# Characterization of Antibody Interaction Using Surface Plasmon Resonance for the Application in Nanoparticle-Based Immunoassays

Master Thesis in Nanobiotechnology

Eglė Deimantavičiūtė

AALBORG UNIVERSITY
STUDENT REPORT

Institute of Physics and Nanotechnology

Aalborg University, Denmark

June 2017

**Department of Physics and Nanotechnology**
**The Faculty of Engineering and Science**
**Aalborg University**
**Skjernvej 4A, 9220 Aalborg Ø**

**Title:**

Characterization of Antibody Interaction Using Surface Plasmon Resonance for the Application in Nanoparticle-Based Immunoassays

**Project period:**

September 2016 - June 2017

**Author:**

Eglė Deimantavičiūtė

**Supervisor:**

Leonid Gurevich

**Copies: 4**
**Number of pages: 104**
**Number of appendices: 1**

**Completed: June 12, 2017**

## Abstract

During this study recombinant dengue type 2 NS1 interactions with a pair of free and nanoparticle conjugated monoclonal antibodies were investigated through kinetic and sandwich analysis using surface plasmon resonance. The antibodies were covalently immobilized using amine coupling method to measure binding events. NS1 association, dissociation kinetics and affinities were evaluated with both antibodies. The inconsistent results indicated the non optimal conditions for the analysis. Kinetics of one antibody, Mer 39, were estimated in a sandwich type analysis, resulting in association constant of 1.13e5 1/M s, dissociation constant of 1.23e-4 1/s and affinity constant of 1.09e-9 M. This type of analysis was used to test NS1 epitope overlap to the said couple of antibodies as well. The investigated antigen did not have the overlapping epitopes to the particular pair. However, the interaction was possible only under specific complex formation sequence. Further research needs to be done to explore the suitability of surface plasmon resonance technique for a comprehensive characterization of nanoparticle conjugated antibodies interaction with the antigen.

# Preface

This master thesis was written by a nanobiotechnology student at the department of Physics and Nanotechnology at Aalborg University. The project lasted from the 1st of September 2016 to 12th of June 2017. The supervisor of the project was Leonid Gurevich. The study was performed in collaboration with BluSense Diagnostics, which a special thanks is given for the project proposal and the supply of proteins and nanoparticles.

References throughout this report will be displayed as a number in brackets like [1]. The number refers to a specific source listed in the bibliography at the end of the report. The position of citation, after or before a full stop, refers to the entire preceding text in one paragraph or to a specific sentence respectively.

Tables, figures and the equations are listed according to the number of the chapter they are in and their sequential position within said chapter. Each figure and table have a brief caption and reference if necessary.

Eglė Deimantavičiūtė Date

# Contents

# Chapter 1

# Introduction

Dengue fever is a widespread viral mosquito-borne disease that poses a threat to more than a half of the worlds population [1]. The disease is caused by one of the four dengue virus serotypes (DENV-1-4) [2]. In recent decades, the geographical expansion of dengue viruses and *Aedes* vector mosquitoes have occurred in tropical and subtropical regions, resulting in a more than 30-fold increase in incidences [3]. The primary and the secondary vectors for DENV transmission are mosquito species *A. aegypti* and *A. albopictus*. *A. aegypti* is highly domesticated species and its population grows alongside urbanization [4]. The Asian tiger mosquito, *A. albopictus*, can survive in temperate regions thus is capable of introducing arboviral diseases in non-endemic areas. This pattern of rapid expansion is a cause for major health and economic concerns world-wide.[3]

Currently, there are no specific antiviral therapy for dengue and, until recently, the only approach for combating the disease were preventive methods like mosquito population and bite control [5]. Even though these methods are effective, due to unfavourable health policies they are not applied continuously [6]. However, the first vaccine has been licensed and granted a marketing authorization in some countries. In addition, the vector competence can be interrupted by implementing mosquito-based immunization strategies. Nevertheless, dengue research, surveillance and patient management still relies on early and accurate diagnosis. [1], [7]

The diagnosis of dengue is based on a detection of certain markers like viral components, antibodies or a combination of both. Enzyme-linked immunosorbent assay (ELISA) is the standard test in endemic areas. [8], [9] However, it requires valuable resources like time, skills and equipment. An effective alternative and a commercially viable method is a detection of the NS1 protein, found in relatively high concentrations in blood during an acute phase of the disease. Even though it is already successfully implemented and used, the sensitivity of this type of assays still can be improved. Thus alternative biosensor technologies for NS1

quantification are being developed. [8], [10]

One of such alternative assays is NS1 detection based on aggregation of magnetic nano particles. This immunoassay is based on an ability of MNPs coated with two different NS1 specific antibodies to capture the antigen and cause aggregation. [10] A way to improve the sensitivity of this immunoassay, is to select an optimal and a well-matched pair of monoclonal antibodies. This can be achieved using surface plasmon resonance (SPR), since it provides information on binding rates, affinity and sites of epitopes. [11] Thus the aim of this study is to characterize NS1 kinetics and epitope overlapping in relation to a pair of monoclonal antibodies using surface plasmon resonance. Additionally, this study aims to measure the binding of free and nanoparticle conjugated antibodies using a sandwich type assay.

## 1.1 Immunoglobulins

### History

In 1890 Behring and Kitasato reported the presence of diphtheria toxin neutralizing agent in the blood. In 1891 Ehrlich made a reference to term antibody in a study, describing the ability of this agent to discriminate between two immune substances. In 1899 the term antigen was used to describe the substance which induces the production of an antibody. [12], [13]

In 1900 Ehrlich proposed a side-chain theory to describe antibody-antigen interactions. He hypothesised that initially antibodies are side chain receptors on cells and later due to excess, they are released into the bloodstream. Also, antibodies were depicted as branched molecules with multiple antigen binding sites and an ability to activate the complement. However, only in 1959 the molecular structure of antibodies was independently published by Gerald Edelman and Rodney Porter. [12], [14]

The modern era of antibody research started after the invention of cells producing monoclonal antibodies in 1975 by Georges Köhler and César Milstein. Nowadays, antibodies are widely used in diverse fields such as biomedical research, therapeutics and diagnostics, since it is possible to develop specific antibodies against a very great variety of antigens. [12]

### Structure and Function

Antibodies or immunoglobulins are heterodimeric proteins produced by the immune systems B-cells in response to foreign or self antigens, such as pathogens, their products, cellular components, toxins [12]. Immunoglobulins are Y shaped and are composed of two indentical light (L) and heavy (H) chains, constructed from two $\beta$ sheets each. The two heavy chains are linked to each other and each heavy chain is linked to a light chain by disulfide and non covalent bonds. Together they form a barrel-shaped structure. [13], [15]

The N-terminal sequences of approximately 110-130 amino acids of both the heavy and light chains vary greatly between different antibodies. This domain is termed variable (V), while remaining domains of the same size are termed constant (C). L chains contain one constant domain, whereas immunoglobulin H chains contain either three or four with a spacer hinge region between the first and second domains. Each V domain can be divided into three regions of variability and four regions of constant sequence, termed the complementarity determining regions (CDR) and the framework regions (FR). The three CDRs of both the heavy and light chains form the antigen binding site. The variable domains are created by

complex gene rearrangement events and after exposure to antigen can be subjected to somatic hypermutation to allow affinity maturation. [12], [16]

Immunoglobulins have not only dual structure but function as well. They have receptor and effector functions. The active regions of immunoglobulins are the two antigen-binding fragments (Fab) and the constant region (Fc). Both heavy and light chains contribute to the Fab regions, while the Fc region consists of the heavy chains only. Antibodies are bivalent and the antigen binding parts of the molecule is located on the tips of the two Fab domains, whereas the stem Fc domain mediate effector functions like activation of complement and binding to Fc receptors. The active parts and structure of antibody are depicted in figure 1.1. [13], [16]

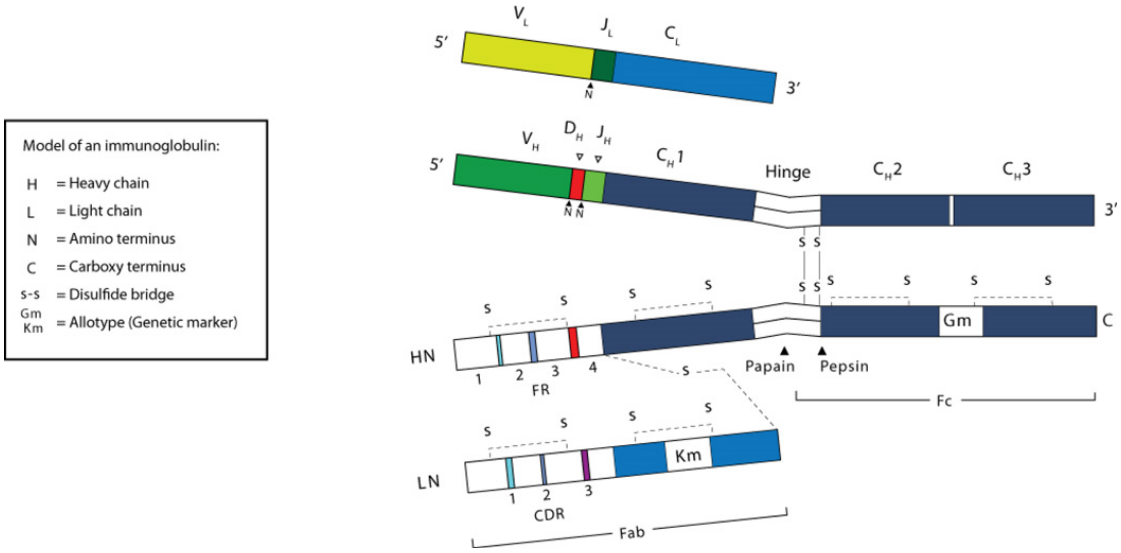


**Figure 1.1:** Two dimensional model of immunoglobulin protein structure. Immunoglobulins gene segments are shown at the top, and the protein structure is shown at the bottom. The structural components illustrated are the disulfide bonds, the heavy and light chains, the hinge, the variable and constant domains and the active Fab and Fc regions. [12]

## Genes of Immunoglobulins

Ig heavy and light chains are each encoded by a separate multigene family and the individual variable and constant domains are each encoded by independent elements, V(D)J gene segments for the V domain and individual C segments for the C domains [13].

V(D)J recombination is a common mechanism that generates immunoglobulin V region diversity through somatic DNA rearrangement. There are as many as hundreds of variable gene segments and a number of diversity (D) and joining (J) segments in the imunoglobulin gene locus. In the case of the light chain gene locus, there are no D segments. Somatic V(D)J rearrangements are able to provide thousands of V(D)J combinatorial sets. V(D)J recombination is often accompanied by nucleotide insertions or deletions at the VD and DJ junction sites and it is a site-specific process mediated by recombination signal sequences (RSSs) flanking the V at the 3' end, D at both 5' and 3' ends, and J at the 5' end genes. Through recombination, a given set of V, D, and J can be used to generate hundreds of different junction sequences, although only one-third of these sequences are in the correct frame for translation.[13], [16], [17],

Another mechanism is somatic hypermutation (SHM), which can intentionally introduce non-template mutations into the variable regions of the transcribed imunoglobulin genes. This mechanism is engaged only after exposure to antigen. SHM occurs at a rate of approximately $10^{-3}$ mutations per base pair per cell division. [13], [17]

## Antigenic Determinants

Immunoglobulins have both common and individual antigenic determinants. Individual determinants, contained within variable domains, are termed idiotypes and are related to the specificity of antibodies. Common determinants are contained within constant domains and are termed isotypes. Differing common determinants within the same species are termed allotypes and represent inherited genetic variations. [16]

## Antibody Classes

Immunoglobulins can be divided into five different classes IgG, IgM, IgA, IgE and IgD, based on differences in their constant regions of the heavy chains [12]. IgG can be split into four and IgA can similarly be split into two subclasses. Antibodies from different classes vary in properties like size, glycosilation status and response to antigen. [16]

IgM is the first immunoglobulin class produced in response to antigen, but class switching later results in expression of IgG, IgA and IgE with the same antigenic specificity. IgM antibodies are associated with a primary immune response. Naive B cells express monomeric IgM on their surface. On maturation and antigenic stimulation, multimeric, usually pentameric IgM is secreted. [12] Given that IgM is expressed early in B-cell development and have not undergone much somatic mutation in response to antigen, IgM antibodies tend to be more polyreactive

than other isotypes, which allows IgM bearing B cells to respond quickly to a variety of antigens. [16]

Similar to IgM, membrane bound IgD participates in receptor signalling. Most IgD B cells also co-express IgM, and IgD can replace IgM and vice versa on said B cells. Circulating IgD is found at very low levels in the serum, with a short serum half-life. Circulating IgD can react with specific bacterial proteins independently of the variable regions of the antibody. The binding of these bacterial proteins to the constant region of IgD results in B-cell stimulation and activation. [12], [16]

IgG is the predominant isotype found in the body and it has the longest serum half-life [16]. IgG antibodies contribute to a secondary immune response. They neutralize many different antigens, including toxins, bacteria, viruses. Based on structural, antigenic, and functional differences in the constant region of the heavy chain, four IgG subclasses were identified. [12]

IgA is critical at protecting mucosal surfaces from toxins, viruses, and bacteria by means of direct neutralization or prevention of binding to the mucosal surface. Although generally a monomer in the serum, IgA at the mucosa, termed secretory IgA is a dimer. There are 2 subclasses of IgA, with structures that differ mainly in their hinge regions. [12], [16],

Although IgE is present at the lowest serum concentration and has the shortest half-life, it is a very potent immunoglobulin. It is associated with hypersensitivity and allergic reactions, as well as the response to parasitic worm infections. [12]

## Monoclonal and Polyclonal Antibodies

A heterogeneous population of antibodies that recognize different epitopes within the same antigen and bind to it with varying affinities are called polyclonal [12]. Polyclonal antibodies are made by immunizing a suitable animal, leading to the production of high titer, high affinity mixture of antibodies against the antigen of interest. However, immunising another animal will not generate antibodies against the same epitopes and the the supply of polyclonal antibodies is limited. [18]

Monoclonal antibodies represent a population of antibodies that recognize a single epitope within an antigen. Monoclonal antibodies are produced by immortalised B-cell, a fusion between a specific antibody-producing B cell with a myeloma cell. This immortal cell line, called hybridoma, can provide a constant supply of monoclonal antibodies. [12]

The main advantage of monoclonal antibodies is monospecificity. The low cross reactivity with non-specific antigens can be useful in evaluating changes in molecular conformation and probing molecular interactions. However, even small changes in the antigenic epitope, due to genetic polymorphism, glycosylation or denaturation, can affect the function of these antibodies. [12] In contrast,

polyclonal antibodies recognize a number of epitopes, thus a change in the epitopes is less significant. In addition, polyclonal antibodies are more stable to changes in pH and salt concentration. Also, polyclonal antibodies often have better specificity. However, the concentration and purity levels of specific antibody in polyclonal mixure is significantly less compared to monoclonal antibodies. [12], [18]

## Antibody-Antigen Interactions

The basic principles of antigen–antibody interaction are those a bimolecular reaction. Also, antibodies do not irreversibly alter the antigen they bind thus the reactions are noncovalent and reversible. [16] The forces involved in the interaction are electrostatic, hydrophobic, van der Waals forces and hydrogen bonds. The contribution of each to the overall interaction depends on the particular antibody and antigen involved. [19] Immunoglobulin-antigen interactions typically take place between the paratope, the site on the molecule at which the antigen binds, and the epitope, which is the site on the antigen that is bound. When the epitope and the paratope come together, they are attracted by long-range electrostatic forces that overcome the hydration energies. After the water molecules are expelled, the interacting molecules approach each other more closely. At this distance, short range forces like van der Waals pull two complementary surfaces together. The strength of the binding depends on the fit between those surfaces. The interaction between an antibody and its antigen can be disrupted by high salt concentrations, extremes of pH, detergents and sometimes by competition with another molecules. [16], [19]

The measure of binding strength, between an antibody and a single epitope, is termed affinity. This interaction is described by the affinity constant $K_a$, the amount of antigen-antibody complex formed at equilibrium:

$$K_a = \frac{[Ab - Ag]}{[Ab][Ag]} \tag{1.1}$$

where $K_a$ is the affinity constant, [Ab-Ag] is the molar concentration of the antibody-antigen complex, [Ab] is the molar concentration of unoccupied antibodies, [Ag] is the molar concentration of free antigen. [16]

Antibodies with high affinity bind larger amounts of antigen with a greater stability in a shorter time than those with low affinity. The stability of antigen-antibody complexes is influenced by presence of additional binding sites on antibodies and antigens. The overall binding intensity between multivalent antibody or multivalent antigen is described as avidity. Avidity is affected by the affinity of the antibody for the epitope, the number of antibody or antigen binding sites, and the structure of the resulting antibody-antigen complexes. [16], [19]

## 1.2 Dengue

### The Emergence of Dengue Throughout History

An illness clinically similar to dengue fever was observed as early as in Chin Dynasty years (265 to 420 A.D.). It was described in a Chinese medical encyclopedia as a water poison, a disease connected to flying insects and water. [4]

In 1779 and 1780 major epidemics occured in Asia, Africa and North America and were thought to be dengue outbreaks [4]. However, in the early nineteenth century dengue was not always distinguished from chikungunya virus infection. In fact, the name dengue more often referred to chikungunya, while the present-day dengue fever was termed differently. The outbreak in Philadelphia in 1780 was identified as dengue epidemic from the historical account of clinical symptoms of break-bone fever described by Benjamin Rush. Additionally, it was observed that dengue manifested once, while break-bone fever was capable of afflicting the same individual twice. Thus the description of the break-bone fever is compatible with the current knowledge of dengue viruses. However, the break-bone fever got the name dengue only because this particular virus was isolated and then labeled before chikungunya. [20]

World War II began a global dengue pandemic. It disrupted the ecologic system and increased a transmission of mosquito-borne diseases in the Southeast Asia and the Pacific. The increased transmission promoted the co-circulation of multiple dengue virus serotypes thus resulting in an emergence of more severe dengue haemorrhagic fever (DHF) epidemics. [21]

Decades later the ever expanding geographic distribution of dengue viruses and *Aedes* vector mosquitoes, resulted in a more than 30-fold increase in incidences in tropical and subtropical regions [3]. Currently, the Eastern Mediterranean, American, South-East Asian, Western Pacific and African regions are endemic and infrequent local cases has been reported in Europe and the United States [22]. At present more than a half of the global population is at risk and around 96 million clinically significant DENV infections are reported annually. However, the actual number of cases are under-reported and misclassified. This significant global burden of dengue makes it one of the most important tropical disease. [1], [5] The global risk and burden of dengue is depicted in figure 1.2.

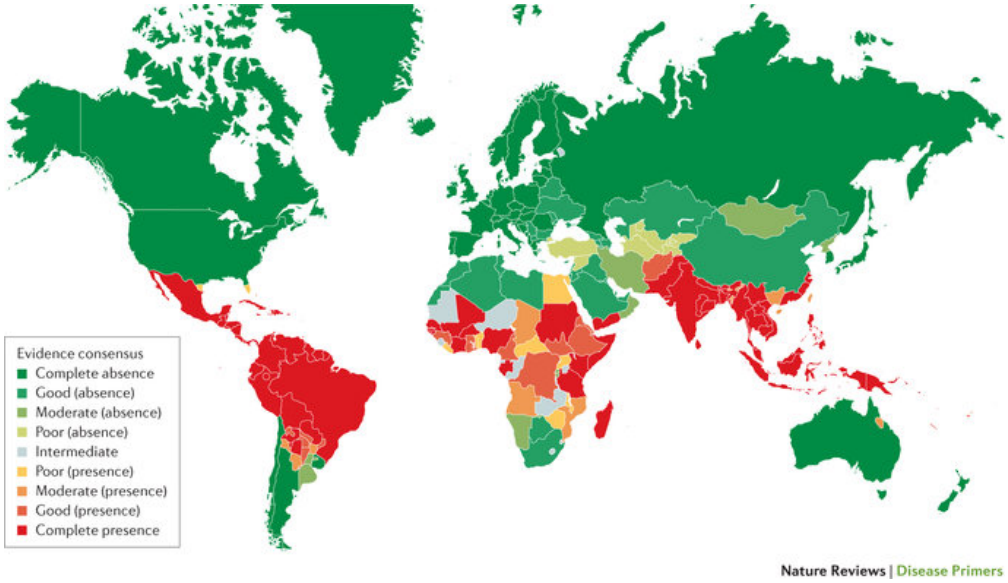


**Figure 1.2:** The global risk and burden of dengue. Complete absence is shown in dark green and complete presence in dark red.[1]

## Causes for The Epidemic Dengue Activity

The causes for the emergence of dengue epidemics are mostly associated with demographic and societal changes like global population growth and urbanization. The urbanization with its side effects like the inadequate housing, water and waste management have created favourable conditions for the transmission of mosquito-borne diseases. [4]

Also, air travel have resulted in a free movement of viruses, through infected humans, to various parts of the globe [23]. Additionally, inadequate public health infrastructures and unfavourable health policies have contributed to the growth of epidemic dengue activity [24]. Other factors are ineffective mosquito control and an expanding *A. aegypti* population. The latter is linked to an increase of mosquito larval habitats like plastics and used tires within the domestic environments. Possibly environmental change will also contribute to the problem in the future. [1], [4]

## Dengue Prevention and Control

Currently, there are no specific antiviral therapy for dengue and, until recently, the only approach for combating the disease were preventive methods like mosquito population and bite control. Such control methods entail active monitoring and

surveillance of vectors, reduction of accessible domestic water habitats and use of insecticides. [4], [5] Additionally, new attempts to control the vector, like genetically modifying male mosquitoes to reduce the number of eggs, are made. Also, the vector competence can be interrupted by infecting mosquitoes with the bacterium *Wolbachia spp.* to limit dengue infection due to competition between the altered and the natural mosquito populations. [25] During the 1950s–1970s the simple vector control strategy was successful in most neotropical locations, but was not sustained ever since [6].

Recently, the first vaccine, comprised of chimeric flaviviruses, containing the structural protein genes of DENV and the non-structural protein genes of the yellow fever virus vaccine strain, has been licensed and granted a marketing authorization in some countries. However, the vaccine has been licensed only for use in children 9 years of age or older and is missing an important segment of the population at risk. Thus there is a need for other dengue vaccine candidates, which currently are being developed and are at various phases of clinical trials. [7], [26]

## Dengue Virus Transmission

The epidemiology of DENV involves both an ancestral sylvatic cycle, among nonhuman primates and arboreal *Aedes* species mosquitoes, and an endemic urban cycle involving humans and the domestic mosquito *Aedes aegypti*. The efficiency of the endemic cycle is greatly enhanced by the ecology and behavior of *A. aegypti*. [27] *Aedes aegypti* mosquitoes are highly domesticated species that feeds on humans, rests indoors and lays its eggs in artificial water containers. These behaviours greatly enhance vector competence and transmission. The viruses are passed on to humans, which serve as an amplification hosts, through the bites of an infective female mosquito. The female mosquitoes become infective when they feed during the viremic phase of illness. Virus infects numerous mosquito tissues, starting with mid-gut cells and lastly reaching the salivary glands, in approximately 10 days. After the incubation a mosquito becomes infective and remains so for life. [4], [28], [29]

## Dengue Viruses

Dengue viruses are classified within the family *Flaviviridae*, genus *Flavivirus*, which contains a number of well known human pathogens, such as Japanese encephalitis virus (JEV), West Nile virus (WNV) and yellow fever virus (YFV). Dengue viruses form a group of four genetically and antigenically distinct serotypes, denoted DENV-1–4. [21], [30] Several phylogenetic genotypes of different geographical origins occur within the serotypes as well [2].

The virions of flaviruses are spherical 40–50 nm particles. Flaviruses have a single-stranded, positive-sense RNA genome of approximately 11 kb, which is surrounded by a nucleocapsid, encased in a host derived lipid bilayer envelope. The genome encodes a single long open reading frame (ORF), flanked by highly structured 5' and 3' untranslated regions (UTRs). Single ORF is translated into a polyprotein that is later processed into three structural proteins, the capsid (C), membrane (M) and envelope (E), and seven non-structural proteins NS1, NS2A, NS2B, NS3, NS4A, NS4B and NS5. The functions of structural and nonstructural proteins are best understood in the context of the viral life cycle. [4], [31]

## Dengue Virus Replication Cycle

Dengue viruses attach to susceptible cells by two known mechanisms [21]. In one case, virus replication cycle, seen in figure 1.3, starts when the envelope protein E binds to the cellular receptors, triggering an uptake of the virion to the host cell by endocytosis. Inside the host cell, the change in pH induces a conformational change in the E protein, which facilitates the fusion between endosomal and viral membranes. The nucleocapsid is released from the viral envelope as a result of the fusion. It then dissociates and the viral genome is released and translated. [32], [33]

The viral genome is replicated via a negative-strand intermediate, which serves as a template for additional positive-strand RNAs. The replication of viral genome occurs inside vesicular packets in the endoplasmic reticulum (ER). The newly formed RNA templates are translated into long polyproteins. The single polyprotein is oriented by its signal sequences and membrane anchor domains and is positioned both on cytosolic and lumen side of endoplasmic reticulum. The individual proteins are formed after processing steps by the viral non-structural NS2B or NS3 and host proteases. [34], [33]

When capsid proteins interact with viral RNAs, a nucleocapsid is formed. It is then enclosed in an envelope by budding into the ER lumen, which has the precursor forms of the membrane protein (prM) and the E proteins embedded in its membrane. When the virions assemble, they are immature thus E proteins are arranged in trimers and make the surface have a spiky appearance. [32], At this stage of maturity, the prM protein prevents the fusogenic activity of envelope glycoproteins. The viral particles reach maturity and become infectious after prM is cleaved by furin proteases during the transportation through the trans-Golgi network. The envelope proteins then rearrange into dimers that lie flat against membrane and gives an appearance of a smooth surface. Lastly, the infectious virions are realesed from the host cell by the processes of exocytosis. [32], [33]

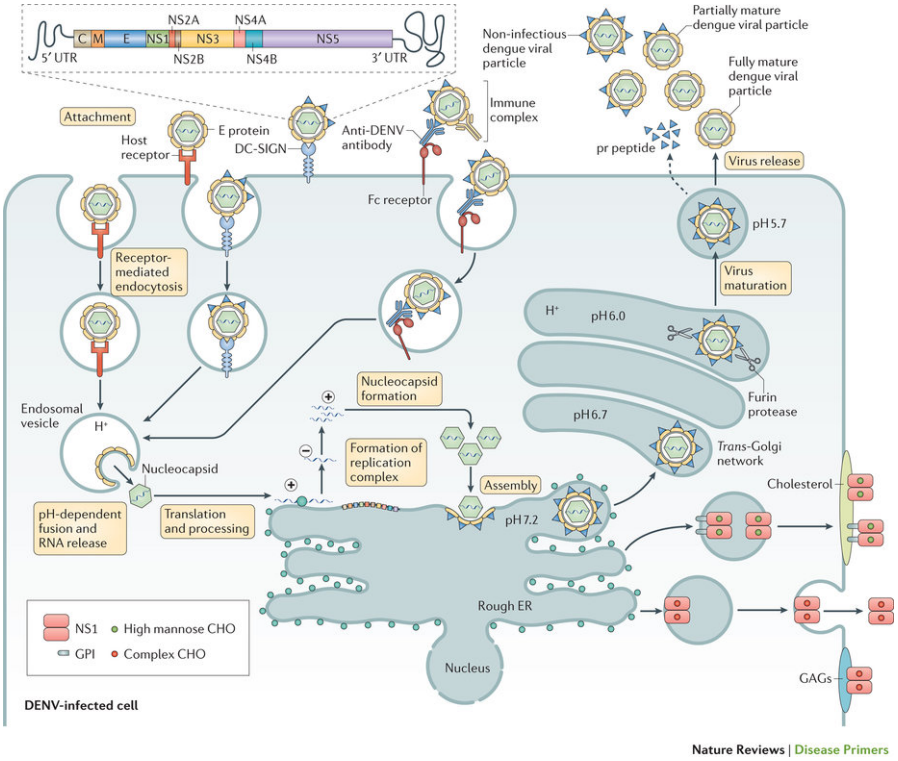


**Figure 1.3:** Dengue virus replication cycle.Viral particles attach to host cells and virus enters through receptor-mediated endocytosis. Inside the cell viral and endosomal membranes fuse and the nucleocapsid is released and disintegrated. Then genomic RNA is translated into a long polyprotein, which is cleaved into individual proteins. NS proteins are located at the site of replication and initiate transcription. The precursor form of the membrane protein (prM) and the E protein, embedded into the ER membrane, enclose the newly formed nucleocapsid as it buds into the ER lumen. This immature particle is trafficked via the secretory pathway that causes rearrangements of the prM and E proteins. The mature virion is formed and released from the host cell. Additionally, NS1 trafficing and glycosilation is depicted. NS1 is either secreted or transported to the cell surface, where it associates with lipids such as cholesterol. [1]

In the other case, dengue viruses can form complexes with non-neutralizing IgG antibodies from previous dengue infection or maternal antibodies. The antigen-antibody complex may attach to macrophages or monocytes via Fc receptors, get inside the cell and replicate. This prossecces is called antibody-dependant enchancment (ADE) and it enables an increased virus production, which contributes to the pathogenesis of severe forms of dengue diseases. [35], [36]

## Dengue Nonstructural Protein 1

The nonstructural glycoprotein (NS1) for dengue virus was first reported in 1970 as a soluble complement-fixing (SCF) antigen in infected cell cultures [37].

Later, the SCF antigen was identified as the viral-encoded 46 kDa glycoprotein gp46 [38]. After the yellow fever virus genome was sequenced, the gene encoding gp46 protein was recognized as the first of the nonstructural proteins and named accordingly in 1985 [39].

NS1 is found at different cellular locations as a cell-membrane-associated dimer, a dimeric intracellular NS1 and a secreted hexameric lipoprotein. Intracellular NS1 plays an essential role in virus replication and has been shown to localize on the ER membrane with viral RNA and other components of replication complexes. Secreted NS1 is highly immunogenic and is a common diagnostic marker for the viral infection. [40], [41]

## NS1 Expression

Initially, NS1 is translated as a part of a long polyprotein that is then translocated into the endoplasmic reticulum for processing. The translocation occurs via a signal sequence corresponding to the final 24 amino acids of viral envelope protein. [42] Within the lumen of the ER, both N and C-terminus of NS1 are cleaved [43]. The cleavage at C-terminus takes place when the ER resident protease recognises the last 8 amino acids of NS1 [31]. Following the processing, a hydrophilic monomeric NS1 is released and then glycosylated by the addition of high-mannose carbohydrates. [44]

## NS1 Glycosilation

Post-translational modifications of nonstructural protein 1 have different glycosylation patterns that are dependant on the host cells and cellular location. Depending on the glycosilation pattern, monomeric NS1 has a molecular weight between 49–55 kDa. DENVs NS1 contain three glycosylation sites, at positions Asn 130, Asn175 and Asn 207. [44]

In mammalian cells, NS1 is found at different cellular locations in multiple oligomeric forms, a cell-membrane-associated dimer, a dimeric intracellular NS1, and a secreted hexameric lipoprotein. mNS1 and sNS1 monomers have differing migration profiles on SDS–PAGE due to the variations in carbohydrate composition.[40], [45]. Membrane-associated dimeric form of NS1 contains only high mannose carbohydrate additions, while the secreted form of NS1 contains complex carbohydrates. This processing occurs, when dimeric NS1 passes through the Golgi compartment where high mannose carbohydrate moieties at Asn 130 are trimmed and processed to a complex carbohydrate form. The glycosilation site at Asn 207 is sterically protected in the oligomeric form, so high-mannose carbohydrate moiety is not processed. [44], [46]

In insect cells, due to the lack of correct glycosilation, NS1 is accumulated and not secreted. Thus the secretion is associated to an addition of complex carbohydrates. [46] Moreover, the removal of either or both glycosylation sites results not only in decreased NS1 secretion but reduced virulence, decreased virus yields and depressed RNA accumulation as well. Hence glycosylation is important for NS1 maturation, in terms of its secretion, role in viral RNA replication and virulence of disease. [44]

## NS1 Oligomerization

NS1 contain all the information needed for oligomerization [47]. Studies demonstrated that soluble hexameric NS1 dissociates into dimers in the presence of detergent molecules and can associate into haxamers after it is removed, seen in the figure 1.4 [41].

After glycosylation, hydrophilic monomers form stable dimeric species, acquiring a partially hydrophobic nature, essential for membrane association. The membrane associated NS1 significantly precedes the formation and secretion of hexameric sNS1. The formation mechanism of hexameric species is unknown.[48] It is possible that dimers are able to dissociate from the ER or Golgi membranes, drag a number of lipids out and then associate with two other dimeric units through hydrophobic domains [49]. However, it is also possible that association of individual dimers is dependent on NS1 concentration. As the concentration of NS1 increases, the dimeric units have higher probability to partner with each other. [48]

## NS1 Structure

NS1 is a 352 amino-acid polypeptide that exists in multiple oligomeric forms. A monomer has a molecular weight of 46–55 kDa, depending on its glycosylation status. The monomeric protein contains 12 cysteines that form 6 disulfide bonds, necessary for protein stability, correct folding, as well for proteins maturation, secretion and the formation of oligomeric species. Initially, monomeric NS1 is hydrophilic, however, it becomes partially hydrophobic after dimerization. [44], [48]

A single NS1 monomer has three domains, a $\beta$-roll, a wing and $\beta$-ladder. A small $\beta$-roll domain continues from amino acids 1 to 29 and forms two $\beta$ hairpins, stabilized by a disulfide linkage at Cys4-Cys15 positions. Within a dimer, the four $\beta$ hairpins intertwine to form a $\beta$ sheet that curves into a roll-like structure. The second domain continues from amino acids 30 to 180 and forms a wing like protrusion. It contains two glycosylation sites at Asn130 and Asn175, a disulfide bond at Cys55-Cys143 and two subdomains. An $\alpha/\beta$ subdomain extends from amino acids 38 to 151 and contain a four-stranded $\beta$ sheet, two $\alpha$ helices and a

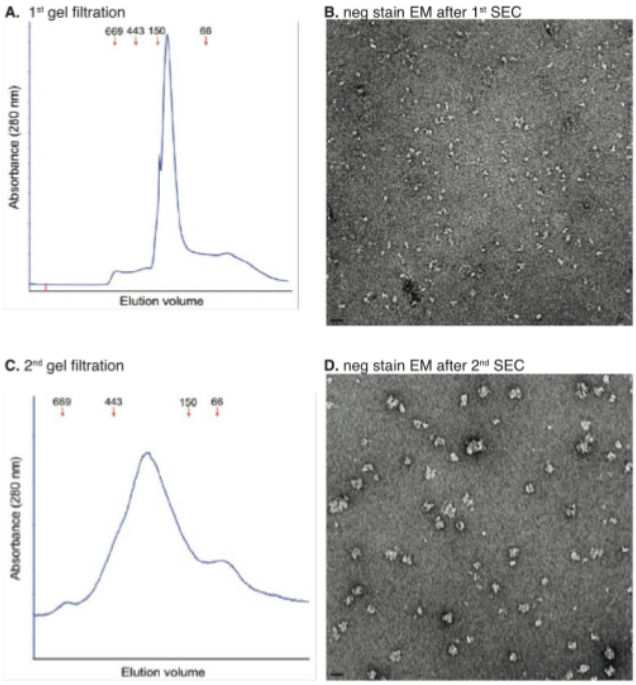


**Figure 1.4:** Detergent effects on NS1. (A) Gel filtration of DEN2 NS1 following affinity purification in the presence of detergent. (B) Negative-stain EM image of the peak fraction from the elution in A. Scale bar in the lower left is 20 nm. (C) Second detergent-free gel filtration of DEN2 NS1. Oligomer formation is evident from the apparent molecular weight of the peak fractions, approximately 300 kDa, corresponding to an NS1 hexamer. (D) Negative-stain EM image of the peak fraction from the elution in C, showing larger particles than seen in B. [41]

20 amino acid long disordered distal tip. A discontinuous connector subdomain extends from amino acids 30 to 37 and 152 to 180. It links the $\beta$ roll to a wing and also links the wing to the central $\beta$-sheet domain. This subdomain shares a disulfide bond at Cys179-Cys223 with the $\beta$-ladder domain. The $\beta$-ladder domain is a main structural feature of NS1 and continues from amino acids 181 to 352. In dimeric species it comprises of 18 $\beta$ strands that form a ladder like structure. The first five $\beta$-strand rungs proceed sequentially toward the end of the ladder. At the end of the domain, amino acids 278 to 352, a conserved tip region contains four strands of the $\beta$ ladder, a small three stranded $\beta$ sheet and three disulfide bonds. The interstrand loops are short, except one, a long spaghetti loop. It extends from amino acids 219 to 272 and is ordered by 57 hydrogen bonds. The 3D and 2D NS1 structure is depicted in figure 1.5. [41]

The hydrophopic character, associated with the dimeric NS1, is attributed to the $\beta$-roll and a connector subdomain of the wing. The connector subdomain contains an important part of the hydrophobic protrusion, a mobile disordered greasy finger loop. This hydrophobic protrusion potentially may be the reason,

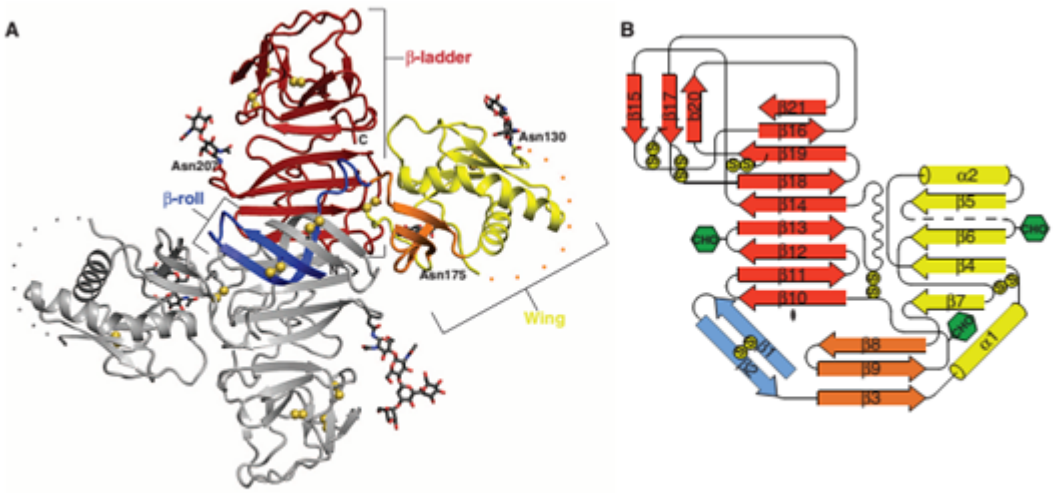


**Figure 1.5:** The structure of NS1. A - NS1 dimer with one monomer in gray and the other coloured by domain. Blue for $\beta$-roll, yellow for wing, orange for connector subdomain, red for central $\beta$-ladder. A disordered region is indicated with dotted lines. B - a diagram for NS1 monomer, where glycosylation sites are indicated with green hexagons and disulfides with yellow circles.[41]

why NS1 associates with the ER membrane. Also it may interact with the viral replication complex through transmembrane proteins NS4A and NS4B, since a dipeptide, implicated in interaction with NS4B, is located in a loop of the $\beta$-roll nearby the hydrophobic surface. [41]

NS1 dimers can also form a symmetric barrel-shaped hexamer, arranged in D3 symmetry. The $\beta$-roll domains and the hydrophobic protrusions face the interior of the hexamer, whereas the outer surface contains the spaghetti loops, glycosylation sites, and disordered wing-domain loop. [41] NS1 hexamer is held together by weak hydrophobic interactions that can be interrupted by the presence of detergent molecules, while the dimeric subunits can only be dissociated by heat or acid treatment. [48]

NS1 is highly immunogenic and has 108 linear epitopes, identified from immune epitope database. The main epitope locations are the most accessible parts of the protein like the wing domains disordered loop, the C-terminal tip of the $\beta$-ladder, and the $\beta$-roll. Another such location is the hydrophobic protrusion. Thus the inside of the hexamer must be accessible to the immune system either before its formation or after dissociation. [41]

## DENV Immune Response and Pathogenesis

Initially, dengue virus infect immature dendritic cells that spread through the lymphatic system to present viral antigens to T-cells, initiating the cellular and humoral immune responses. However, infected cells have an impaired ability to communicate with adaptive immune cells and to produce interferons and cytokines. [50]

The first line of defence against the virus is production of interferons (IFN)-$\alpha/\beta$, which induce intracellular antiviral activity and initiates the adaptive response. However, dengue virus can evade innate immunity by undermining antiviral responses and inhibiting cellular signalling cascades. It has been shown that IFNs are less activated in cases of severe disease. citeinter Another factor contributing to the severity of the disease is over-production of cytokines, believed to be a product of T-cell activation and infection of cells such as keratinocytes, dendritic cells and endothelial cells. Moreover, the high levels of the complement activation products C3a and C5a correlate with the severity of illness as well. [50], [51]

Adaptive immune response to dengue virus has both protective and detrimental aspects. On one hand, infection with one of DENVs provide long-term immunity to the specific serotype. On the other hand, the remaining cross-reactive immune response to other serotypes has the potential to increase the severity of dengue infection. The adaptive immune response to dengue infection consists of the production of antibodies that are primarily directed against the virus envelope proteins, the precursor membrane (preM) and non-structural protein 1. IgM antibodies increase after the decline of viremia and have the highest activity in a primary infection, whereas IgG antibodies exceed IgM production during secondary infection. [50], [52]

The pathogenic role of antibodies in dengue infections have been demonstrated in relation to several mechanisms such as antibody-dependent enhancement(ADE), antibody-dependent complement activation and antibody-dependent cellular cytotoxicity. The enhanced virus replication is mediated primarily by pre-existing, non-neutralizing antibodies to the virion surface antigens that enhance access of the virion-antibody complex to Fc receptor bearing cells. Antibodies specific to membrane-bound NS1 can also direct complement-mediated lysis of infected cells and contribute to antibody-dependent cellular cytotoxicity. [51], [53]

The memory B and T-cells are reactivated during secondary infection. B-cells synthesize antibodies with higher affinity for the first infecting virus than for the second infecting virus. The stimulation of T-cell memory results in the production of heterotypic $CD4+$ and $CD8+$ cells that have a diminished capacity to kill but nonetheless release inflammatory cytokines that contribute to disease severity. [50]

## Dengue Illness

Infection with dengue virus is classified as either dengue with or without clinical presentation that may vary in severity from a mild undifferentiated fever to a severe, life-threatening illness. The severity of clinical manifestation depends on a number of risk factors like the strain and serotype of the infecting virus and the immune status, age, and genetic background of the human host. An infection with one of the four dengue viruses generates only type-specific immunity thus a secondary infection with heterologous types can occur. [4], [5] The course of of dengue infection is depicted in figure 1.6.

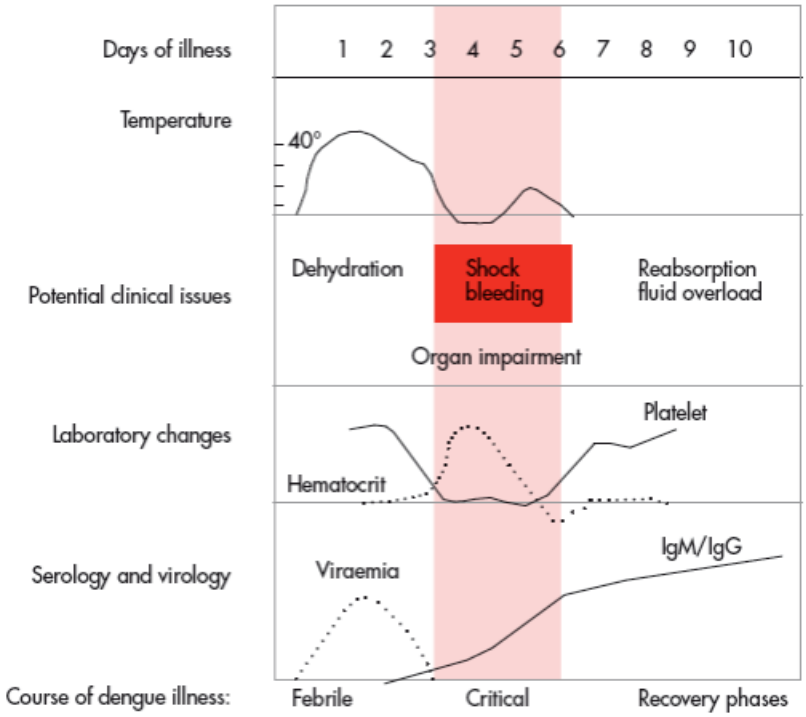


**Figure 1.6:** The course of of dengue infection [54].

Dengue fever is a most common manifestation of DENV infection and is primarily seen in adults and older children. It occurs during both primary and secondary infections. [55] The illness is characterized by the sudden onset of fever and a variety of non-specific symptoms like headache, retro-orbital pain, abdominal pain, nausea and vomiting, muscle and joint pains, fatigue, and rash. Generally, dengue fever is self-limiting and rarely fatal. The acute phase of illness lasts for 3 to 7 days, but the convalescent phase may be prolonged for weeks. [4], [5]

The more severe forms of dengue infection are classified as dengue haemorrhagic fever (DHF) and dengue shock syndrome (DSS). Dengue haemorrhagic fever (DHF) usually follows a secondary dengue infection and primarily affects children. However, it may follow a primary infection in infants due to maternally acquired dengue antibodies. [4] The clinical course of DHF is divided into febrile, leakage, and convalescent phases. The acute febrile phase of DHF is difficult to distinguish from dengue fever. [5] However, as fever subsides, characteristic symptoms of circulatory failure or plasma leakage may appear. In less severe cases, most patients recover spontaneously or after a period of fluid replacement. In severe cases, plasma leakage and coagulopathy, accompanied by bleeding can lead to a fall in blood pressure and to a circulatory shock and organ impairment. Patients with DSS have high mortality rates. However, early diagnosis and fluid replacement therapy with good clinical management can decrease fatality rates up to 1%. [4], [5], [55]

## Dengue Diagnostics

Accurate and efficient dengue diagnostic tools are necessary for dengue research, surveillance and control. An early and reliable diagnosis can improve clinical management and vector control measures. Additionally, it can provide data on vaccine evaluation, the epidemiology and health burden of dengue. [9] Depending on the purpose of diagnosis, different types of confirmation methods can be used and combined for relevant results. Currently, the established confirmation methods are virus isolation, genome or antigen identification and serological studies. [9],[56] The diagnostic markers of dengue infection and their timelines are shown in figure 1.7.

Dengue virus can be directly detected and serotype identified during an early acute phase of infection from serum, plasma, whole blood and infected tissues. Even though a viral culture or a nucleic acid amplification are very effective techniques that offer sufficient accuracy and specificity, the procedures are rarely available for decentralized diagnostics in dengue endemic countries. [56]

A common simplified method of diagnosis is the NS1 antigen detection. High concentrations of this antigen can be detected in patients with the primary and the secondary dengue infection up to 9 days after the onset of illness. However, in many cases the virus serotype, the infection type and stage limit the sensitivity and reliability of these tests. However, NS1 detection is a promising method, especially, if used in combination with serological methods. [8], [9]

Serological assays are commonly used at the end of the acute phase, when viremia and viral products are undetectable. Different patterns of antibody responses are observed during the primary and the secondary dengue infection thus the type of infection can be determined by IgM/IgG capture ELISA. [9] In primary

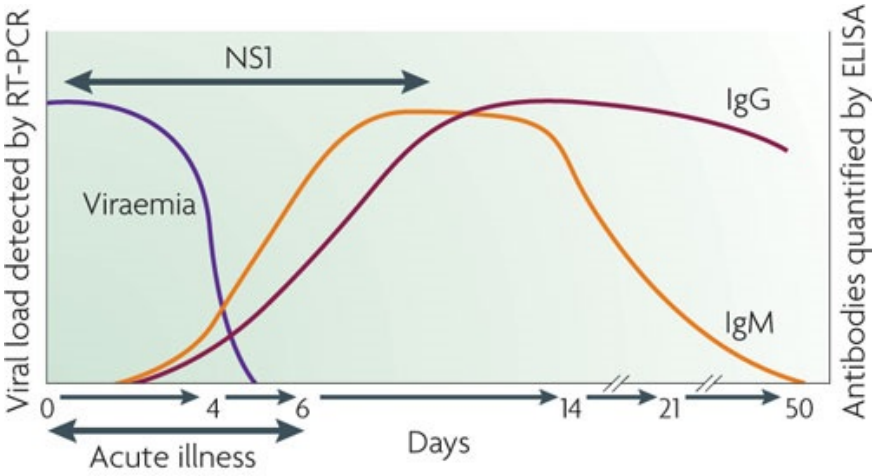


**Figure 1.7:** The diagnostic markers of Dengue infection, their timelines and appropriate tests [9].

infections, immunoglobulin M (IgM) is detected 5 or more days after the onset and immunoglobulin G (IgG) is detected from 10–15 days. In secondary infections, IgM are usually at lower titers than in primary infections while a secondary immune response generates high levels of IgG through the stimulation of memory B cells. However, it is difficult to use serology to identify dengue serotypes because the antibodies often demonstrate some degree of cross-reactivity with other dengue viruses. Moreover, a recent vaccination or infection of antigenically related flaviviruses can interfere with the diagnosis as well. [8], [9]

## NS1 Detection Based on Aggregation of MNPs

Currently, the standard DENV NS1 test is ELISA [8]. However, alternative biosensor technologies for NS1 quantification using fluorescent nanoparticles, surface plasmon resonance and electrochemical detection are being developed. One of such alternative immunoassays is NS1 detection based on aggregation of magnetic nanoparticles. [10] Figure 1.8 illustrates the principle and instrumentation of this assay.

The magnetic nanoparticles used in this assay have their surfaces treated against non specific binding with human serum albumin. The HSA monlayer is then used to anchor, via bio-orthogonal Cu-free click chemistry, high-affinity monoclonal antibodies, targeting two different epitopes on the NS1 protein. The NS1 detection proceeds in three steps. Firstly, the biomarker molecules diffuse and in a process are captured by the antibody-coated magnetic nanoparticles. Then

a pulsating magnetic field during the field-on period concentrates and during the field-off period lets the particles to diffuse. The diffusive motion randomizes the angular orientations of the nanoparticles and facilitates biomarker induced internanoparticle binding. The internanoparticle binding gives clusters of nanoparticles, which are detected by optical scattering at applied magnetic rotation frequencies. The signal reveals the number and size of clusters in solution. Since the MNPs have a negligible magnetic moment, a homogeneous suspension of non-aggregated particles is not expected to produce a modulation of the transmitted light intensity. [10]

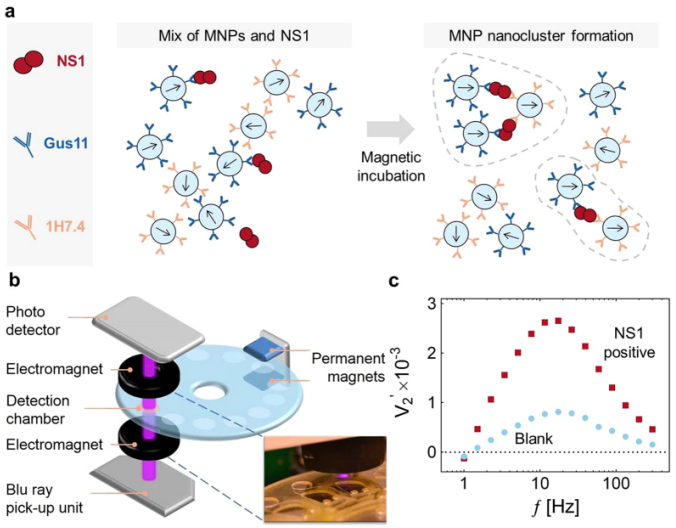


**Figure 1.8:** The instrumentation and principle of NS1 detection using antibody-conjugated magnetic nanoparticles [10].

## 1.3 Surface Plasmon Resonance Biosensor

### Introduction to Surface Plasmon Resonance Biosensors

In the beginning of the twentieth century, Wood detected an anomalous diffraction pattern of light and dark bands when visible polarized light reflected on a metal grating, due to the excitation of electromagnetic surface waves [57]. In the late sixties, Kretschmann and Otto demonstrated optical excitation of surface plasmons by the method of attenuated total reflection [58], [59]. Since then, surface plasmons have been studied and and implemented in optical sensors. [60]

Surface plasmon resonance biosensor is one of the most successful plasmonic biosensor. In 1983 the first SPR biosensing experiments were performed with antibody antigen interactions by Liedberg. The experiments demonstrated that the binding kinetics could be resolved for different analyte concentrations thus making the high performance of the technique evident. [60], [61] Since then SPR biosensors have become an important tool in studying biomolecular interactions and detection of chemical and biological substances in areas such as diagnostics, environmental monitoring, food safety and security. [62]

SPR-based biosensors can measure the interactions of biomolecules directly in real time without the need for labelling. The ability to measure interactions in real time allows to quantitatively determine kinetic parameters, thermodynamics and concentration, or qualitatively characterize relationships between ligands and analytes. [63] SPR-based biosensors are used to study a large variety of biomolecular mechanisms, ranging from protein–protein, antibody–antigen, and receptor–ligand interactions to the characterization of low molecular weight compounds. [64]Additionally, progress in surface chemistries enables the use of SPR-based platforms to facilitate capture of hydrophobic compounds such as lipids to study membrane-associated receptors. [65].

### Surface Plasmons

Plasmons are described as charge density waves that arises due to collective coherent motion of conduction electrons. Surface plasmons (SP) propagate along the interface between mediums that have dielectric constants of opposite signs like a dielectric and a metal. [60], [66], [67] SP is characterized by the propagation constant and electromagnetic field distribution [60]. The field of a surface plasmon is transversemagnetic (TM) polarized, its vector of intensity of magnetic field lies in the plane of metal-dielectric interface and is perpendicular to the direction of propagation [68]. When the intensity of the magnetic field reaches its maximum at the metal-dielectric interface, it decays into both the metal and dielectric. However, the electromagnetic field of an SPW is mainly localized in the dielectric. Hence

the propagation constant of the surface plasma wave is very sensitive to changes in the refractive index of the dielectric. [60], [66] The propagation constant of surface plasmons can be expressed as:

$$\beta_{SP} = \frac{w}{c}\sqrt{\frac{\varepsilon_M \varepsilon_D^2}{\varepsilon_M + \varepsilon_D^2}} \tag{1.2}$$

where w is the angular frequency, c is the speed of light in vacuum, $\varepsilon_M$ is permittivity of the metal and $\varepsilon_D$ is the permittivity of the dielectric. [69]

## Optical Excitation of Surface Plasmons

A light wave can couple to a surface plasmon at an interface between metal and dielectric if the component of light's wavevector that is parallel to the interface matches the propagation constant of the surface plasmon. As the propagation constant of a surface plasmon at a metal-dielectric interface is larger than the wavenumber of the light wave in the dielectric, surface plasmons cannot be excited directly by light incident onto a smooth metal surface. The wavevector of light can be increased to match that of the surface plasmon by the attenuated total reflection or diffraction. [60], [70] Prism couplers represent the most frequently used method for optical excitation of surface plasmons. In the Kretschmann configuration of the attenuated total reflection (ATR) method, a light wave passes through a high refractive index prism and is totally reflected at the base of the prism, generating an evanescent wave penetrating a thin metal film, shown in figure 1.9. [71]

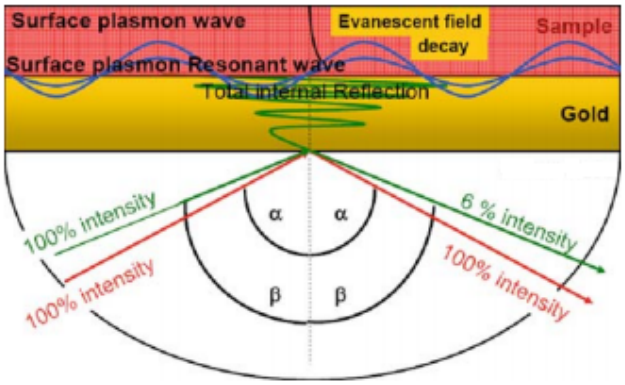


**Figure 1.9:** SPR effect at attenuated total reflection (ATR). An SPR sensor is shown in the Kretschmann configuration. Al prism is covered with a sensor chip with a gold layer on which a ligand can be immobilized. The surface is irradiated with polarized visible light. Under conditions of attenuated total reflection (angle $\alpha$) a dip in the intensity of reflected light is observed and the electrons in the gold layer absorb the energy of the light, resulting in a surface plasmon resonant wave. [71]

The evanescent wave propagates along the interface with the propagation constant, which can be adjusted to match that of the surface plasmon by controlling the angle of incidence. Thus, the matching condition

$$\frac{2\pi}{\lambda} n_p \sin(\theta) = Re\left\{\beta_{SP}\right\} \tag{1.3}$$

can be fulfilled, allowing the evanescent wave to be coupled to the surface plasmon. $\theta$ denotes the angle of incidence, $n_p$ denotes the refractive index of the prism and $\beta_S P$ denotes the propagation constant of the surface plasmon. [72]

## The Principle of SPR Biosensor

SPR sensors measure changes in the refractive index occurring at the surface of a metal film supporting a surface plasmon. A surface plasmon excited by a light wave propagates along the metal film, and its evanescent field probes the medium in contact with the metal film. A change in the refractive index of the dielectric gives rise to a change in the propagation constant of the surface plasmon, which through the coupling condition alters the characteristics of the light wave coupled to the surface plasmon. [69]

The coupling of incident light wave to an SP is accompanied by a transfer of energy and results in a drop of the intensity of the reflected light wave. As the coupling occurs only within a narrow range of angles of incidence or wavelengths, the excitation of SP produces a narrow dip in the angular or wavelength

spectrum of the reflected light, seen in figure 1.10. [71] Based on these characteristics, the reflected light wave is measured by the SPR sensor. On the basis of which characteristic of the light wave modulated by a surface plasmon is measured, SPR sensors are classified as sensors with angular, wavelength, intensity, or phase modulation.[72]

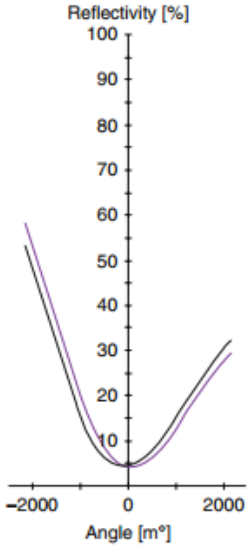


**Figure 1.10:** SPR signal. The SPR signal measured as a dip in intensity of reflected light. [71]

In SPR sensors with angular modulation, a monochromatic light wave is used to excite a surface plasmon. The strength of coupling between the incident wave and the surface plasmon is observed at multiple angles of incidence. The excitation of surface plasmons is observed as a dip in the angular spectrum of reflected light. The angle of incidence yielding the strongest coupling is measured and used as a sensor output. [66], [71]

In SPR sensors with wavelength modulation, a surface plasmon is excited by a light wave containing multiple wavelengths. The excitation of surface plasmons is observed as a dip in the wavelength spectrum of reflected light. The wavelength yielding the strongest coupling is measured and used as a sensor output. SPR sensors with intensity modulation are based on measuring the strength of the coupling between the light wave and the surface plasmon at a single angle of incidence and wavelength, and the intensity of light wave serves as a sensor output. [69], [71]

In SPR sensors with phase modulation the shift in phase of the light wave coupled to the surface plasmon is measured at a single angle of incidence and

wavelength and used a sensor output. Figure 1.11 shows a schematic overview of SPR biosensor principles of operation. [67], [71]

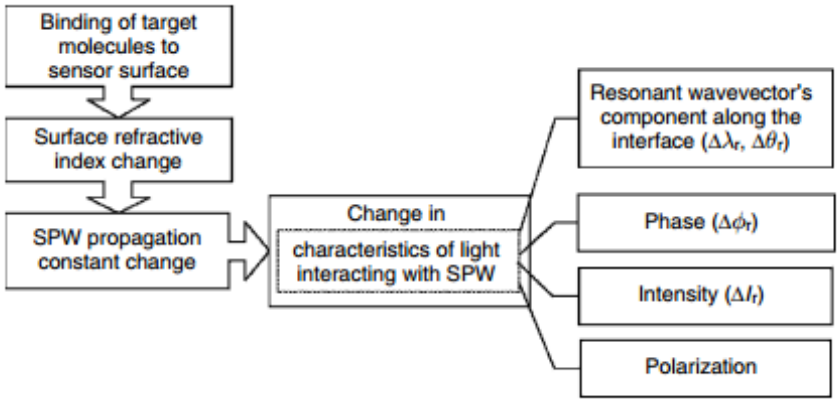


**Figure 1.11:** Schematic overview of operation of Surface plasmon resonance biosensor [66].

Surface plasmon resonance affinity biosensors use surface plasma waves to probe biomolecular interactions occurring at the surface of sensor. SPR sensor bind to the biorecognition elements, producing an increase in the refractive index at the sensor surface. The change in the refractive index produced by the capture of biomolecules depends on the concentration and properties of analyte molecules at the sensor surface. [71], [73] If the binding occurs within a thin layer at the sensor surface of thickness $h$, the sensor response is proportional to the binding-induced refractive index change, which can be expressed as:

$$\Delta n = (\frac{dn}{dc})\frac{\Gamma}{h} \tag{1.4}$$

where $(dn/dc)$ denotes the refractive index increment of the analyte molecules and $\Gamma$ denotes the surface concentration in mass/area. [72]

## Performance Characteristics

The most significant performance characteristics of SPR biosensor are sensitivity, resolution, accuracy, reproducibility and lowest detection limit. The sensitivity of an SPR affinity biosensor depends on two factors, the sensitivity to the change of the refractive index and efficiency of the conversion of the binding to a change in the refractive index. The sensitivity of sensor output depends on the method of excitation of surface plasmons.[66], [74]

In general, the sensitivity of the effective index of a surface plasmon to refractive index depends on the distribution of the refractive index change. There

are two cases in the distribution of the refractive index change, the change in the refractive index that occurs within the whole sample and the change in the refractive index that occurs only within a very short distance from the sensor surface. The surface refractive index sensitivity is proportional to the bulk refractive index sensitivity and the ratio of the thickness of the layer within which the surface refractive index change occurs and the penetration depth of the surface plasmon. As the penetration depth of a surface plasmon on gold increases with increasing wavelength, the surface refractive index sensitivity of the effective index decreases with the wavelength more quickly than the bulk refractive index sensitivity. [66], [74]

The sensor resolution describes the minimum change of the evaluated parameter which can be distinguished by the detector device. Systematic noise can disguise signal changes and is therefore important to keep to a minimum to obtain high resolution. Accuracy describes the degree to which a sensor output represents the true value of the measured parameter. Repeatability refers to the capacity of a sensor to reproduce output reading under the same measurement conditions over a short interval of time. The lowest detection limit describes the lowest concentration of analyte that can be measured by the sensor. [66], [74]

## Experimental Design

A typical SPR experiment involves a selection of a suitable sensor chip, ligand immobilization, recording the response to an analyte injection, surface regeneration and data analysis [75]. The example of a an experimental run in a form of sensorgram is depicted in figure 1.12. Carefully planned SPR experiments can provide information on binding rates of association and dissociation, strength of an interaction, as well as the overlapping sites of epitopes. [73]

## Sensor Chip

Sensorchip selection depends on the ligand that needs to be immobilized, the analyte that binds to the ligand and the purpose of the assay. A typical sensor chip is a glass chip coated with a thin layer of metal, usually gold and it can be fictionalized by an additional chemical coating. Ligands are attached to this coating via covalent or non-covalent bonds. The coating or immobilization matrix consists of a layer of hydrophilic polymers, such as dextran, carboxymethyl dextran, polyglycerol, polyethylene glycol among others, and it minimizes non-specific binding. [65], [76]

These hydrophilic polymers form highly flexible, non-cross-linked, brush-like structures. The three-dimensional nature of the hydrogels formed by these poly-

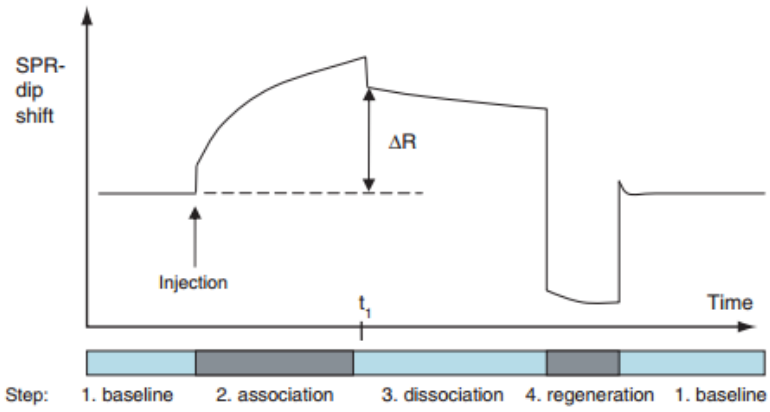


**Figure 1.12:** Typical sensorgram of a molecular interaction. The various phases of a SPR experiment are shown. [65]

mers offers large surface area, important for binding of small ligands. Planar immobilization matrices have a lower binding capacity and are suitable for studying interactions between proteins and other large molecules. Figure 1.13 shows a schematic representation of the ligand, immobilized in a hydrogel, capturing the analyte. [65], [76]

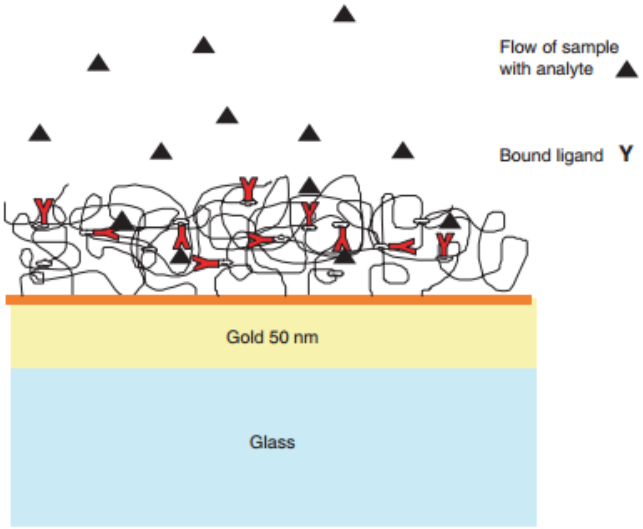


**Figure 1.13:** A schematic representation of the ligand, immobilized in a hydrogel, capturing the analyte. [65]

## Pre-concentration

Before ligand immobilization a pre-concentration step is performed. The purpose of pre-concentration is to concentrate the protein to very high levels thus driving the coupling reaction. Pre-concentration is driven by an electrostatic interactions between the negatively charged sensor chip matrix and positively charged protein. The protein is diluted into a buffer with a low ionic strength to minimize charge screening. Electrostatically bound protein should dissociate rapidly and completely when injection of running buffer resumes, because the proteins net positive charge will decrease and because electrostatic interactions will be screened by the high ionic strength of the running buffer. If protein fails to dissociate, it implies non-specific binding. [65], [75]

## Ligand Immobilization

Proteins are the most widely used immobilization partners in SPR-based assays. Immobilisation can either be direct, by covalent coupling, or indirect, through capture by a covalently coupled molecule. Indirect immobilisation can only be used for proteins that have a suitable binding sites or tag for the covalently coupled molecule. However, it is the method of choice in most cases. Proteins are rarely inactivated by indirect coupling, the crude protein samples can be used and all the molecules are immobilised in a known and consistent orientation. The major advantage of direct covalent immobilisation is that it can be used for any pure protein mixture. However, proteins couple heterogeneously and the binding of analyte can be decreased. [75], [77],[78]

All covalent coupling methods utilize free carboxymethyl groups on the sensor chip surface. The individual amino acids supply the functional moieties that can be utilized for immobilization to the sensor surface. There are three main types of functional groups, amine, thiol or aldehyde. Different physical properties related to charge balance and distribution, size, and thermodynamic stability make every protein unique with respect to immobilization conditions and success. Antibodies are the most homogeneous protein class and are also the most frequently used recognition elements for different types of applications. Antibodies, are among the easiest molecules to immobilize. The probability for immobilization via the Fc region is high thus the active antigen binding regions are exposed to interactions with an analyte. [65], [75], [78]

The immobilization via amine coupling follows protocol, seen in figure 1.14. Firstly, the carboxymethyl groups are activated with 1-Ethyl-3-(3-dimethyl- aminopropyl)carbodiimide (EDC) and N-hydroxysuccinimide (NHS), thus creating a highly reactive succinimide ester which reacts with amine and other nucleophilic groups on proteins. Then protein is injected and after the coupling reaction the

remaining activated carboxymethyl groups are deactivated by injecting very high concentrations of ethanolamine. The activity of the immobilized protein should be evaluated before proceeding to regeneration. [75], [79]

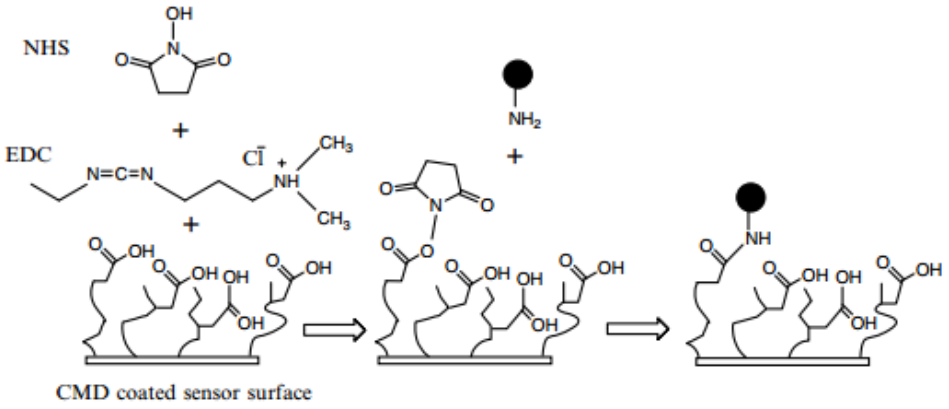


**Figure 1.14:** Covalent binding via amine coupling. EDC interacts with the carboxyl groups located on the surface, resulting in an unstable O-acyl isourea intermediate. Addition of NHS creaates a stable active ester, capable of substituting with the ligand. EDC is most reactive at pH 4 - 5, thus activation mixture contains 4-morpholine ethanesulfonic acid monohydrate (MES), which gives a pH value 4.5. [79]

## Regeneration

Optimal surface regeneration is identified empirically and can be difficult and time consuming. A good regeneration is very important for the stability and reproducibility of assay. In order to reuse the sensor chip surface the analyte must be removed without damaging the ligand. [80] However, some regeneration solutions can have undesired effects on the ligand. Not only regeneration solutions can cause loss of ligand function, they can cause non-specific binding, baseline drifting and changes to sensor chip matrix. Regeneration is affected not only by ligand or sensor chip but analyte concentration as well. Thus higher analyte concentration requires harsher regeneration conditions. [75], [80]

The most frequent regeneration method used, is the injection a low pH-buffer such as 10 mM Glycine pH 1.5 - 2.5. Most proteins become partly unfolded and positively charged at low pH thus the protein binding sites will repel each. Other procedures use high pH, high salt or specific chemicals to break the interactions. Also, a mixture of the different regeneration solutions can be used to target several binding forces simultaneously. [80]

The effect of the regeneration solution can be evaluated from:

$$R_{eff} = (\frac{R_A - R_{reg}}{R_A - R_0})100\% \tag{1.5}$$

where $R_{eff}$ is regeneration effect, $R_{reg}$ is the baseline response after regeneration injection, $R_0$ is the baseline response before analyte injection. [75]

## Data Processing

High quality data is needed to obtain relevant results. The quality of data is improved by optimizing experimental design. Data obtained from biosensors are usually affected by the position on the resonance unit scale, noise, non-specific responses and other artefacts that complicate presentation. Therefore raw data need to be processed to ensure their comparability. [73]

SPR-based biosensors have at least two flow-cells since one is used as a reference to subtract possible non-specific signal and correct for refractive index changes, injection noise and instrument drift. Several software packages are available for data analysis such as Scrubber or Tracedrawer. [81] The first step in data processing is to zero the response just before the analyte injection. This can be performed by subtracting an average of the response in a small interval just prior to the start of the injection. The second step is to align the responses so that all injections start at the same point. Then a double referencing is performed to improve the quality of the data. In the first step, signal collected from the reference flow-cell is subtracted and the second step is the subtraction of an average of the responses obtained for a set of buffer injections.[73] Lastly, global analysis of interaction data in order to extract accurate estimates of the binding constants is performed. Global analysis means that all the responses within a data set are fit simultaneously using the same set of rate constants. Global analysis of a wide range of analyte concentrations provides a method to discriminate between different reaction models. Figure 1.15 depicts processed and fitted SPR results of kinetic analysis. [73], [81]

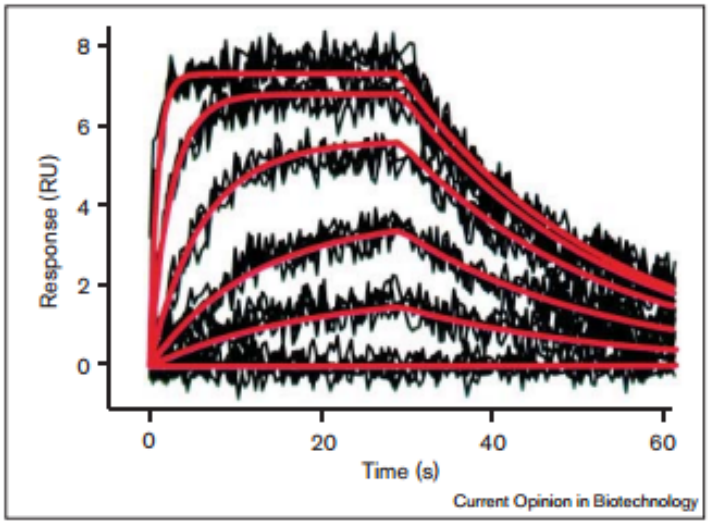


**Figure 1.15:** Proccessed and globally fitted kinetic data obtained by SPR [73].

## Kinetic analysis

To determine the kinetic constants of a label-free biomolecular interaction through SPR analysis, the sensorgram must be fitted to a kinetic model using a mathematical algorithm. There are several different binding models with which to perform the interaction analysis. However, it is recommended that SPR interactions be fitted to the simplest model possible. [75], [82]

The most commonly used binding model for SPR biosensors is the Langmuir model. It describes a 1:1 interaction in which one ligand molecule interacts with one analyte molecule. In theory, the formation of the ligand-analyte complex follows second-order kinetics. However, because the majority of SPR biosensors are fluidics-based and capable of maintaining a constant analyte concentration in a continuous liquid flow, complex formation actually follows pseudo–first-order kinetics. In addition, this model assumes that the binding reactions are equivalent and independent at all binding sites. It also assumes that the reaction rate is not limited by mass transport. Many interactions adhere to this model, in which the interaction is described as:

$$A + L \underset{k_d}{\overset{k_a}{\rightleftharpoons}} AL \tag{1.6}$$

where L represents the ligand, A is the analyte, the rate of complex formation is represented by the association constant $k_a$ and the rate of complex decay is represented by the dissociation constant $k_d$. [81], [83], [82]

Analysis of the sensorgram curve in the association phase, in which binding is measured while the analyte solution flows over the ligand surface, allows determination of the rate of complex formation:

$$\frac{d[AL]}{dt} = k_a[A][L] - k_d[AL] \tag{1.7}$$

where t is time and [AL], [A] and [L] are the concentrations of complex, analyte and ligand.[81]

In the dissociation phase, the analyte concentration is reduced to zero by the injection of running buffer. Thus the rate of complex dissociation is:

$$\frac{d[AL]}{dt} = -k_d[AL] \tag{1.8}$$

Since complex [AL] formation is directly proportional to a change in response $R_t$ and $R_{max}$ is equivalent to $[L]_{max}$, the equation 1.5 can be rewritten as:

$$\frac{dR_t}{dt} = k_a[A](R_{max} - R_t) - k_d R_t \tag{1.9}$$

After integration the equation is transformed into:

$$R_t = \frac{R_{max}[A]}{K_D + [A]}[1 - e^{-(k_a[A]+k_d)t}] \tag{1.10}$$

The change in the amount of complex formed or the change in response units over time is linearly related to $k_a$, $k_d$ and the analyte concentration. The equation describes the level of response at equilibrium and also the time taken to reach a certain response level during the association phase. [81]

The rate of complex dissociation follows exponential decay:

$$R_t = R_0 e^{-k_d t} \tag{1.11}$$

where $R_0$ is the response at the initiation of dissociation. This equation describes time taken to reach a certain response level during the dissociation phase. This equation is not applicable if dissociation is incomplete due to rebinding. [81]

A frequently occurring condition in kinetic SPR analysis is that the apparent association and dissociation rate of a molecular interaction does not correspond to the physical rates. In certain cases the on-rate is so high that diffusion of analyte from the bulk into the sensor matrix becomes rate limiting, and that, as a consequence, the concentration of analyte near the sensor matrix is lower than

in the bulk. [73], [83] For the dissociation phase a high on-rate implies that a dissociated analyte can rebind to an empty binding site, before it diffuses from the matrix environment. In such case, the observed dissociation rate is slower than the physical off-rate. To determine whether a particular interaction is limited by mass transport, injections of an analyte sample at different flow rates should be made. If the association curves are different, then this interaction is mass transport limited. In contrast, if the association curves are independent of the flow rate, then diffusion is not the rate-limiting factor. [84]

Also, there are four complex binding models for analysing non-Langmuir interactions like the heterogeneous analyte, heterogeneous ligand, two-state and bivalent analyte models. However, they are used only with biological justification and conclusions based on analyses with these complex models should be confirmed with additional experiments. [81], [82]

## Epitope Mapping

Epitope mapping on the biosensor can be used to characterize both antigens and monoclonal antibodies. Typical epitope mapping experiments on the biosensor involve immobilizing the primary antibody on the surface, then capturing the antigen and testing whether a secondary antibody is capable of binding to the antigen. Using this method it is possible to screen a variety of monoclonal antibodies specific to different epitopes presented on the antigen. [81]

# Chapter 2

# Materials and Methods

| Chemicals | Description | Supplied by |
|---|---|---|
| Acetic Acid | Lot: SZBF0220V | Sigma Aldrich |
| Disodium hydrogen phosphate dihydrate | Lot: 441 | Merck |
| Ethanol | Batch SE10012182 | Kemetyl |
| Ethanolamine | Batch 045K0644 | Sigma Aldrich |
| Glycerol | Lot: STBC1888V | Sigma Aldrich |
| Glycine | Lot: 0F008040 | Biochemica |
| Hydrochloride | Lot: SZBG2220 | Fluka |
| Immersion oil | WA18406 | SAFC |
| N-(3-Dimethylaminopropyl) N'-ethylcarbodiimide hydrochloride (EDC) | Lot: BCBN0730V | Fluka |
| N-hydroxysuccinimide (NHS) | Lot: BCBF6027V | Sigma Aldrich |
| Potassium chloride | Lot: 1121871 | Fluka |
| Potassium phosphate monobasic | Lot: SLBR1363V | Sigma Aldrich |
| Sodium chloride | - | - |
| Sodium dodecyl sulfate (SDS) | Lot: STBD6276V | Sigma Aldrich |
| Sodium hydroxide | Lot: SZBE2520V | Sigma Aldrich |
| Sodium tetraborate decahydrate | Lot: 1355809 | Fluka |
| 2-(N-Morpholino)ethanesulfonic acid (MES) monohydrate | Lot: 1275145 | Fluka |
| Triton X-100 | Lot: 023K0005 | Sigma Aldrich |

**Table 2.1:** A list of chemicals used for the experiments.

| Biological Samples | Description | Supplied by |
|---|---|---|
| **Monoclonal Antibodies** | | |
| NS1 DENV 2-3 (BBI5) | BM405-K9A1 Lot: 1017-201<br>1.78 mg/mL mouse mAb IgG<br>PBS pH 7.2 with 0.1% sodium azide | BBI Solutions |
| NS1 DENV 1-4 (Mer39) | C01839M Lot: 1A01217<br>1.88 mg/mL mouse mAb $IgG_1$<br>PBS pH 7.2 with 0.1% sodium azide | Meridian |
| NS1 DENV 1-4 (Mer39) | C01839M 1.56 mg/mL | BluSense Diagnostics |
| **Nanoparticles** | | |
| Mer39 conjugated | PCC-D-114-1 Mer39 10 mg/mL | BluSense Diagnostics |
| BBI5 conjugated | PCC-D-114-3 BBI5 10 mg/mL | BluSense Diagnostics |
| **Antigens** | | |
| Recombinant DENV 2 NS1 | 5 mg/mL | BluSense Diagnostics |
| Recombinant DENV 2 NS1 | Batch 161220 0.46 mg/mL in PBS | BIO-RAD |

**Table 2.2:** A list of all monoclonal antibodies, nanoparticle samples and antigens used for the experiments.

| Equipment | Description | Supplied by |
|---|---|---|
| SPR Spectrophotometer | SR75000C | Reichert |
| Autosampler | SR8100 | Reichert |
| Diverter Valve | SR8600 | Reichert |
| Pump | SR8500 | Reichert |
| Screw cap and clear vial kit | Lot: 000016299 | Agilent |
| 400 µL flat bottom glass insert | Lot: 3377662800 | Agilent |
| Sensor chip HC 1000 m | Lot: SC HC1000m1114.a | Xantec |
| Sensor chip HC 200 m | Lot: SC HC200M0217.a | Xantec |
| Sensor chip CMD 50 m | Lot: SC CMD50M0416 and m0914.a | Xantec |
| Bottle filter top | Lot: 20030488 250 mL 0.2 µm PES | TPP |

**Table 2.3:** A list of equipment used for the experiments.

## 2.1 Materials

The following sections will present an overview of all the solutions and experimental protocols used during this study.

### Running Buffer

Phosphate-buffered saline (PBS) solution with no additives was used as as a running buffer. Several batches of 500 mL PBS was made by dissolving 8 g/L sodium chloride, 0.2 g/L potassium chloride, 1.44 g/L disodium hydrogen phosphate dihydrate and 0.24 g/L dihydrogen potassium phosphate monobasic in Milli-Q water. Hydrochloric acid was used to adjust the pH of resulting solution to 7.4. Lastly, the buffer was degassed. Additionally, PBS buffer used to prepare protein samples was filtered through 0.2 µm sterile syringe filters.

### Rinsing Solutions

The 0.5% sodium dodecyl sulphate (SDS) rinsing solution was made by dissolving 25 mg SDS in Milli-Q water to a total volume of 5 mL.

The 50 mM glycine rinsing solution was made by dissolving 37 mg glycine in Milli-Q water to a total volume of 10 mL. Sodium hydroxide was used to adjust the pH of resulting solution to 9.5. Lastly, it was filtrated through 0.2 µm sterile syringe filter.

The elution buffer was prepared by dissolving 5.84 g sodium chloride and 3.81 g disodium tetraborate decahydrate in 100 mL Milli-Q water. The resulting concentrations were 1 M and 0.1 M. The pH of the elution buffer was adjusted to 9.0 using hydrochloric acid. Before application, precipitates were dissolved by stirring and heating.

### Coupling Solution

Coupling buffers were made by mixing 14.37 µL acetic acid with Milli-Q water to a total volume of 50 mL, achieving concentration of 5 mM. The pH of resulting solution was adjusted to 4.5 with sodium hydroxide. Coupling buffers were prepared freshly for every experimental run. Additionally, coupling buffer solutions were filtered through 0.2 µm sterile syringe filters.

### Activation Solution

The activation solution was prepared by dissolving 173 mg N-hydroxysuccinimide (NHS) and 160 mg 4-morpholine ethanesulfonic acid monohydrate (MES) in 15 mL Milli-Q water, achieving concentrations of 100 mM and 50 mM. The pH of the

solution was adjusted to 5.0 with sodium hydroxide. Then the resulting solution was separated into 1.5 mL aliquots and stored at -20 °C. Immediately before use, 14 mg N'(3-dimethylaminopropyl)N-ethylcarbodiimide hydrochloride (EDC) was added to a defrosted aliquot, obtaining a concentration of 50 mM EDC.

### Quenching Solution

1 M ethanolamine was used as a quenching solution. It was made by mixing 3.07 mL ethanolamine with Milli-Q water to a total volume of 50 mL. Hydrochloric acid was used to adjust the pH to 8.5.

### Antibody Solutions

Mer 39 antibody samples were prepared from different stock solutions, first 10.4 µM and second 12.57 µM. 400 nM antibody solutions for pre-concentration and antibody immobilization were made by using coupling buffer pH 4.5 and 38.46 µL of first stock or 31.82 µL of second stock per 1 mL. 400 nM BBI5 antibody samples were made from 11.87 µM stock by adding 33.69 µL to coupling buffer pH 4.5 up to 1 mL.

The Mer 39 antibody samples for sandwich assays were made in concentrations 40, 20, 10 and 5 nM for kinetic analysis and 40 nM to test binding. The 40 nM BBI5 antibody samples were made only to test the binding capacity. The samples were prepared in filtered PBS buffer.

To test the nanoparticle conjugated antibody binding, a 0.6 µL nanoparticle sample, conjugated to Mer 39 or BBI5, was added to 420 µL PBS.

### Antigen Solutions

Two NS1 stock solutions, 108.7 µM and 10 µM, were used. Antigen solutions were added to filtered PBS to prepare the injection samples. The first stock was used to prepare 360, 272, 136, 68, 34, 17 and 8.5 nM solutions by diluting the 360 nM sample. Also, concentrations 100, 50, 25 and 12.5 were prepared the same way. The second stock solution was used to prepare 160, 80, 40, 20, 10 and 5 nM samples individually or once using previous sample as stock. 420 µL insert vials were used to minimize the waste.

### Regeneration Solutions

Glycine-hydrochloride solutions with added glycerol were used for regeneration. The solutions were made by adding 15 mg of glycine and 2.00 mL of glycerol into Milli-Q water to a total volume of 20 mL, resulting in 10 mM and 10%

concentrations. Hydrochloric acid was used to adjust the pH to either 2.0 or 2.2. Additionally, these solutions were filtered through sterile syringe filters.

The hydrochloride regeneration solution was prepared by mixing hydrochloric acid with Milli-Q water, achieving a concentration of 15 mM. Also, the solution was sterile filtrated.

0.5% SDS 15 mM HCl regeneration solution was prepared by adding 25 mg SDS into 15 mM HCl solution to a total volume of 5 mL.

2 M NaCl 15 mM HCl regeneration solution was prepared by adding 0.58 g NaCl into 15 mM HCl solution to a total volume of 5 mL.

## 2.2 Methods

### Sensor Chip Installation and Rinsing

In order to install a new sensor chip the sapphire prism surface was cleaned with an ethanol-soaked cleaning lens tissue. A small droplet of immersion oil was added onto the clean prism surface. Then the defrosted sensor chips either CMD 50 m, HC 200 m or HC1000m were placed and the flow cell mounted. The sensor chips used and a brief description are presented in table 2.1. The installed sensor chip was was rinsed with Milli-Q water at a flow rate 50 µL/min until baselines stabilized. Then the sensor chip and flow system were rinsed with SDS and glycine rinsing solutions, followed by the use of elution buffer. Afterwards, the flow rate was set to 20 µL/min and the system was left to equilibrate. The rinsing procedure can be seen in table 2.2.

| Sensor Chip | Description |
|---|---|
| HC1000 m | Polycarboxylate 1000 nm hydrogel coating, medium charge and surface density |
| HC 200 m | Polycarboxylate 200 nm hydrogel coating, medium charge and surface density |
| CMD50 m | Carboxymethyldextran 50 nm hydrogel coating, medium density |

**Table 2.4:** A list and descriptions of sensor chips used.

| Rinsing Protocol | |
|---|---|
| 1. Infuse flow rate 50 µL/min | 7. 4 min injection of glycine rinsing solution |
| 2. Pump Refill | 8. 1 min dissociation |
| 3. 5 min injection of SDS rinsing solution | 9. 4 min injection of glycine rinsing solution |
| 4. 1 min dissociation | 10. 2 min dissociation |
| 5. 4 min injection of glycine rinsing solution | 11. 3 min injection of elution buffer |
| 6. 1 min dissociation | |

**Table 2.5:** An overview of rinsing protocol.

### Antibody Immobilization

Prior to immobilization a pre-concentration test was performed under set conditions, antibody concentration 400 nM and coupling buffer pH 4.5. In order to immobilize the antibodies, sensor chip surface was activated using the solution containing EDC and NHS. The injection of activation solution was followed by an injection of coupling buffer. The diverter valve was activated so that flow only occurred in the left channel and double injections of 400 nM and 150 nM antibody samples were made. 45 minutes after, the diverter valve was deactivated and quenching solution was injected three times to deactivate any remaining active groups. A protocol of the immobilization process is shown in table 2.3. Before further experiments, running buffer was exchanged from water to PBS.

| Antibody Immobilization | |
|---|---|
| 1. Infuse Flow Rate 20 uL/min | 9. Pump Refill |
| 2. Pump Refill | 10. Diverter Valve Deactivated |
| 3. 10 min Injection of Activation Solution | 11. 5 min Injection of Quenching Solution |
| 4. 2 min Injection of Coupling buffer | 12. 5 min Injection of Quenching Solution |
| 5. Diverter Valve Activated | 13. 5 min Injection of Quenching Solution |
| 6. 10 min Injection of Antibody Solution | 14. 5 min Dissociation |
| 7. 10 min Injection of Antibody Solution | 15. 5 min Wait |
| 8. 45 min Wait | |

**Table 2.6:** An overview of a protocol used to immobilize antibodies.

### Data Collection

Measurements for kinetic analysis on directly immobilized antibody were performed, at 25 °C at flow rate 25 µL/min, by injecting a selected concentration of NS1 solution for 10 minutes followed by 10 minutes of dissociation. Afterwards, the regeneration solution was injected for 15 to 30 seconds followed by 5 minute dissociation period. If regeneration was insufficient, an additional injection was

made. The kinetic analysis of sandwich antibody or antibody-nanoparticle complex were performed by, firstly, injecting antigen solution for 10 minutes, followed by 10 minutes dissociation and 10 minute injection of relevant sample. After 10 minutes dissociation, a regeneration solution was injected for 30 seconds.

### Data Processing

The relevant data was transferred to a TraceDrawer, a data fitting software, for editing. Firstly, the baseline difference between injections were zeroed and starting points of injections were aligned. Then the reference channel and blank responses were subtracted for double referencing. The treated data was then kinetically evaluated by defining the start of association and dissociation phases and model-fitting data. The parameters of fit were global $B_{max}$, $k_a$, $k_d$ and constant BI. A models evaluated were one to one and one to one with depletion corrected. For sandwich analysis the $B_{max}$ was set to local to account for varying antigen response levels.

# Chapter 3

# Results

The results are divided into four sections, sensor chip installation and rinsing, immobilization, binding and regeneration and kinetic analysis. Each section describes comparable results combined from all experimental runs. One experimental run corresponds to a complete set of experiments performed on one sensor chip. All runs have assigned numbers, which will be used to describe and discuss the results. An overview of the type of data obtained during the runs, and, additionally, a type of sensor chip used, is presented in table 3.1.

The aims of this study were to characterize the kinetics of recombinant dengue virus type 2 NS1 antigen and the overlapping of its epitopes in relation to a pair of monoclonal antibodies BBI5 and Mer39 using surface plasmon resonance. Additionally, the binding of free and nanoparticle conjugated BBI5 and Mer 39 was evaluated by performing a sandwich analysis.

| **Run No.** | **Type of Sensor Chip** | **Type of Analysis** |
|---|---|---|
| Run 1 | HC1000 m | NS1 kinetics and regeneration |
| Run 2 | CMD50 m | NS1 kinetics |
| Run 3 | CMD50 m | Ab-NP binding and regeneration |
| Run 4 | CMD50 m | Regeneration |
| Run 5 | CMD50 m | NS1 kinetics and Ab binding |
| Run 6 | HC 200 m | NS1 kinetics and Ab binding |
| Run 7 | HC 200 m | NS1, Mer 39 kinetics and Ab, Ab-NP binding |
| Run 8 | CMD50 m | NS1, Mer 39 kinetics and Ab, Ab-NP binding |
| Run 9 | CMD50 m | Ab, Ab-NP binding |

**Table 3.1:** An overview of sensor chips used and the type of results obtained on a particular set of experiments. Ab stands for antibody and Ab-NP for antibody-nanoparticle complex.

## 3.1 Sensor Chip Installation and Rinsing

The sensor chips installed were either HC 1000, HC 200 or CMD 50. The appearance of signal validated installations as correct. After the signal equilibrated, the rinsing procedure was performed and a stable baseline was obtained. The procedure is described in previous chapter. A typical sensorgram of the rinsing step is depicted in figure 3.1.

In addition, the baselines before and after rinsing procedure are displayed in table 3.2. A variation in baseline signals was observed between different and same type of sensor chips. Rinsing procedure, generally, reduced the baselines, with exception to sensor chips CMD 50 and HC 200 from the runs 4 and 7.

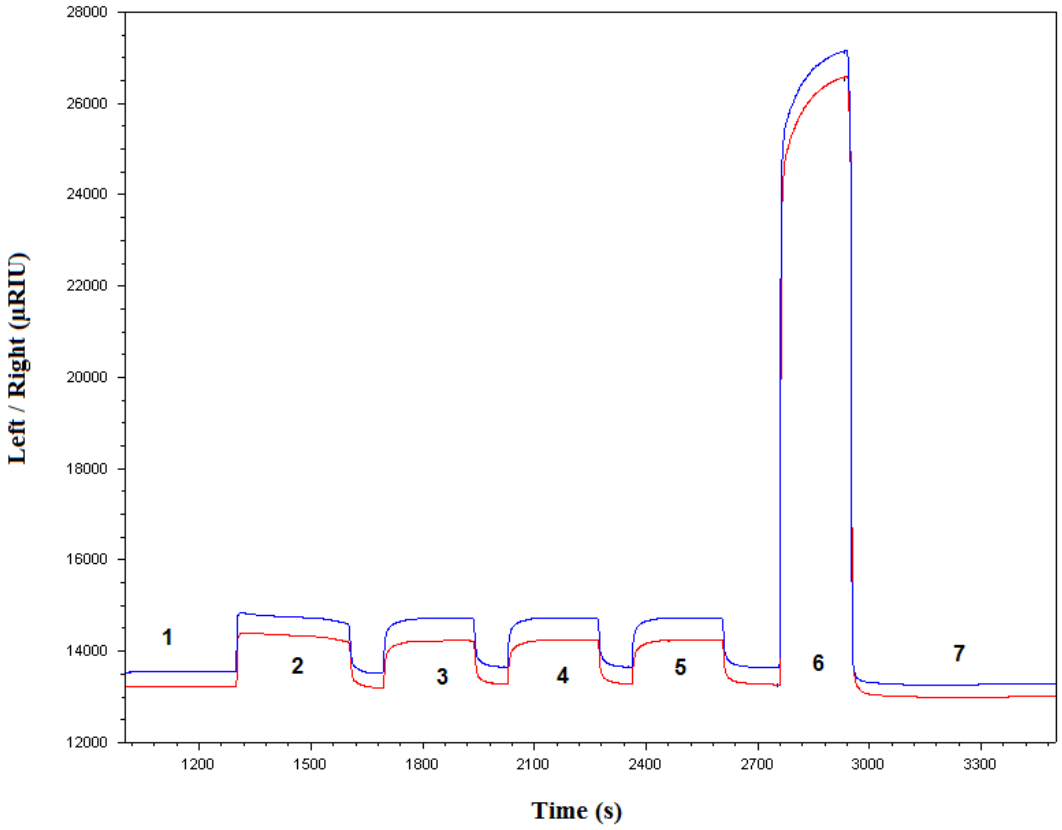


**Figure 3.1:** A typical sensorgram of the rinsing step. 1 - baseline before rinsing; 2 - injection of SDS rinsing solution; 3, 4, 5 - injections of glycine rinsing solution; 6- injection of elution buffer; 7 - baseline after rinsing. Blue and red represent the signals of working and reference channels. This sensorgram was obtained during the second experimental run.

| Run No. | Sensor Chip | Baseline 1 (µRIU) (L:R) | Baseline 2 (µRIU) (L:R) |
|---|---|---|---|
| Run 1 | HC1000 m | 16404 : 15902 | 15616 : 14911 |
| Run 2 | CMD50 m | 15362 : 12685 | 15300 : 12557 |
| Run 3 | CMD50 m | 13530 : 13224 | 13268 : 13011 |
| Run 4 | CMD50 m | 12388 : 12221 | 12465 : 12260 |
| Run 5 | CMD50 m | 12822 : 12517 | 12679 : 12424 |
| Run 6 | HC 200 m | 13254 : 13031 | 12988 : 12748 |
| Run 7 | HC 200 m | 13058 : 12684 | 13036 : 12783 |
| Run 8 | CMD50 m | 12872 : 12549 | 12668 : 12429 |
| Run 9 | CMD50 m | 12799 : 12493 | 12699 : 12434 |

**Table 3.2:** Baseline before (1) and after (2) rinsing newly inserted sensor chip. L - left channel and R - right channel, µRIU - response units.

## 3.2 Antibody Immobilization

Firstly, a pre-concentration test was performed to concentrate the antibodies on a sensor chip surface. The test was not conducted during the run 3, because the remaining supply of antibody was saved for immobilization. The concentration of antibodies used for all pre-concentration tests were 400 nM. Also, the tests were performed using a coupling buffer with a set condition of pH 4.5.

High pre-concentration responses were observed for all the sensor chips. Two different pre-concentration profiles were noted. Firstly, the injected antibodies dissociated from the surface before or after injection of elution buffer was made. Secondly, the pre-concentration response intensity when compared to immobilization varied in different runs. Even though the concentration of antibodies used for immobilization was the same, 400 nM, the pre-concentration responses were either lower or higher.

The higher pre-concentration responses were noted to correspond to HC sensor chips. The reason for this was thought to be higher surface charge density compared to CMD. Moreover, the surface activation step might have reduced the density of negative charges on HC sensor chips, resulting in lower immobilization response. The dissociation of pre-concentration sample before injection of elution buffer was observed only for sensor chips CMD 50 with immobilized Mer 39. The overview of pre-concentration profiles for all the runs is presented in table 3.3.

Two different antibodies, Mer39 and BBI5, were immobilized. The Xantec immobilization protocol was used and it was consistent through all the runs, except run 3. Run 3 due to the ending supply of antibody, resulted in lower concentration and, as mentioned above, absence of pre-concentration test. Additionally, Mer 39 conjugated nanoparticles were immobilized on top of the pre-existing layer of Mer 39. However, this immobilization will be described in next section. A typical immobilization sensorgram can be seen in figure 3.2.

| Run No. | Type of Sensor Chip | Dissociation Profile | Response Profile |
|---|---|---|---|
| Run 1 | HC 1000 m | Did not dissociate | Higher |
| Run 2 | CMD 50 m | Did not dissociate | Lower |
| Run 3 | CMD 50 m | - | - |
| Run 4 | CMD 50 m | Dissociated | Lower |
| Run 5 | CMD 50 m | Dissociated | Lower |
| Run 6 | HC 200 m | Did not dissociate | Higher |
| Run 7 | HC 200 m | Did not dissociate | Higher |
| Run 8 | CMD 50 m | Did not dissociate | Lower |
| Run 9 | CMD 50 m | Partly Dissociated | Lower |

**Table 3.3:** Different pre-concentration profiles: Dissociation occured before or after elution buffer was injected; Pre-concentration signal levels compared to immobilization signal.

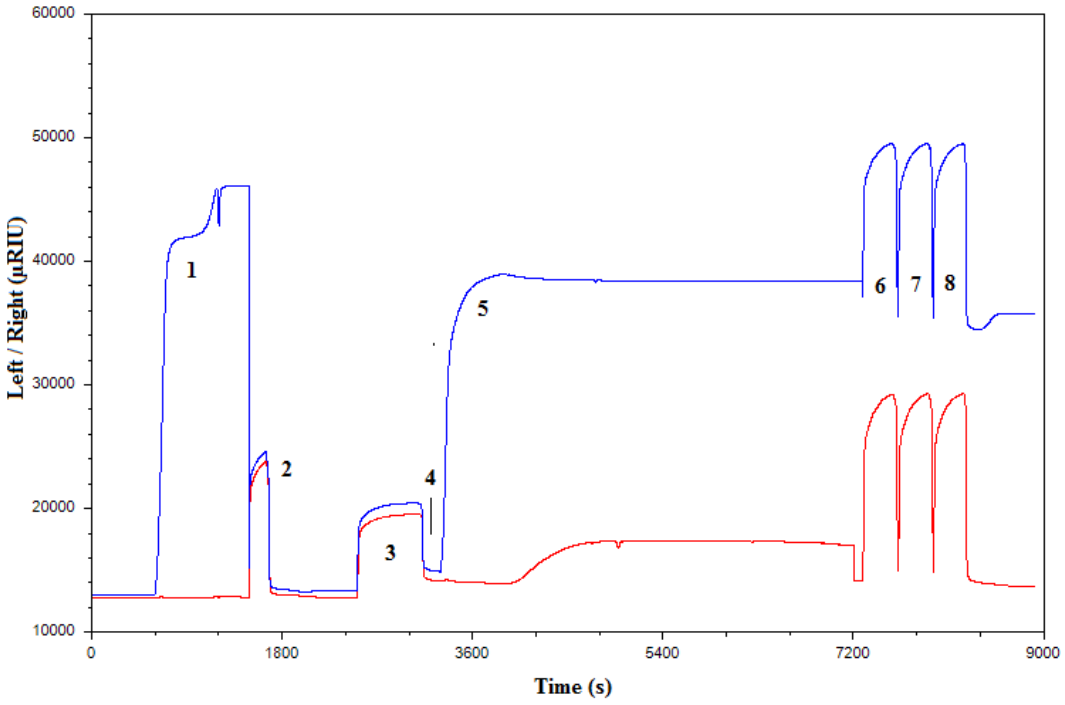


**Figure 3.2:** A typical immobilization sensorgram, illustrating immobilization procedure identical to all the runs. This sensorgram was obtained from run 8 and has a pre-concentration profile with higher response and no dissociation. A sensorgram depicting different pre-concentration profile is presented in appendix. Different numbers represent injections of 1 - antibody sample, 2 - elution buffer, 3 - activation solution, 4- coupling buffer, 5 - antibody sample and 6, 7, 8 - quenching solution. The baseline increase in reference channel (red) is attributed to drifting and is not considered relevant since the baseline decreased with quenching.

An overview of a type of sensor chip, the name of an antibody and its concentration, the difference between baselines before and after activation, baselines after activation solution and after quenching injections and immobilization yields are displayed in table 3.4. CMD 50 sensor chips did not give consistent immobilization yields. Also, the level of increase in signal, after activation solution was injected, did not account for the differing yields. However, Run 2 and 3 were performed on older sensor chips while runs 4, 5, 6, 9 were conducted with fresh supply. Moreover, different supply of antibodies were used for run 2, 3 and runs 4, 5, 9.

| Run No. | Sensor Chip | Antibody | Concentration(nM) | Activation response(µRIU) | Baseline 1 (µRIU)(L:R) | Baseline 2 (µRIU)(L:R) | Yield(µRIU) |
|---|---|---|---|---|---|---|---|
| Run 1 | HC 1000 m | Mer39 | 400 | 1661 | 16918 : 16111 | 46715 : 15174 | 29797 |
| Run 2 | CMD 50 m | Mer39 | 400 | 601 | 15338 : 12529 | 20775 : 12804 | 5437 |
| Run 3 | CMD 50 m | Mer39 | 250 | 849 | 13254 : 13006 | 18309 : 13098 | 5055 |
| Run 4 | CMD 50 m | Mer39 | 400 | 954 | 12498 : 12234 | 22288 : 12862 | 9790 |
| Run 5 | CMD 50 m | Mer39 | 400 | 728 | 12797 : 12469 | 26178 : 12998 | 13381 |
| Run 6 | HC 200 m | Mer39 | 400 | 1591 | 13250 : 12702 | 35682 : 13652 | 22432 |
| Run 7 | HC 200 m | BBI5 | 400 | 1485 | 13216 : 12768 | 34595 : 13384 | 21379 |
| Run 8 | CMD 50 m | BBI5 | 400 | 736 | 12743 : 12408 | 19791 : 13038 | 7048 |
| Run 9 | CMD 50 m | Mer39 | 400 | 717 | 13536 : 13073 | 26033 : 13103 | 12497 |

**Table 3.4:** An overview of immobilization data. Baseline before (1) and after (2) immobilization. L - left channel and R - right channel.

## 3.3 Binding and Regeneration

This section describes results obtained and observations made from all the experimental runs in chronological order. The kinetic results will be presented in the next section.

### Run 1 and 2

During the first experimental run, sensor chip HC 1000 and immobilized Mer 39, NS1 antigen injections were made, in concentrations 360, 272, 136, 68, 34, 17 and 8.5 nM to select regeneration conditions and to estimate kinetic constants. A 10 mM glycine and 10 % glycerol solution pH 2 was initially tested for two 360 nM antigen injections. The regeneration time selected was 30 s and two repeated injections had to be made to better recover the baseline. The regeneration effectiveness was calculated to be 83 % and 80 % and was assumed insufficient. Thus a 15 mM hydrochloric acid solution was tested and used during this and some other experimental runs. The regeneration effectiveness for remaining NS1 concentrations are presented in table 3.5.

Regeneration effect on the baseline increased with the decrease in concentrations. However, the effectiveness of regeneration of two last injections were inconsistent with the downward trend. After multiple subsequent regenerations, the

baseline only increased. The reference channel signal showed the upward trend as well, presented in appendix. Thus hydrochloric acid had an effect on the sensor chip's matrix. The drift in working channel baseline is depicted in figure 3.3.

| **Run No.** | **272 nM (2)** | **136nM** | **68 nM** | **34 nM** | **17 nM** | **8.5 nM** |
|---|---|---|---|---|---|---|
| Run 1 | 97 %; 104 % | 115 % | 116 % | 142 % | 113 % | 61 % |
| **Nr.** | **100 nM (2)** | **50 nM (2)** | **25 nM (2)** | **12.5 nM (2)** | **-** | **-** |
| Run 2 | 97 %; 96 % | 119 %; 132 % | 174 %; 156 % | 231 %; 184 % | - | - |

**Table 3.5:** Regeneration effectiveness obtained using 15 mM HCl as a regeneration solution for antigen concentrations 272, 136, 68, 34, 17 and 8.5 nM on sensor chip HC 1000 with immobilized Mer 39. The table also presents regeneration effectiveness from run 2 using sensor chip CMD 50. The same regeneration solution was used for second run. However, antigen concentrations and regeneration time, 20 s, were different. (2) - indicates the number of antigen injections.

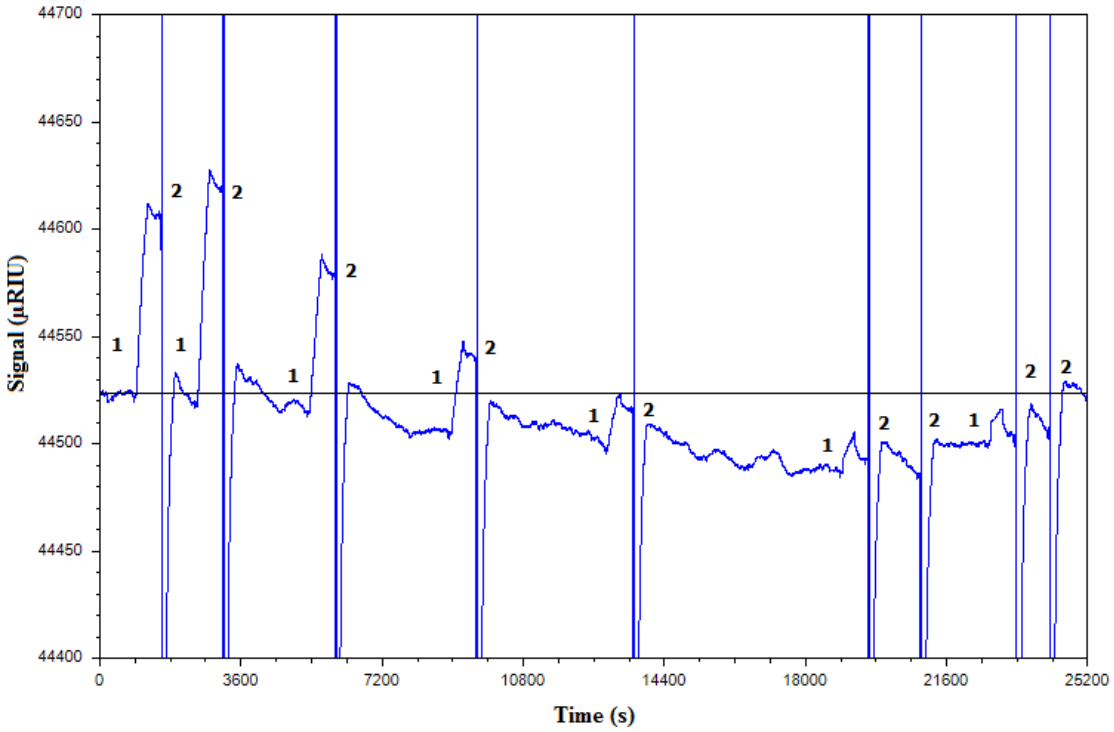


**Figure 3.3:** 15 mM HCl regeneration effects on the working channel baseline. 1 - injection, 2 - regeneration.

After processing data from run 1 NS1 injections, the loss in response was noted. Figure 3.4 shows the difference between a response from freshly prepared 360 nM NS1 sample and few hours old 262 nM sample.

During the second run with immobilized Mer 39 NS1 antigen injections were made in duplicates and in concentrations 100, 50, 25 and 12.5 nM in this exact

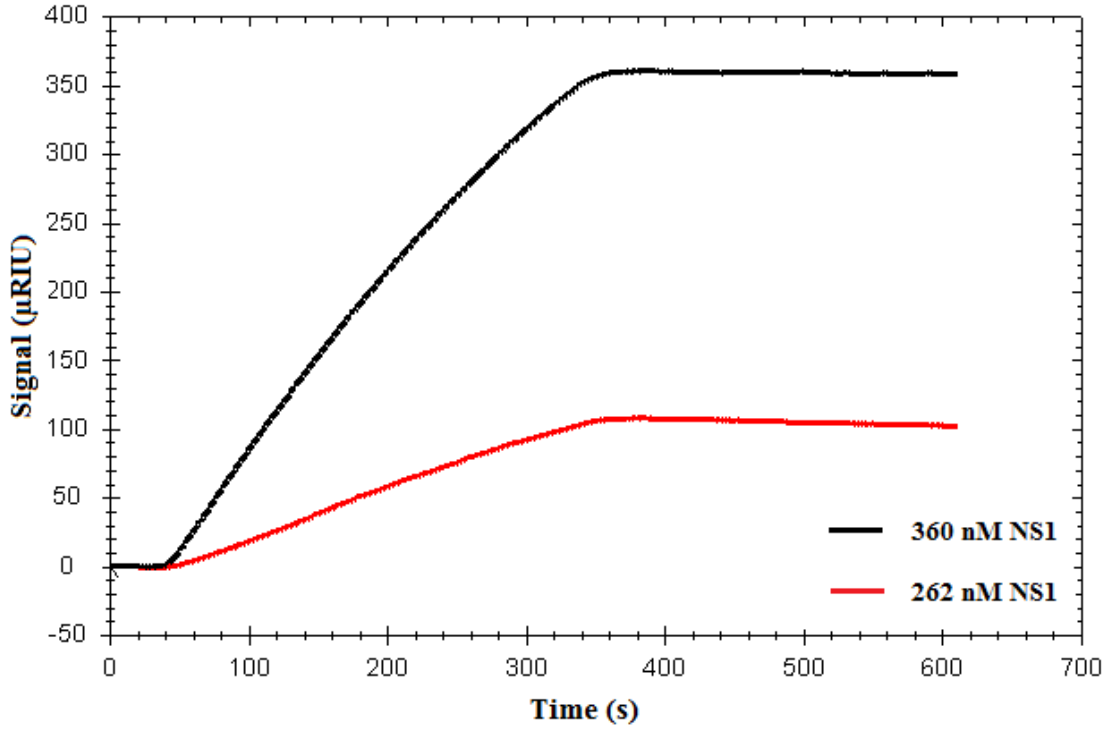


**Figure 3.4:** The difference between a response from freshly prepared 360 nM NS1 sample (black) and few hours old 262 nM sample (red. The data was obtained during run 1 with HC 1000 sensor chip and immobilized Mer 39.

order. The sensor chip selected CMD 50 was intended to better suit the purpose of performing kinetic analysis. The regeneration conditions were changed by reducing injection time to 20 s, in order to reduce the downward/upward drifting trend. Table 3.3 displays regeneration effectiveness during run 2. Even though, the regeneration time was reduced, the baseline drift remained.

### Run 3

Run 3 was performed for the purpose of testing nanoparticle conjugated antibodies in a sandwich assay. The sensor chip used and antibody immobilized were CMD 50 and Mer 39. The first injection of 100 nM antigen sample gave rise to uncharacteristically high non-specific response, 1346 µRIU and 1222 µRIU for working and reference channels. Also, the injected NS1 completely dissociated. The subsequent injection of nanoparticle conjugated BBI5 responded the same,with high 1096 µRIU and 1035 µRIU respnses for working and reference channels and dissociation. The regeneration with 15 mM HCl gave large increase in both baselines. The increase could at least partly be attributed to baselines be-

ing not fully equilibrated. However, HCl regeneration solution did cause upward drift in previous experiment 1.

The next antigen and BBI5-NP injections showed significantly lower responses in both channels, 228 µRIU and 151 µRIU for NS1 and 152 µRIU and 100 µRIU for BBI5-NP. Thus the intensity of the first responses and even dissociation of antigen may be attributed to the presence of non-covalently bound antibody, since regeneration was not yet performed. Second regeneration with hydrochloric acid increased the baseline again. Figure 3.5 illustrates the described injections.

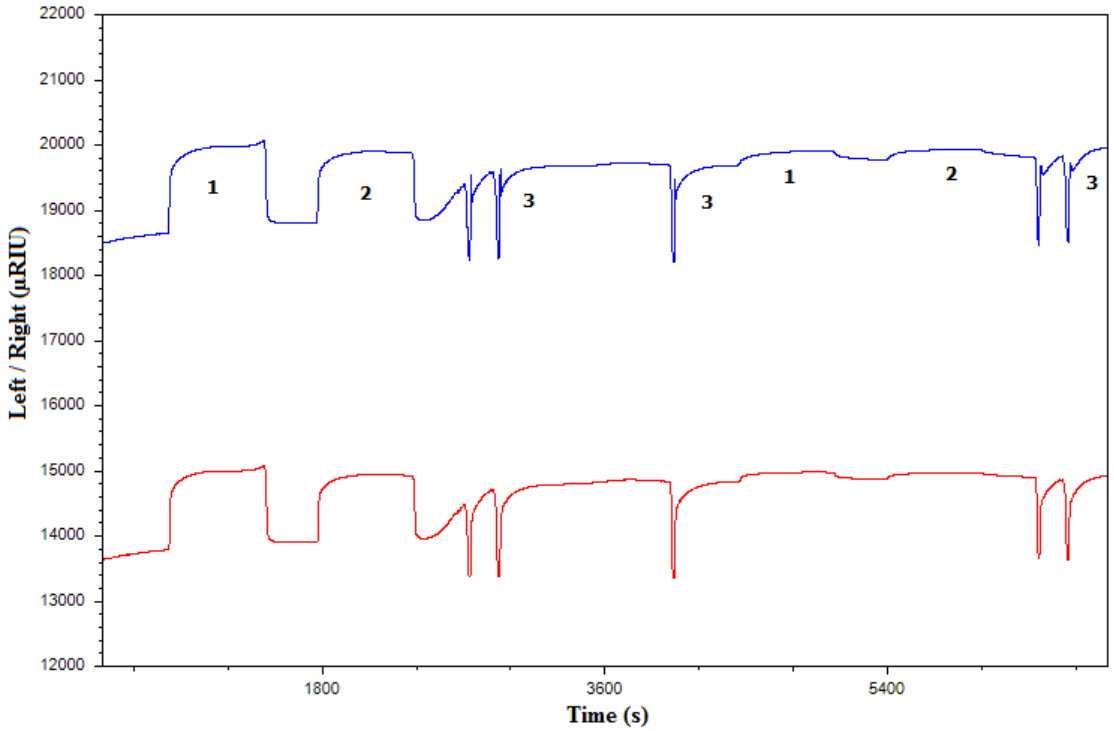


**Figure 3.5:** Subsequent injections of 100 nM NS1 and BBI5-NPs, followed by regeneration with 15 mM HCl. 1 - injection of antigen, 2 - injection of BBI5-NPs and 3 - regeneration. Red signal corresponds to reference channel and blue to a working channel. The experiment was performed on sensor chip CMD 50 with immobilized 250 nM Mer 39.

Upon subtraction of reference channel the second injection of 100 nM antigen gave a response of 50 µRIU, while BBI5-NPs completely dissociated. The third injection of antigen gave a 151 µRIU response and 35 % regeneration after two injections. Then 15 nM HCl 2 M NaCl regeneration solution was tested and the effectiveness of two 30 s injections was found to be 93 %.

The following two antigen injections gave high non-specific signal again, 306 µRIU and 124 µRIU for first and 420 µRIU and 144 µRIU for second injections. Moreover, antigen completely dissociated again. Nevertheless, Mer39-NPs were in-

jected after antigen and showed binding, seen in figure 3.6. Regeneration, achieved with multiple injections of 15 nM HCl 2 M NaCl, recovered 77 % of previous baseline.

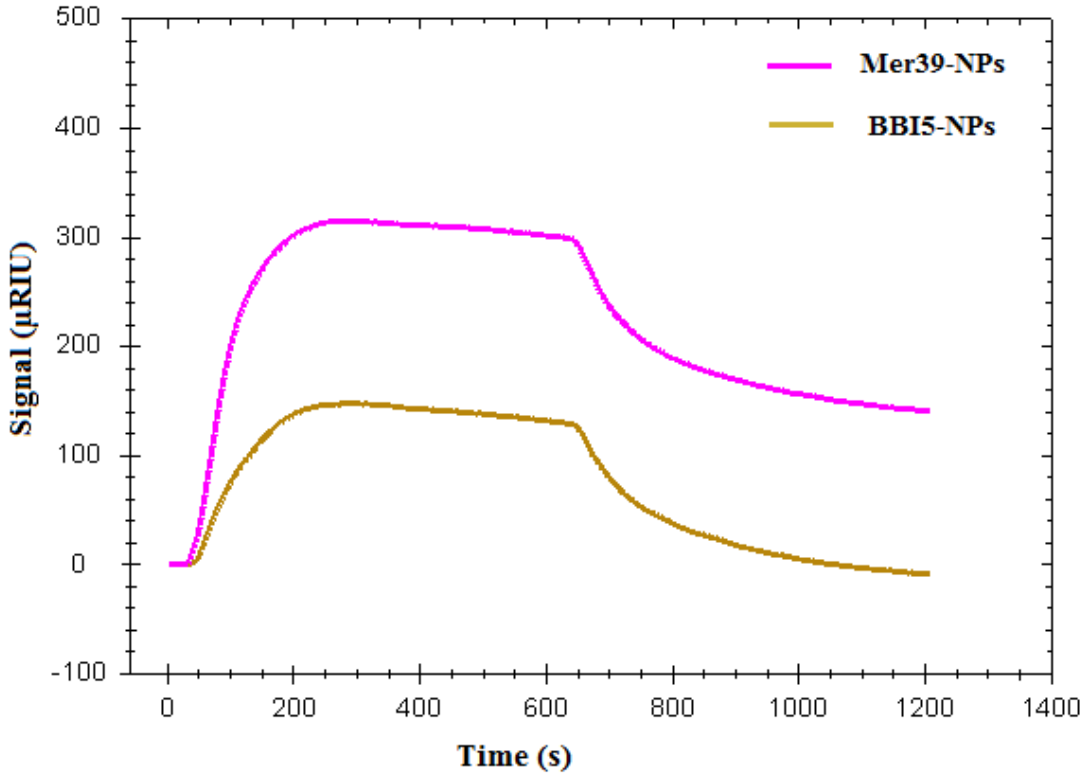


**Figure 3.6:** The binding curves of BBI5-NPs (brown) and Mer39-NPs (pink) obtained during run 3, sensor chip CMD with 250 nM Mer 39. The concentration of antigen was 100 nM for both injections of nanoparticle samples.

The next 100 nM injection of antigen did not dissociate and gave response of 230 µRIU after subtraction of reference signal. This pattern of changing signal intensity of 100 nM antigen injections could partly be attributed to the need to often prepare new samples, thus introducing significant systematic error and reducing the quality of data. However, the inconsistencies are too great to be only related to antigen. No binding was observed between immobilized Mer39-NS1 complex and BBI5 conjugated nanoparticles, seen in figure 3.6. The effectiveness of regeneration was 32 % and 15 nM HCl 2 M NaCl solution was estimated as ineffective.

### Run 4

New stock solutions of antibodies and antigen were used during run 4 and all the following experiments. The activity of immobilized Mer 39 was tested with 10 nM NS1 sample, which gave 125 µRIU signal before and 110 µRIU after regeneration with 15 nM hydrochloric acid.

All previously used regeneration solutions were retested and a new regeneration with 15 mM HCl 0.1% SDS solution was attempted. SDS solution was tested because detergent molecules can break active NS1 hexamer into dimers. The effectiveness of each regeneration solution is presented in table 3.6. All four regeneration solutions after first injection decreased the baseline dramatically. Upon second try, hydrochloric acid increased the baseline by 17% instead of recovering it and SDS solution regenerated only 6%.

Additionally, regeneration with SDS decreased the signal intensity of injected antigen which was partly recovered after using different method, seen in figure 3.7. However, it negatively affected the activity of immobilized antibody Mer 39.

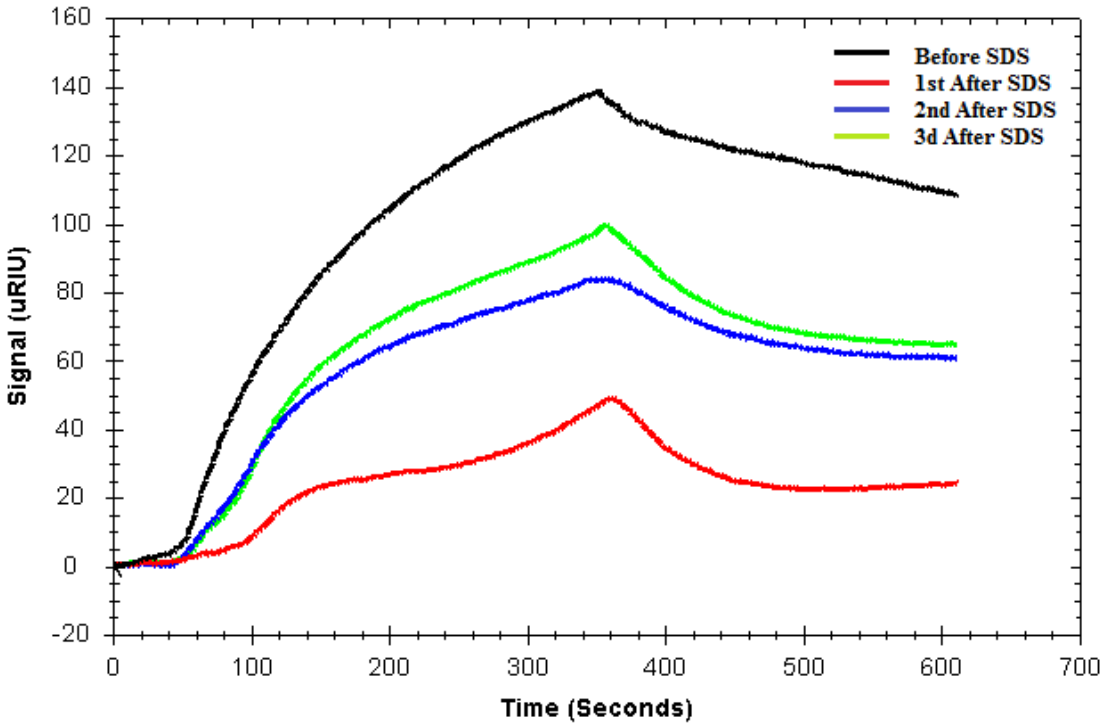


**Figure 3.7:** 10 nM NS1 signal intensity before (black) and after (red) recovering baseline with 15 mM HCl 0.1% SDS. The blue and green curves represent the recovered signal to antigen. The data was obtained during run 4 on sensor chip CMD 50 with immobilized Mer 39.

| Regeneration solution | 10 nM | 10 nM | Injection time (s) | Regeneration injections |
|---|---|---|---|---|
| 15 mM HCl | 636% | Increased | 20 | 1 and 2 |
| 15 mM HCl 0.1% SDS | 1052% | 6% | 20 | 1 |
| 15 mM HCl 2M NaCl | 854% | 125% | 30 | 1 |
| 10 mM Glycine 10% Glycerol pH 2 | 355% | 207% | 30 | 1 |

**Table 3.6:** The effectiveness of four different regeneration solutions. The regeneration data was obtained during run 4 with sensor chip CMD 50 and immobilized Mer 39 by injecting 10 nM NS1 solutions.

### Runs 5 and 6

Runs 5 and 6 were performed for the purpose of estimating NS1 kinetics and testing antibodies Mer 39, BBI5 in a sandwich assay. Sensor chip CMD 50 was used for run 5 and HC 200 for run 6. The change was made in order to reduce the non-specific signal.

The activity of immobilized Mer 39 on CMD 50 sensor chip was tested with 10 nM NS1 sample, which gave 139 µRIU signal before and 157 µRIU after regeneration with glycine solution pH 2. The signal intensity of both injections were 1993 µRIU and 364 µRIU for working and 1045 µRIU and 188 µRIU for reference channels, indicating high levels of non-specific response.

The activity of immobilized Mer 39 on HC 200 sensor chip was tested with 10 nM NS1 sample, which gave 137 µRIU signal before and 108 µRIU after regeneration with glycine solution pH 2.2. The signal intensity of both injections were 209 µRIU and 166 µRIU for working and 128 µRIU and 59 µRIU for reference channels.

The levels of non-specific response were reduced with the change in sensor chip from CMD to HC. However, during the initial experiments with CMD sensor chips, the nonspecific response was not observed. But the experimental runs 1, 2 and 3 were performed with older batch of sensor chips and different stock solutions of NS1 and Mer 39. The change in running buffer injection (blank) response levels, obtained from kinetic runs, are presented in table 3.7.

| Run No. | Sensor Chip | Left Channel (µRIU) | Right Channel (µRIU) |
|---|---|---|---|
| Run 1 | HC1000 m | 16 | 11 |
| Run 2 | CMD50 m | 17 | 9 |
| Run 5 | CMD50 m | 95 | 90 |
| Run 6 | HC 200 m | 23 | 17 |
| Run 7 | HC 200 m | 13 | 10 |
| Run 8 | CMD50 m | 72 | 62 |

**Table 3.7:** Blank response levels during kinetic analysis experiments.

Also, two glycine regeneration solutions were tested pH 2 and pH 2.2. The effectiveness of pH 2 solution for low antigen concentrations 20 nM and 10 nM for

20 s were 157 % 197 %. Thus a milder regeneration solution pH 2.2 was selected. Regeneration time was adjusted in accordance to concentration, 15 s for 5, 10 nM and 30 s for 20, 40, 80 nM. The antigen was injected in random order on both first and second days of experiments. The regeneration effectiveness using glycine regeneration solution pH 2.2 during runs 5 and 6 is presented in table 3.8.

The baselines of working and reference channels and regeneration effects are illustrated in figure 3.8. The glycine regeneration solution gave a more stable reference channel baseline. The adjusted time combined with milder regeneration solution gave more stable baseline for run 6 as well.

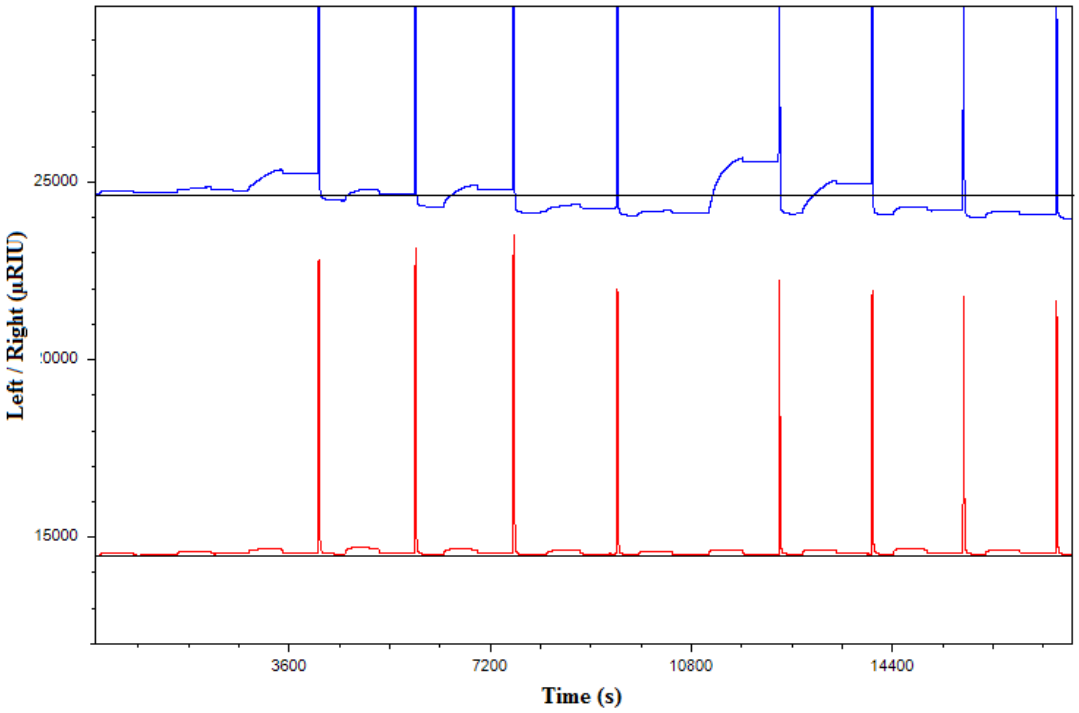


**Figure 3.8:** The baselines of working (blue) and reference (red) channels and regeneration effects on them. The baselines are extracted from run 5 experiments.

| Run No. | 80 nM | 40 nM | 20 nM | 10 nM | 5 nM |
|---|---|---|---|---|---|
| Run 5 | 101% | 104% | 131% | 157% | 185% |
| Run 5 (2) | 95%(x2); 106% | 109%; 102% | 186%; 120% | 157%; 155% | 194%; 131% |
| Run 6 | 107%(x2) | 122% | 131% | 100% | 156% |
| Run 6 | 100% | 105% | 116% | 187% | 183% |

**Table 3.8:** Regeneration with 10 mM glycine 10 % glycerol pH 2.2 during kinetic runs. Run 5 (2) - regeneration effectiveness with duplicates on a second day of experiments using CMD 50 with immobilized Mer 39. Run 6 - first day of experiments using HC 200 with immobilized Mer 39.(x2) - two regeneration injections.

The activity loss of immobilized Mer 39 antibodies were noted since the response to antigen injections significantly dropped every day. Figure 3.9 shows 20 nM NS1 injections on day 1, 2 and 3 during run 5.

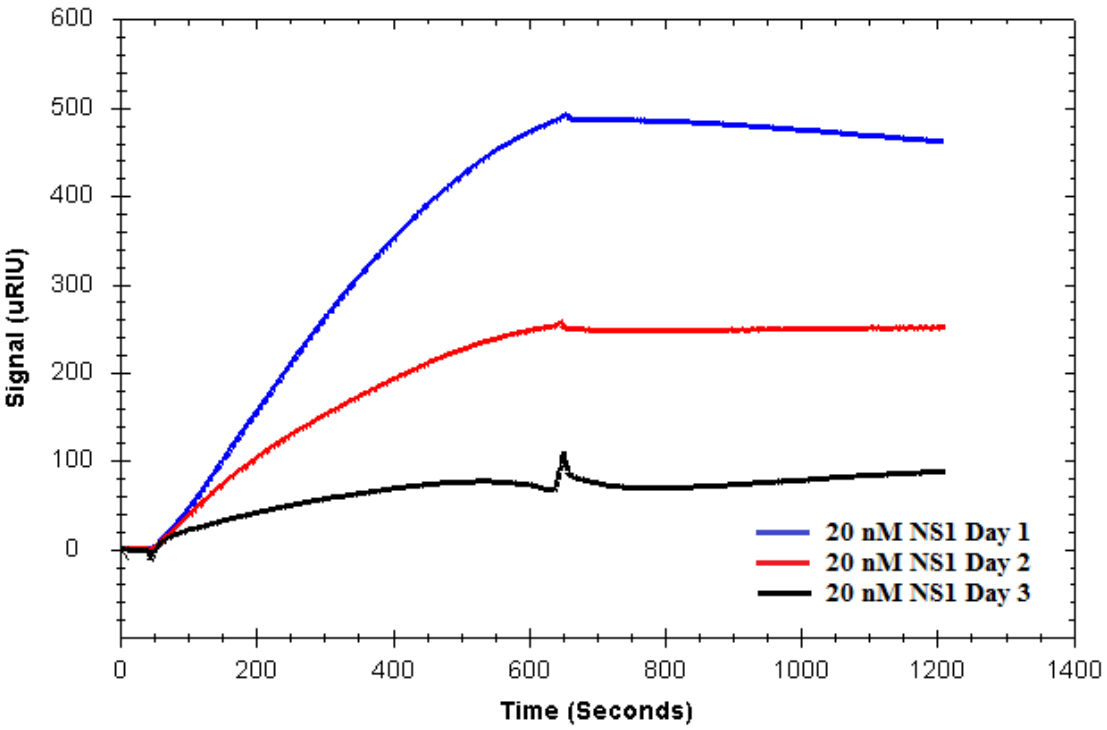


**Figure 3.9:** Response to injection of 20 nM NS1 during 3 days of experiments of run 5 on sensor chip CMD 50 with immobilized Mer 39. Day 1 - blue , day 2 - red and day 3 - black.

Table 3.9 shows the signal intensities for different antigen concentrations on different chips, run 5 CMD 50 and run 6 HC 200, and different days, first (1) and second (2). The response loss was evident with high antigen concentrations like 80, 40 and 20 nM. The inconsistencies in lower concentrations might be attributed

to the systematic error previously mentioned. Unexpectedly, the response levels obtained with sensor chip CMD 50 during run 5 were higher than HC 200.

| Run No. | 80 nM | 40 nM | 20 nM | 10 nM | 5 nM |
|---|---|---|---|---|---|
| Run 5 (1) | 1397 | 766 | 448 | 124 | 54 |
| Run 5 (2) | 907 | 518 | 244 | 119 | 32 |
| Run 6 (1) | 1235 | 726 | 448 | 341 | 138 |
| Run 6 (2) | 1047 | 582 | 330 | 185 | 55 |

**Table 3.9:** Response levels (µRIU) of antigen injections during runs 5 and 6 on first (1) and second (2) days. The antibody immobilized during both runs were Mer 39 on sensor chips CMD 50 for run 5 and HC 200 for run 6.

In addition, binding of 40 nM Mer 39 and BBI5 antibodies were tested upon a 10 nM injections of antigen during both runs. Run 5 and 6 binding curves of Mer 39 and BBI5 can be seen in figure 3.10.

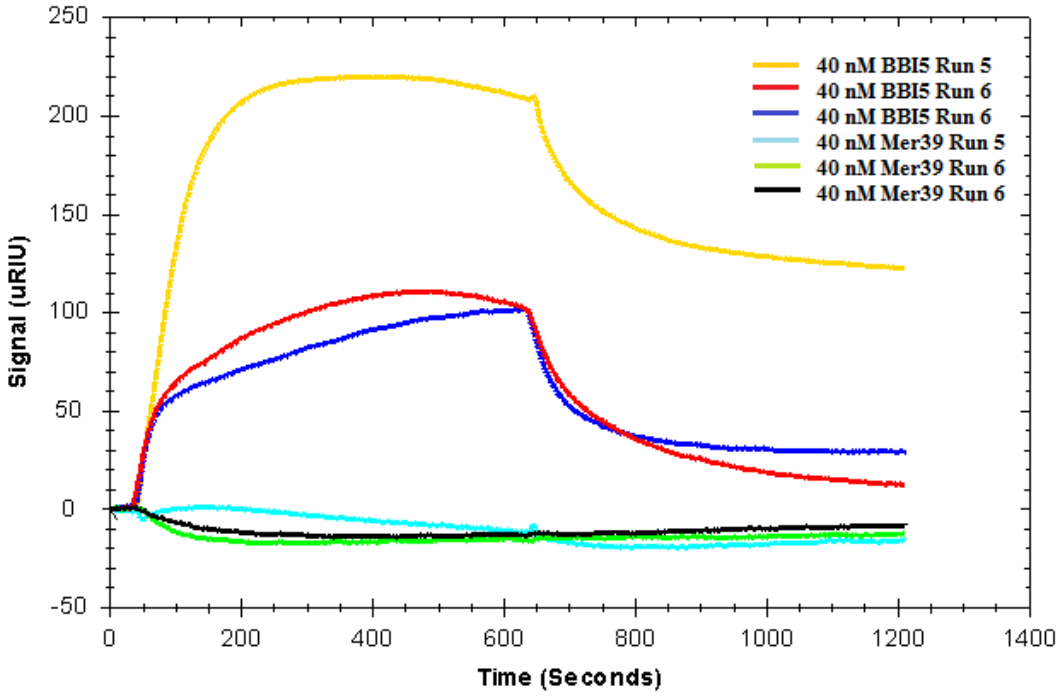


**Figure 3.10:** Run 5, CMD 50 with Mer 39, and 6, HC 200 with Mer 39, binding curves of 40 nM Mer 39 and BBI5 using 10 nM antigen injections as a base. Run 5: BBI5 - yellow; Mer - light blue. Run 6: BBI5 - red, blue; Mer - black, green.

Figure 3.10 also illustrates the inconsistency of data, since the level of BBI5 binding during run 5 could not be reproduced during run 6 and the following runs.

However, as mentioned before, antigen showed higher binding signals during run 5 than run 6 which could be the case with the antibody as well. Mer 39 did not show any binding, which was contrary to the results obtained during run 3 with Mer39-NPs.

### Runs 7 and 8

Runs 7 and 8 were performed for the purpose of estimating NS1 kinetics when immobilized antibody was BBI5. Also, free and nanoparticle conjugated antibodies Mer 39 and BBI5 were tested in a sandwich assay. Moreover, Mer 39 kinetic constants were estimated. Sensor chip HC 200 was used for run 7 and CMD 50 for run 8. The switch was made because the last HC 200 sensor chip was used in run 7.

The activity of immobilized BBI5 on HC 200 sensor chip was tested with 10 nM NS1 sample, which gave 205 µRIU signal before and 140 µRIU after regeneration with glycine solution pH 2.2. The signal intensity of both injections were 335 µRIU and 176 µRIU for working and 161 µRIU and 27 µRIU for reference channels.

The activity of immobilized BBI5 on CMD 50 sensor chip was tested with 10 nM NS1 sample, which gave 103 µRIU signal before and 88 µRIU after regeneration with glycine solution pH 2.2. The signal intensity of both injections were 250 µRIU and 128 µRIU for working and 164 µRIU and 68 µRIU for reference channels.

Regeneration was performed with glycine solution pH 2.2 and regeneration time was adjusted in accordance to NS1 concentrations, 15 s for 5, 10, 20 nM and 30 s for 40, 80, 160 nM. The concentrations were injected in random order on first and second days of experiments for run 7 and first day for run 8. The regeneration effectiveness of runs 7 and 8 is presented in table 3.10.

| **Run No.** | **160 nM** | **80 nM** | **40 nM** | **20 nM** | **10 nM** | **5 nM** |
|---|---|---|---|---|---|---|
| Run 7 | 98% | 101% | 97% | 117% | 111% | 139% |
| Run 7 | 106% | 103% | 108% | 101% | 181% | 250% |
| Run 8 | - | 99% | 99% | 109% | 116% | 281% |

**Table 3.10:** Regeneration with 10 mM glycine 10% glycerol solution pH 2.2. The data was obtained from runs 7 on the first and second day and run 8 first day of experiments. Antigen injections of differing concentrations were injected in random order. Run 7 sensor chip was HC 200with BBI5 immobilized and run 8 was sensor chip CMD 50 with BBI5 as well.

Table 3.11 shows the signal intensities for different antigen concentrations. The responses to NS1 injections, when antibody immobilized was BBI5, seemed to be more consistent and did not show a drop in signal on day 2, indicating that BBI5 was more resilient to experimental conditions than Mer 39.

| Run No. | 160 nM | 80 nM | 40 nM | 20 nM | 10 nM | 5 nM |
|---|---|---|---|---|---|---|
| Run 7 (1) | 546 | 412 | 390 | 216 | 167 | 90 |
| Run 7 (2) | 537 | - | 414 | 317 | 175 | 58 |
| Run 8 | - | - | 358 | 136 | 55 | 23 |

**Table 3.11:** Response to NS1 injections during runs 7, HC 200 with BBI5, and 8, CMD 50 with BBI5, on first (1) and second (2) days.

The activity of immobilized BBI5 antibodies was tested with 20 nM NS1 injections on day 1, 2 and 3, seen in figure 3.11. The differing response between day 1 and 2 was not attributed to activity loss but rather to dilution and time effects on antigen, since both responses could be seen on a third day.

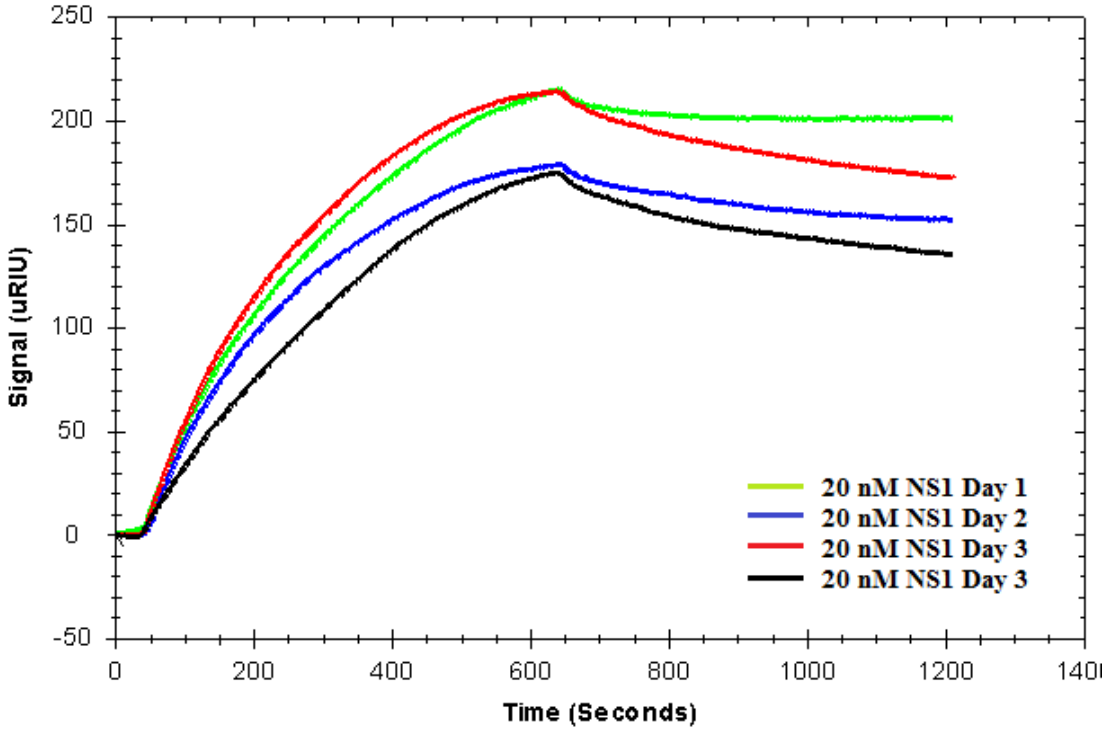


**Figure 3.11:** 20n M NS1 response levels during 3 days of experiments during run 7, sensor chip HC 200 with immobilized BBI5. Day 1 - green , day 2 - blue and day 3 - red and black.

Additionally, simple mass transport and antigen activity loss tests were performed during run 8, sensor chip CMD 50 with BBI5 immobilized. The mass transport test was performed by changing flow rates, 10, 20 and 30 µL/min, seen

in figure 3.12. The mass transport may have been observed since the curves did not overlap on top of each other. However it might be the artefact of sample preparation.

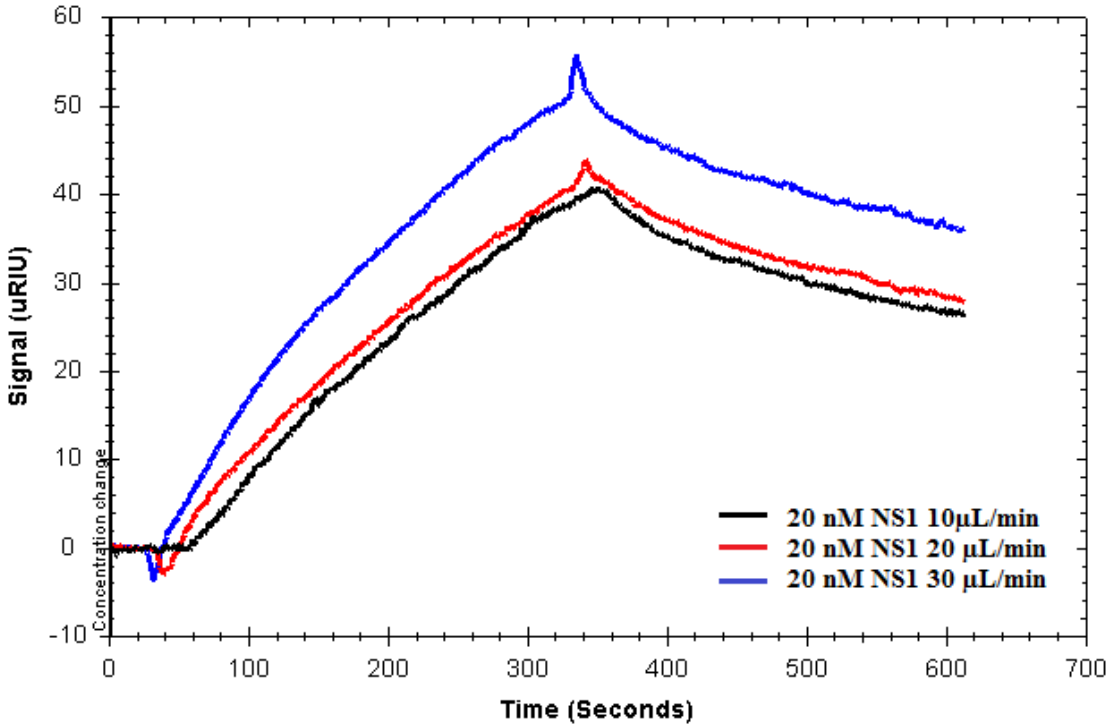


**Figure 3.12:** A mass transport test performed by changing flow rates 10, 20 and 30 µL/min. 20 nM NS1 injection onto CMD 50 with immobilized BBI5 gave responses, shown in black, red and blue.

The activity test was performed by preparing 20 NS1 nM sample and measuring its activity after 30 minutes, 105 minutes and 195 minutes, shown in figure 3.13. The signal levels to antigen decreased with time when BBI5 was immobilized just like with Mer 39. The reason for the drop in signal might be the concentration related dissociation of hexamers into dimers, resulting in a loss of active component.

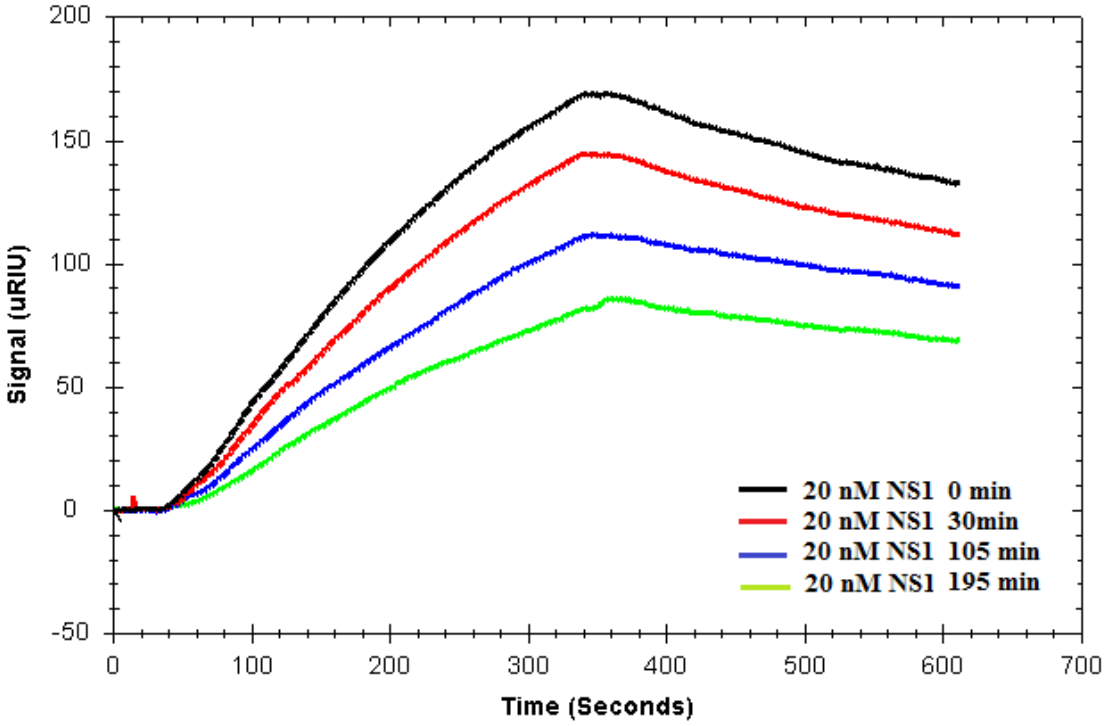


**Figure 3.13:** An antigen signal loss test performed on sensor chip CMD 50 with BBI5 immobilized. A 20 nM NS1 was prepared and its activity measured immediately and after 30, 105 and 195 minutes, shown by black, red, blue and green curves.

During run 7 a binding of Mer 39 was observed when conducting a sandwich assay. The binding curves of 40 nM Mer 39 and BBI5 can be seen in figure 3.14. After significant binding of Mer 39 was observed, kinetic analysis was performed. Also, regeneration effectiveness was calculated and is presented in table 3.12. The regeneration time was set to 30 s, since both antigen and antibody needed to be removed.

| **Run No.** | **Sensor Chip** | **40 nM** | **20 nM** | **10 nM** | **5 nM** |
|---|---|---|---|---|---|
| Run 7 | HC 200 m | 103% | 118% | 113% | 100% |
| Run 8 | CMD 50 m | 98% | 113% | 114% | 116% |

**Table 3.12:** Regeneration of captured antibodies Mer 39 with 10 mM glycine and 10% glycerol solution pH 2.2. 20 nM NS1 was used as a base for injections. Sensor chips used during run 7 was HC 200 with immobilized BBI5 and CMD 50 with BBI5 for run 8.

-

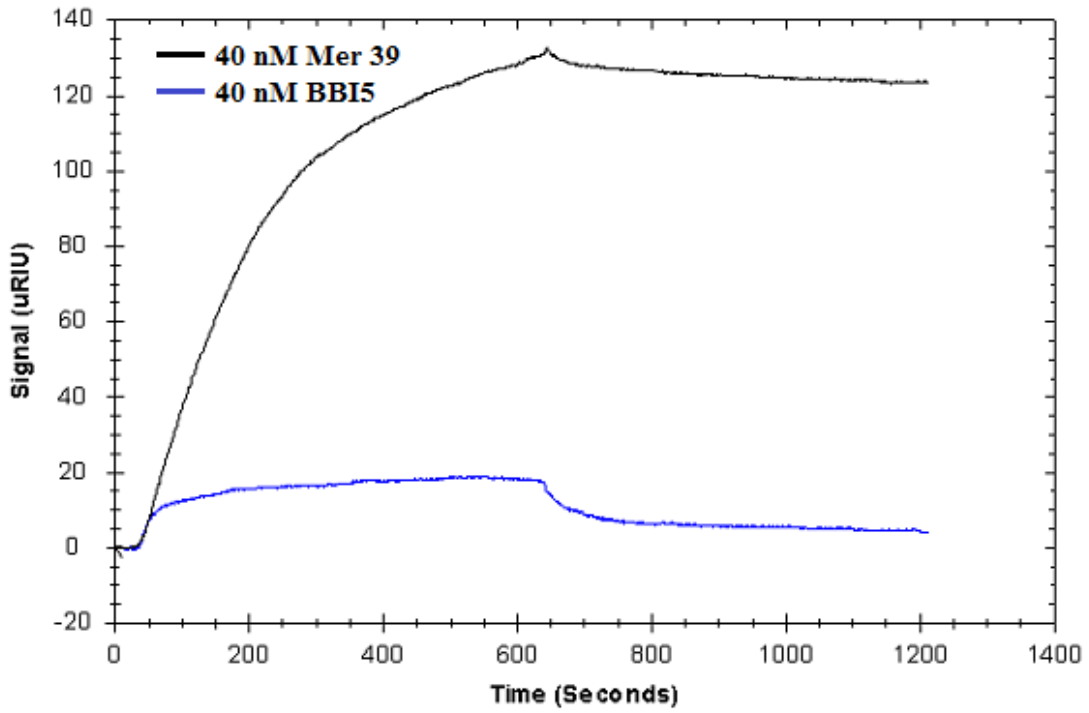


**Figure 3.14:** Binding curves of 40 nM Mer 39 in black and BBI5 in blue obtained during run 7 using sensor chip HC 200 with immobilized BBI5. The antigen concentration used prior to injections of antibodies were 20 nM.

Table 3.13 shows the signal intensities for different antibody concentrations on different chips HC 200 run 7 and CMD 50 run 8. As expected, the signal is lower when using CMD 50 than with HC 200.

| Run No. | Sensor Chip | 40 nM | 20 nM | 10 nM | 5 nM |
|---|---|---|---|---|---|
| Run 7 | HC 200 m | 131 | 92 | 72 | 41 |
| Run 8 | CMD 50 m | 77 | 68 | 56 | 35 |

**Table 3.13:** Responses to Mer 39 injections in a sandwich assay when prior antigen injection wass 20 nM for both experimental runs 7 and 8 when immobilized antibody was BBI5, run 7 sensor chip was HC 200 and run 8 sensor chip was CMD 50.

The binding of nanoparticle conjugated Mer39 and BBI5 was tested during run 7 and can be seen in figure 3.15. Different antigen concentrations, 10 nM and 20 nM, were used as a base for injections. Both nanoparticle samples demonstrated a some level of binding. The higher response belongs to BBI5-NPs and the lower to Mer39-NPs. Firstly, the results were contrary because free BBI5 did not show

any binding while Mer 39 did. Secondly, the response level to Mer 39 was similar to that of BBI5-NPs. In addition, the different concentrations of antigen used as a base, did not change the response levels to Ab-NPs.

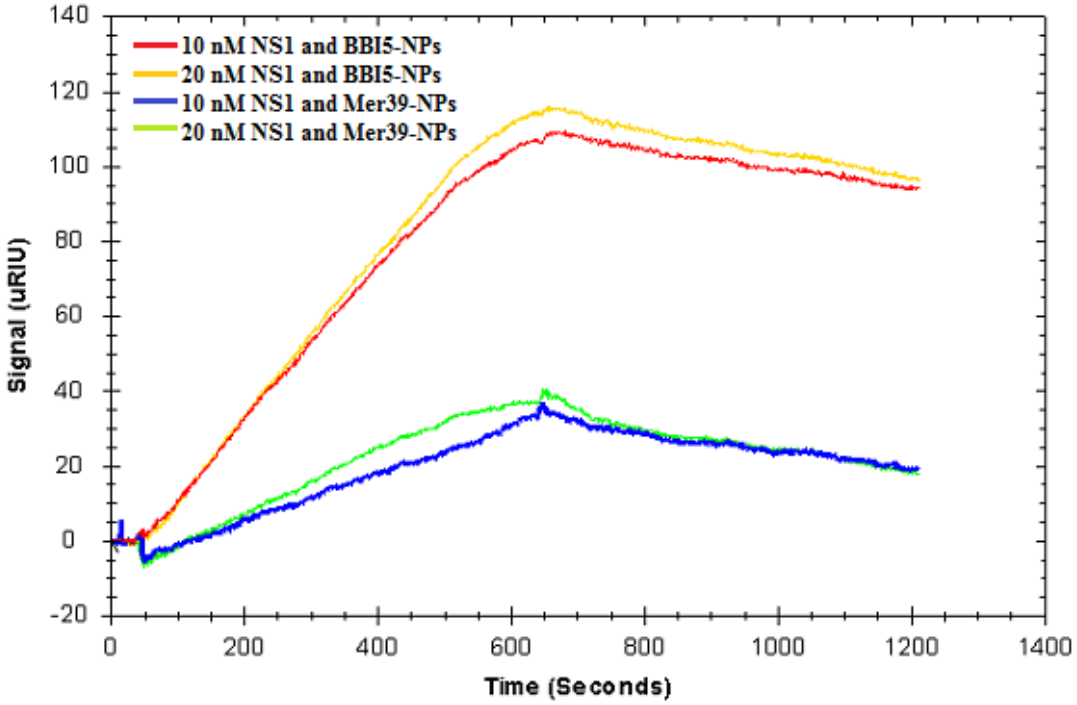


**Figure 3.15:** Binding curves of Mer 39 and BBI5 conjugated to nanoparticles obtained during run 7 usinng HC 200 sensor chip with immobilized BBI5. Different concentrations of NS1, 10 and 20 nM were used as a base for antibody-nanoparticle injections. 10 nM NS1 BBI5-NPs - red; 10 nM NS1 Mer39-NPs - blue; 20 nM NS1 BBI5-NPs - yellow; 20 nM NS1 Mer39-NPs - green.

During run 8 a double nanoparticle sandwich assay was performed on CMD 50 sensor chip with BBI5 antibody immobilized, depicted in figure 3.16. It was performed by subsequently injecting 20 nM NS1, BBI5-NPs, 20 nM NS1 and Mer 39-NPs without regeneration. The assay with switch in nanoparticle injection placement was performed as well. Figure 3.17 shows the subtracted curves for both double sandwich assays. The nanoparticle samples gave differing responses when the first injection was Mer39-NPs complex, while injection gave the same binding curve when it was BBI5-nanoparticles. The new batch of nanoparticles were used during this run, thus Mer 39 was expected to give a higher response than BBI5. However, when the distance from the sensor chip surface increases, the response decreases, explaining differing nanoparticle sample profiles. Also, this

could explain why the response to free antibody was higher compared to antibody-nanoparticle complex.

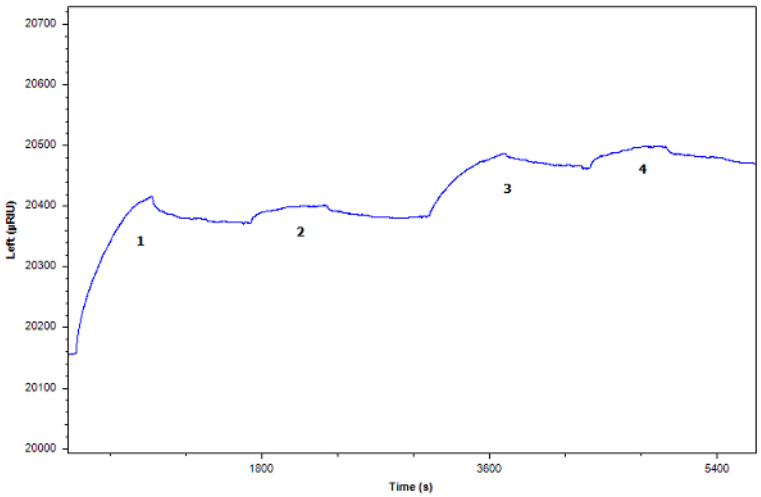


**Figure 3.16:** A double nanoparticle sandwich assay, performed on CMD 50 sensor chip with BBI5 antibody immobilized. Injections of 1 - 20 nM NS1, 2 - BBI5-NPs, 3 - 20 nM NS1 and 4 - Mer39-NPs.

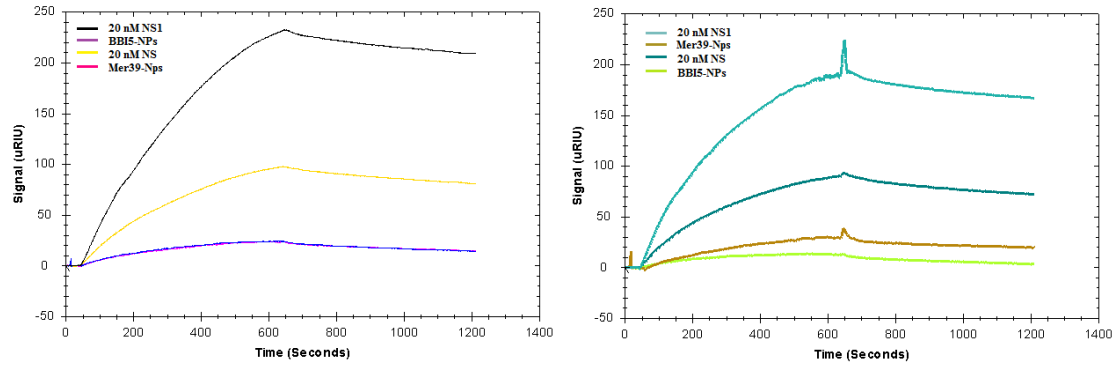


**Figure 3.17:** Figure on the left shows the curves of injections: black - NS1 20 nM, purple - BBI5-NPs, yellow - 20 nM NS1 and pink- Mer39-NPs. Figure on the right shows the curves of injections: blue - NS1 20 nM, brown- Mer39-NPs, blue - 20 nM NS1 and green- BBI5-NPs. The curves were obtained from double nanoparticle sandwich assay, performed on CMD 50 sensor chip with BBI5 antibody immobilized.

### Run 9

The binding of free and nanoparticle conjugated antibodies was tested with Mer39-NS1 complex on CMD 50 sensor chip, shown in figure 3.18. Surprisingly,

BBI5-NPs did not completely dissociate while free BBI5 did. The response levels seemed to decrease if antibody was conjugated to nanoparticles. However, during previous runs a much higher responses were obtained. Mer 39 antibody did not show any binding.

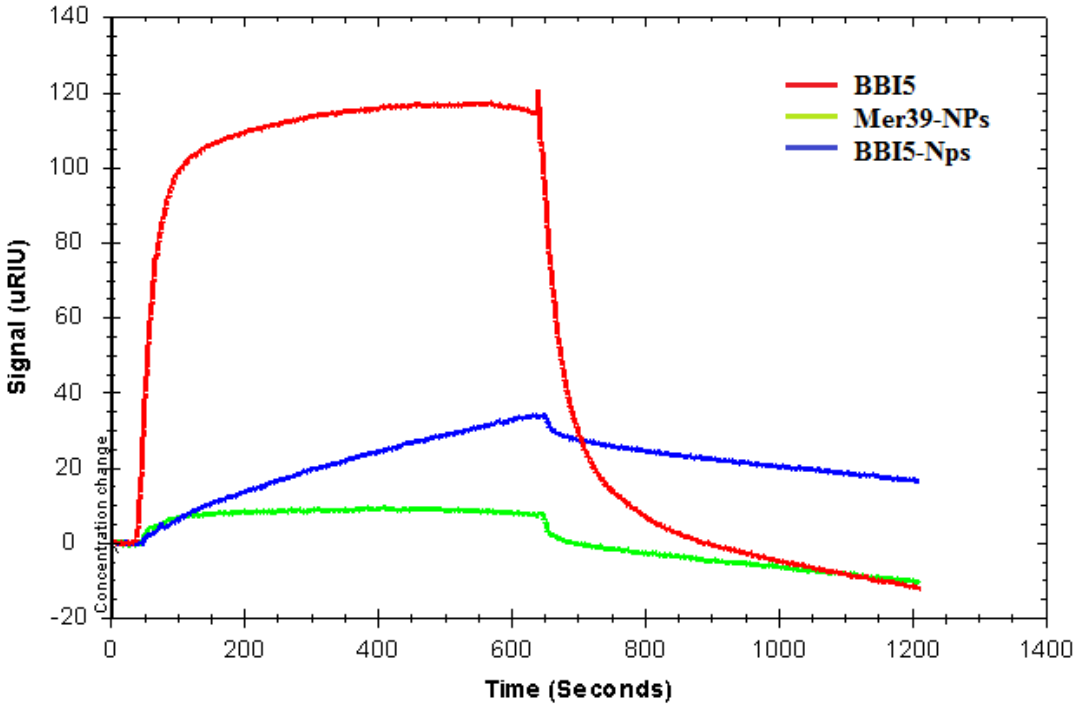


**Figure 3.18:** The binding of free and nanoparticle conjugated antibodies with Mer39-NS1 complex on CMD 50 sensor chip. The injection responses to BBI5 (red), Mer39 (green) and BBI5-NPs(blue)using 20 nM NS1 as a base.

Additionally, immobilization of Mer 39 nanoparticles was done to demonstrate that antigen binds to the complex. The binding responses of 20 nM antigen are shown in figure 3.19. Antigen could not be regenerated after injection and the baseline increased with every attempt.

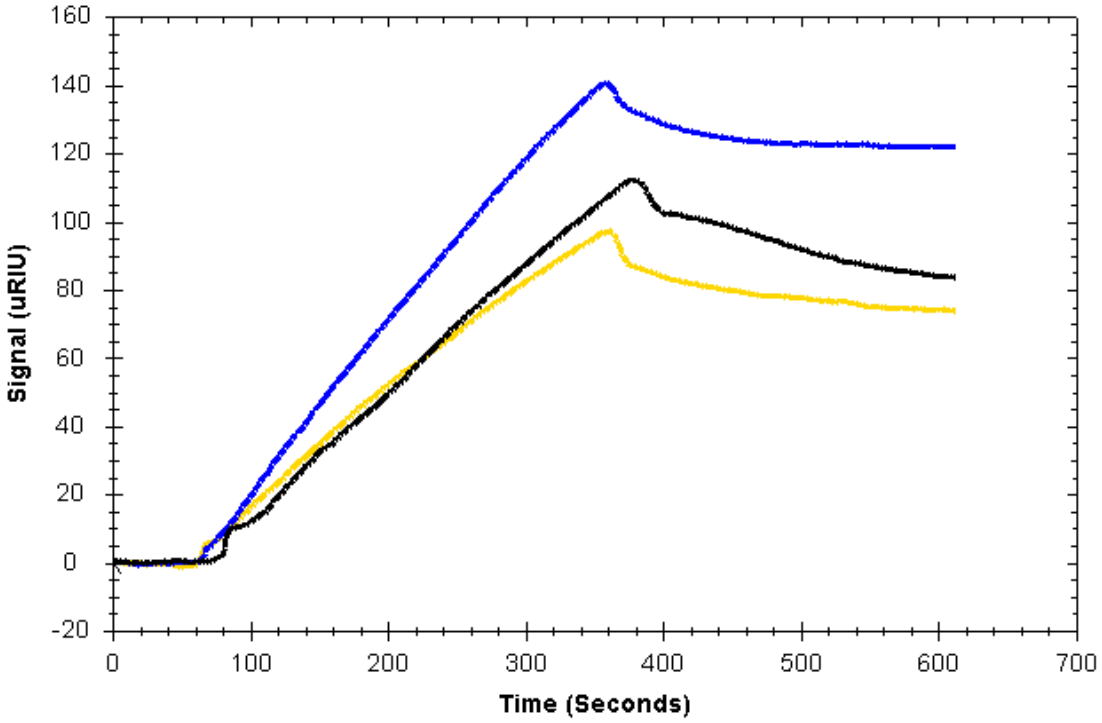


**Figure 3.19:** Responses to 20 nM NS1 injections onto immobilized Mer39-NPs on CMD 50 sensor chip.

## 3.4 Kinetic Analysis

The kinetics of recombinant dengue 2 NS1 antigen with immobilized Mer39 or BBI5 were measured on sensor chips HC 1000, HC 200 and CMD 50. One to one model was selected to fit all kinetic data. Antibody kinetics are better fitted with a bivalent interaction model, however with small enough concentrations the one to one model is valid. The kinetic data obtained was not high in quality thus it did not produce a good enough fit. For that reason literature was used to screen the obtained measurements for validation.

The runs that produced affinity constants less than 1 nM or more than 100 nM were assumed inaccurate. The limits for association and dissociation constants, 1e2 - 1e5 and 1e-2 - 1e-5, were set according to literature. [11]

### Mer39-NS1

The kinetics of recombinant dengue 2 NS1 antigen with immobilized Mer39 were measured during runs 1, 2, 5 and 6. The association constants varied consid-

erably between the runs. While dissociation constants were in the same order of magnitude when using one to one model, displayed in table 3.14.

| **Run No.** | **Sensor Chip** | $B_{max}$ **(µRIU)** | $k_a$ **1/M*s** | $k_d$ **1/s** | $K_d$ **M** | $chi^2$ |
|---|---|---|---|---|---|---|
| Run 1 | HC 1000 | 213.57 | 7.88e3 | 1.27e-4 | 1.61e-8 | 2.53 |
| Run 2 | CMD 50 | 11058.07 | 3.70e2 | 4.34e-4 | 1.17e-6 | 223.61 |
| Run 5 (1) | CMD 50 | 3093.52 | 1.60e4 | 2.90e-4 | 1.81e-8 | 3349.99 |
| Run 5 (2) | CMD 50 | 2551 | 1.05e4 | 2.74e-4 | 2.58e-8 | 1049.48 |
| Run 6 (1) | HC 200 | 2027 | 2.37e4 | 2.46e-4 | 1.04e-8 | 1966.64 |
| Run 6 (2) | HC 200 | 2628.81 | 1.29e4 | 3.26e-4 | 2.54e-8 | 2428.06 |

**Table 3.14:** An overview of kinetic constants obtained from globally fitting one to one model to data from runs 1, 2, 5 and 6 day (1) and day (2).

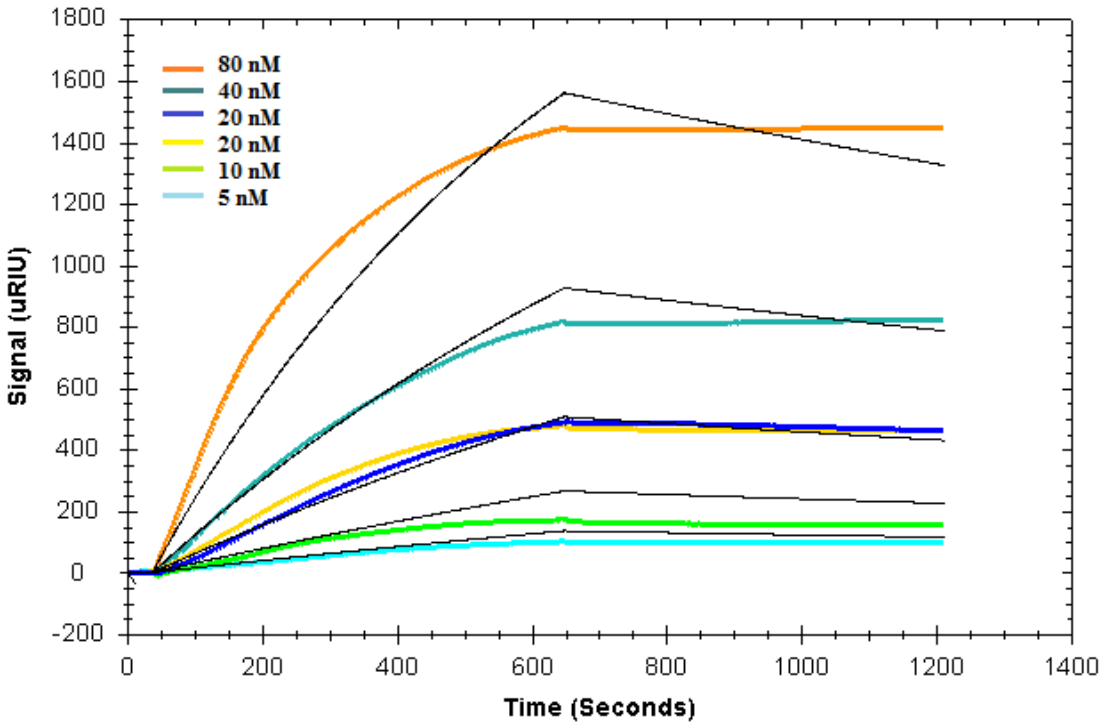


**Figure 3.20:** A global fit of data with one to one model from run 5 experiments on CMD 50 sensor chip with immobilized Mer 39 on day 1. The antigen was injected in random order in concentrations 80, 40, 20, 10 and 5 nM.

One to one model was not the best fit for the data collected from runs 5 and 6, seen in figure 3.20. Other one to one model with depletion corrected was fitted to the same data, seen in figure 3.21. The values for depletion model were $B_{max}$

2853.79 (µRIU), $k_a$ 2.79e4 1/M*s, $k_d$ 6.07e-5 1/s, $K_d$ 2.17e-9 M and $chi^2$ 1221.50. Even though the depletion model fitted better, the dissociation constant changed in order of magnitude and was not in the selected confidence interval anymore.

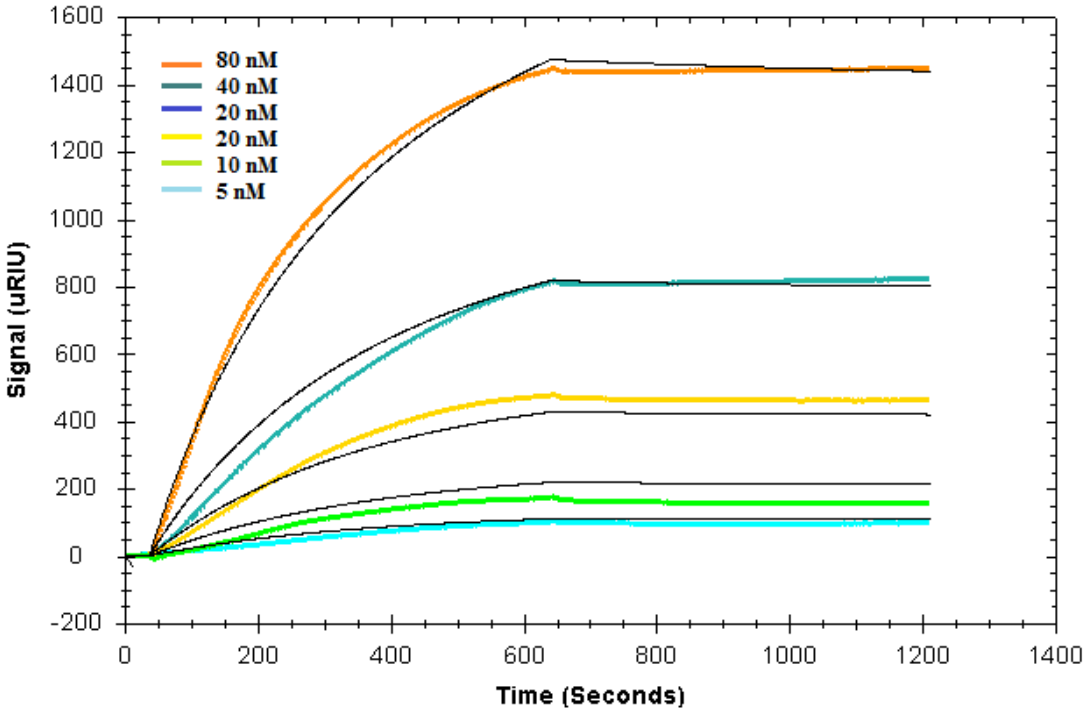


**Figure 3.21:** A global fit of data, one to one model with depletion corrected, obtained from run 5 experiments on CMD 50 sensor chip with immobilized Mer 39 on day 1. The antigen was injected in random order in concentrations 80, 40, 20, 10 and 5 nM.

### BBI5-NS1

The kinetics of recombinant dengue 2 NS1 antigen with immobilized BBI5 were measured during runs 7 and 8 on sensor chips HC 200 and CMD 50, displayed in table 3.15.

One to one model was poor fit for the data collected from runs 7 and 8, Figure 3.21 shows fitted data from run 7 day 2. One to one model with depletion corrected, fitted to the same data, was tested. The values for depletion model were $B_{max}$ 527.37 (µRIU), $k_a$ 8.32e4 1/M*s, $k_d$ 4.31e-4 1/s, $K_d$ 5.17e-9 M and $chi^2$ 604.66. In this case, the depletion model did not fit better. However, the constants remained similar and did not change in order of magnitude. The unusual profile of injection responses were hard to fit to any model. Despite that, the response profile was reproducible during both run 7 and run 8 experiments.

| Run No. | Sensor Chip | $B_{max}$ (µRIU) | $k_a$ 1/M*s | $k_d$ 1/s | $K_d$ M | $chi^2$ |
|---|---|---|---|---|---|---|
| Run 7 (1) | HC 200 | 521.48 | 7.77e4 | 5.57e-4 | 8.08e-9 | 795.25 |
| Run 7 (2) | HC 200 | 528.98 | 6.89e4 | 4.40e-4 | 5.66e-9 | 448.64 |
| Run 8 | CMD 50 | 4944.87 | 4.38e3 | 9.98e-4 | 2.28e-7 | 1031.69 |

**Table 3.15:** An overview of kinetic constants obtained from globally fitting one to one model to data from runs 7 and 8 day (1) and day (2).

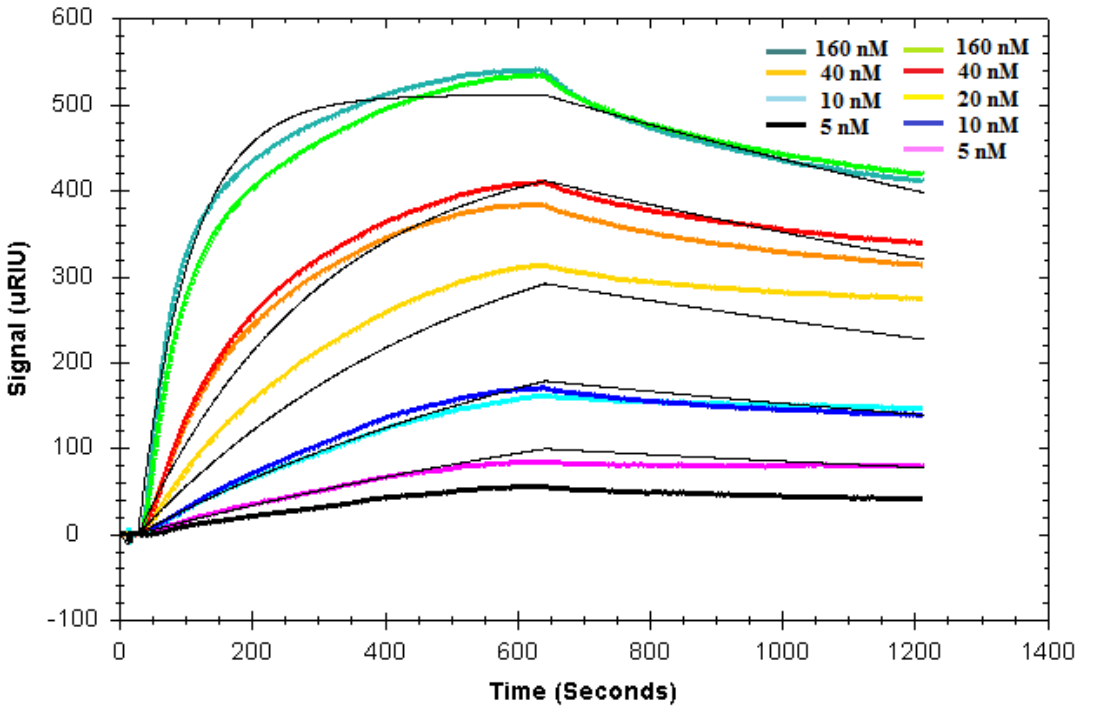


**Figure 3.22:** A global fit of data, one to one model, obtained from run 7 experiments on HC 200 sensor chip with immobilized BBI5 on day 2. The antigen was injected in duplicates, random order and in concentrations 160, 40, 20, 10 and 5 nM.

### Sandwich Assay Kinetic Analysis of Mer 39

The kinetics of monoclonal Mer 39 antibody with immobilized BBI5-NS1 were measured during runs 7 and 8 on sensor chips HC 200 and CMD 50. The local $B_{max}$ was set for the fit to account for different NS1 response levels, seen in figure 3.22, before injection of Mer 39. The $B_{max}$ 152 was observed for 5 nM Mer 39 with a base NS1 response 200 µRIU. The $B_{max}$ 126 was observed for 40 nM Mer 39 when NS1 response was around 150 µRIU. Thus providing justification for the local fitting of the parameter. The kinetic constants are presented in table 3.16.

| **Run No.** | **Sensor Chip** | $B_{max}$ **(µRIU)** | $k_a$ **1/M*s** | $k_d$ **1/s** | $K_d$ **M** | $chi^2$ |
|---|---|---|---|---|---|---|
| Run 7 | HC 200 | Local | 1.13e5 | 1.23e-4 | 1.09e-9 | 4.09 |
| Run 8 | CMD 50 | Local | 1.19e5 | 1.51e-4 | 1.27e-9 | 12.46 |

**Table 3.16:** Overview of kinetic data accumulated during sandwich assay kinetic analysis of Mer39 run 7 and run 8, sensor chips HC 200 and CMD 50 with immobilized BBI5.

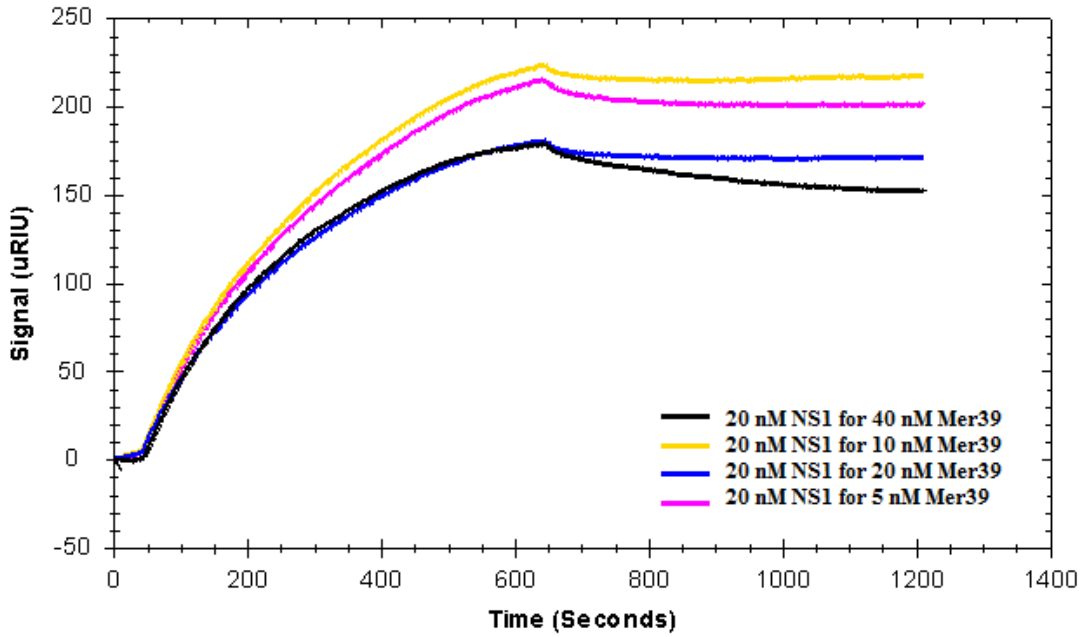


**Figure 3.23:** The differing response levels to 20 nM NS1 injections used as a base during sandwich assay kinetic analysis of Mer39 run 7 sensor chip HC 200 with immobilized BBI5 .

The kinetic results obtained from sandwich analysis were regarded as the most reliable and self consistent between different sensor chips. The fitted data from run 7 is shown in figure 3.24. The remaining figures of fitted data from all the runs are presented in appendix.

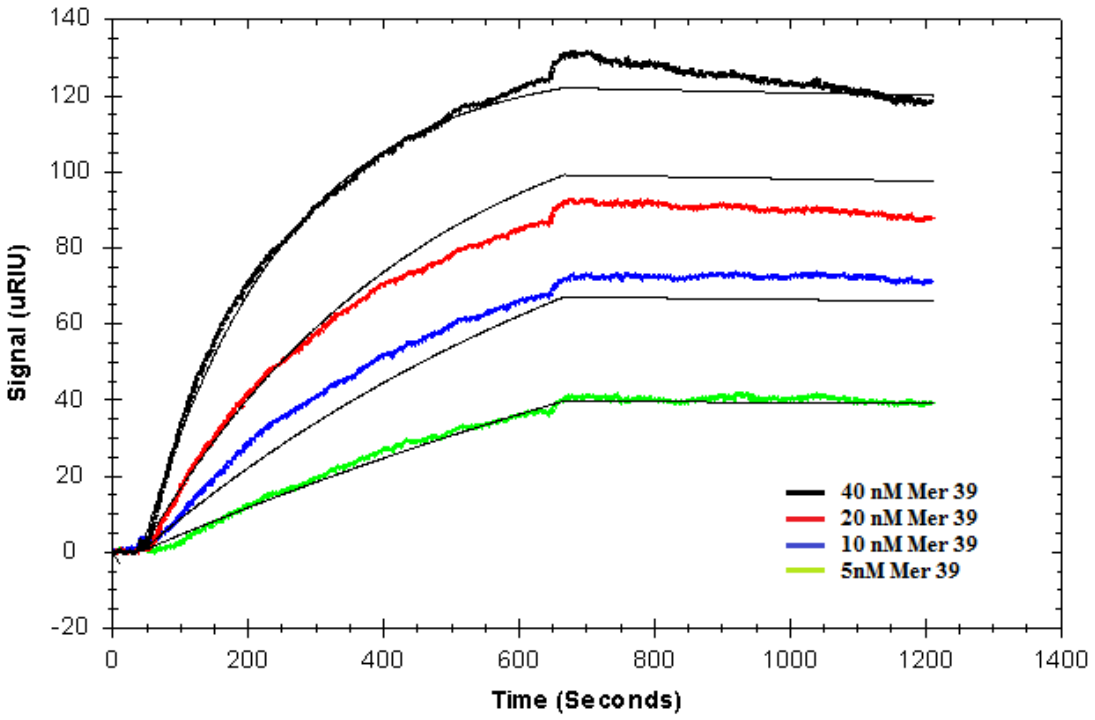


**Figure 3.24:** Data, acquired during sandwich assay kinetic analysis of Mer39 run 7 with sensor chip HC 2000 and immobilized BBI5, fitted with one to one model and parameter of local $B_{max}$. Mer 39 was injected in concentrations 40, 20, 10 and 5 nM on top of 20 nM NS1 base.

# Chapter 4

# Disscussion

Irregular patterns were observed with pre-concentration, immobilization yield, nonspecific noise, NS1 activity and response variations, responses to injections of free and nanoparticle conjugated antibodies and fitting the kinetic data. Not only some of these patterns were irregular but also uncontrollable and not reproducible.

Firstly, different type of sensor chips HC and CMD were noted to have certain advantages or disadvantages when compared to each other. Sensor chips HC 1000 and HC 200 were intended to be used for low or medium molecular weight analytes, while CMD 50 could be used for large molecules over 150 kDa [85]. Even though the CMD 50 is more suitable for kinetic analysis and large molecules like NS1, 300 kDa, it was not noted during the study. In fact, HC hydrogels gave consistent immobilization yields and lower nonspecific signal. According to manufacturer, HC sensor chips were specifically designed to reduce the nonspecific responses [85]. Contrary, varying immobilization yields under the same conditions with sensor chips CMD 50 were noted and the variation could not be accounted by activation step.

Moreover, the immobilization yields were high for all the sensor chips used, resulting in high maximum analyte response. The recommendations for this parameter differ depending on the type of analysis. For kinetic measurements, after analyte injection a response of approximately 100 µRIU is desired [86]. The minimal value of this parameter during the study was 10874 µRIU using molecular mass of NS1 hexamer. The $R_{max}$ is calculated:

$$R_{max} = \frac{MW_A \cdot R_L}{MW_L} \cdot V_L \tag{4.1}$$

where $V_L$ is ligand valency, MW is molecular weight of analyte and ligand and $R_L$ is immobilization yield [11]. In fact, the most self-consistent kinetic results were obtained during a sandwich assay, when the ligand was NS1 giving a response

of only 200 µRIU. Really, illustrating the importance of optimal experimental conditions in obtaining high quality results.

In addition, the activity loss of antigen was noted as quickly as 30 min after sample preparation. The antigen samples were prepared by adding NS1 stock solution to PBS buffer. According to manufacturer, NS1 stock solution buffer is PBS with no additives as well. however, the stock solution remained active while diluted samples did not. An active form of NS1 is considered to be hexameric. A study proposed a theory that NS1 haxamers were formed after a certain concentration of dimers were present [48]. Thus the diminishing response to NS1 could mean that hexamers are dissociating into dimers when concentrations are at nM level. Also, the short maximum activity period suggests dissociation rather than degradation. Due to the unstable nature of NS1 a systematic error was introduced since samples needed to be prepared individually. Thus negatively affecting the quality of data and kinetic analysis results.

Also, different stabilities of immobilized Mer 39 and BBI5 were observed. BBI5 monoclonal antibody was noted to be more stable under experimental conditions compared to Mer 39. Mer 39 demonstrated a decreasing activity on different days of experiments and were usable for first two days. While BBI5 did not show loss in activity during all 3 days of experiments. The manufacturer states that Mer 39 is intended as a detection antibody, which could explain its activity loss when immobilized. BBI5 can be used as both detection and capture antibody.

Unstable working and reference channel baselines, due to regeneration, were thought to interfere with the evaluation of kinetic parameters by skewing the response curves upon subtraction of both reference and blank responses. Since the experiments were conducted manually, the time after regeneration was insufficient, up to 10 minutes, to reach new equilibrium.

The models used to fit kinetic data were one to one and in some cases depletion corrected for comparison. It was assumed that one to one did not provide a good fit due to low quality of data when estimating NS1 kinetics. Thus model providing a better fit was tried for comparison. The one to one depletion corrected model estimates the depletion of ligand sites. This model is not commonly applied to flow system based measurements. [87] Also, it did not seemed obvious for the particular case of NS1, since ligand depletion was not expected. Contrary, ligand immobilization yields were high. However, the depletion of NS1 could be plausible, since low concentrations were used. The unusual responses to 160, 80 and 40 nM NS1 were observed when BBI5 was immobilized. 80 nM and 40nM responses were interchangeable, while 160 nM gave an increase again. This might indicate a two state interaction dependent on concentration.

Additionally, puzzling results of free and nanoparticle conjugated antibodies were observed. The only consistent and reproducible binding was noted for Mer

39 antibody when BBI5 was immobilized thus suggesting non overlapping epitopes. However, the BBI5 did not stay bound to NS1 when Mer 39 was immobilized. The significant binding without dissociation was observed once during run 5. The symmetric 3 dimeric structure of hexamer, theoretically have a number of repeating epitopes. However their accessibility to antibodies is not known. Also, a conformation related epitopes could be at play.

Lastly, a high binding responses was observed once for Mer39-NPs and BBI5-NPs under contrary experimental conditions, immobilized Mer 39 and BBI5 respectively. However, the stability of samples and their contents and purity from free antibodies are not known and thus can not be dismissed. A few low non-discriminative responses were recorded for both nanoparticle samples in cases of both Mer 39 and BBI5 immobilized. On one hand, the presence of nanoparticles could reduce the SPR signal due to the increasing distance from the surface. On the other hand, if the nanoparticle immobilized antibodies are not stable and degrade, the low curves could indicate non-specific binding, since NS1 is called sticky protein for its ability to non-specifically bind to variety of proteins during the course of dengue infection.[48]

# Chapter 5

# Conclusion

Recombinant dengue type 2 NS1 was characterized in relation to a pair of monoclonal antibodies Mer 39 and BBI5 for the use in nanoparticle-based immunoassays. Surface plasmon resonance biosensor was used to discern the kinetic constants, epitope overlapping and interactions of nanoparticle conjugated antibodies, mentioned above. For this purpose antibodies, either Mer 39 or BBI5, were covalently immobilized by amine coupling to different hydrogels HC 1000, HC 200 and CMD 50. Through experiments, the binding kinetics of NS1 to both antibodies and Mer 39 kinetics in a sandwich assay were estimated. Due to certain non-optimal experimental conditions and unidentified artefacts, NS1 kinetic constants were unreliable. However, the said constant were within valid range according to literature. Additionally, the kinetic constants of Mer 39 were consistent and were estimated to be $k_a$=1.13e5 1/M s, $k_d$= 1.23e-4 1/s and $K_D$=1.09e-9 M. Also, it was noted that NS1 epitopes for BBI5 and Me 39 did not overlap. However, the complex was not successfully formed in cases when Mer 39 was immobilized. The binding measurements of nanoparticle-antibody complexes were inconsistent. However it was observed that nanoparticles did not eliminate Mer 39 binding to NS1 when said Mer39-NPs complex was immobilized.

# Chapter 6

# Outlook

This chapter will present few ideas by which this study could be expanded and improved. Firstly, the lack of accurate and reproducible data was apparent. Thus an optimization of experimental protocols would be the first step. Three different immobilization strategies could be employed. An immobilization yield could be lowered by adjusting activation solution, antigen could be the one immobilized or antibody capture based immobilization could be attempted. Antibody capture immobilization would be a convenient because antibody concentration can be adjusted. NS1 immobilization would eliminate the need to prepare fresh samples constantly and the error inherent in that.

Different experimental conditions call for different regeneration strategies. However, regeneration caused artifacts, were thought to significantly impact the quality of data. Thus regeneration free stair like experiments could be attempted.

Additionally, it would be interesting to clarify thee activity loss of antigen, which could be done by simple Native-PAGE experiment.

Also, the suitability of surface plasmon resonance for the purpose of study could be evaluated by using different technique. The different method could be analytical ultracentrifugation. Since this methods estimates binding characteristics in solutions, it would be suitable to clarify the nature of Mer39-NS1-BBI5 interactions and the interaction stoichiometry between NS1 and both antibodies.

Lastly, additional experiments like thermodynamic analysis using SPR or AFM imaging of NS1 samples or immobilized molecules onto the SPR sensor chip could enrich or diversify the results.

# Bibliography


[1] Maria G Guzman, Duane J Gubler, Alienys Izquierdo, Eric Martinez, and Scott B Halstead. Dengue infection. *Nature reviews. Disease primers*, 2:16055, 2016.

[2] Edward C Holmes and S Susanna Twiddy. The origin, emergence and evolutionary genetics of dengue virus. *Infection, genetics and evolution*, 3(1):19–28, 2003.

[3] Samir Bhatt, Peter W Gething, Oliver J Brady, Jane P Messina, Andrew W Farlow, Catherine L Moyes, John M Drake, John S Brownstein, Anne G Hoen, Osman Sankoh, et al. The global distribution and burden of dengue. *Nature*, 496(7446):504–507, 2013.

[4] Duane J Gubler. Dengue and dengue hemorrhagic fever. *Clinical microbiology reviews*, 11(3):480–496, 1998.

[5] World Health Organization. Dengue guidelines for diagnosis, treatment, prevention and control. 2009.

[6] Duane J Gubler. Dengue and dengue hemorrhagic fever in the americas. *Puerto Rico health sciences journal*, 6(2):107–111, 1987.

[7] Alan L Rothman and Francis A Ennis. Dengue vaccine: The need, the challenges, and progress. *Journal of Infectious Diseases*, 214(6):825–827, 2016.

[8] Vu Ty Hang, Nguyen Minh Nguyet, Vianney Tricou, Sutee Yoksan, Nguyen Minh Dung, Tran Van Ngoc, Tran Tinh Hien, Jeremy Farrar, Bridget Wills, Cameron P Simmons, et al. Diagnostic accuracy of ns1 elisa and lateral flow rapid tests for dengue sensitivity, specificity and relationship to viraemia and antibody responses. *PLoS Negl Trop Dis*, 3(1):e360, 2009.

[9] Rosanna W Peeling, Harvey Artsob, Jose Luis Pelegrino, Philippe Buchy, Mary J Cardosa, Shamala Devi, Delia A Enria, Jeremy Farrar, Duane J Gubler, Maria G Guzman, et al. Evaluation of diagnostic tests: dengue. *Nature Reviews Microbiology*, 8:S30–S37, 2010.

[10] Paula Antunes, Daniel Watterson, Mattias Parmvi, Robert Burger, Anja Boisen, Paul Young, Matthew A Cooper, Mikkel F Hansen, Andrea Ranzoni, and Marco Donolato. Quantification of ns1 dengue biomarker in serum via optomagnetic nanocluster detection. *Scientific reports*, 5, 2015.

[11] Dongmei Hu, Scott R Fry, Johnny X Huang, Xixia Ding, Liwen Qiu, Yuxian Pan, Yue Chen, Jing Jin, Catriona McElnea, Joe Buechler, et al. Comparison of surface plasmon resonance, resonant waveguide grating biosensing and enzyme linked immunosorbent assay (elisa) in the evaluation of a dengue virus immunoassay. *Biosensors*, 3(3):297–311, 2013.

[12] William E Paul. *Fundamental immunology*. Number ISBN: 9781451117837 in 8th ed. Raven Press New York, 2013.

[13] Harry W Schroeder and Lisa Cavacini. Structure and function of immunoglobulins. *Journal of Allergy and Clinical Immunology*, 125(2):S41–S52, 2010.

[14] Meirion B Llewelyn, Robert E Hawkins, and Stephen J Russell. Discovery of antibodies. *Bmj*, 305(6864):1269–1272, 1992.

[15] P Casali and EW Schettino. Structure and function of natural antibodies. In *Immunology of Silicones*, pages 167–179. Springer, 1996.

[16] Bruce Alberts, Dennis Bray, Karen Hopkin, Alexander Johnson, Julian Lewis, Martin Raff, Keith Roberts, and Peter Walter. *Essential cell biology*. Garland Science, 2013.

[17] David G Schatz and Patrick C Swanson. V (d) j recombination: mechanisms of initiation. *Annual review of genetics*, 45:167–202, 2011.

[18] Neil S Lipman, Lynn R Jackson, Laura J Trudel, and Frances Weis-Garcia. Monoclonal versus polyclonal antibodies: distinguishing characteristics, applications, and information resources. *ILAR journal*, 46(3):258–268, 2005.

[19] David M Webster, Andrew H Henry, and Anthony R Rees. Antibody-antigen interactions. *Current opinion in structural biology*, 4(1):123–129, 1994.

[20] Donald E Carey. Chikungunya and dengue: a case of mistaken identity? *Journal of the History of Medicine and Allied Sciences*, 26(3):243–262, 1971.

[21] Erik A Henchal and J Robert Putnak. The dengue viruses. *Clinical microbiology reviews*, 3(4):376–396, 1990.

[22] Maria G Guzman and Eva Harris. Dengue. *The Lancet*, 385(9966):453–465, 2015.

[23] DJ Gubler. Arboviruses as imported disease agents: the need for increased awareness. In *Imported Virus Infections*, pages 21–32. Springer, 1996.

[24] Duane J Gubler. Aedes aegypti and aedes aegypti-borne disease control in the 1990s: top down or bottom up. *The American journal of tropical medicine and hygiene*, 40(6):571–578, 1989.

[25] Cameron P Simmons, Jeremy J Farrar, Nguyen van Vinh Chau, and Bridget Wills. Dengue. *New England Journal of Medicine*, 366(15):1423–1432, 2012.

[26] Scott B Halstead and Philip K Russell. Protective and immunological behavior of chimeric yellow fever dengue vaccine. *Vaccine*, 34(14):1643–1647, 2016.

[27] Scott C Weaver and Nikos Vasilakis. Molecular evolution of dengue viruses: contributions of phylogenetics to understanding the history and epidemiology of the preeminent arboviral disease. *Infection, Genetics and Evolution*, 9(4):523–540, 2009.

[28] Goro Kuno. Review of the factors modulating dengue transmission. *Epidemiologic reviews*, 17(2):321–335, 1995.

[29] Louis Lambrechts, Thomas W Scott, and Duane J Gubler. Consequences of the expanding global distribution of aedes albopictus for dengue virus transmission. *PLoS Negl Trop Dis*, 4(5):e646, 2010.

[30] Richard J Kuhn, Wei Zhang, Michael G Rossmann, Sergei V Pletnev, Jeroen Corver, Edith Lenches, Christopher T Jones, Suchetana Mukhopadhyay, Paul R Chipman, Ellen G Strauss, et al. Structure of dengue virus: implications for flavivirus organization, maturation, and fusion. *Cell*, 108(5):717–725, 2002.

[31] Thomas J Chambers, Chang S Hahn, Ricardo Galler, and Charles M Rice. Flavivirus genome organization, expression, and replication. *Annual Reviews in Microbiology*, 44(1):649–688, 1990.

[32] Franz X Heinz and Steven L Allison. Structures and mechanisms in flavivirus fusion. *Advances in virus research*, 55:231–269, 2000.

[33] Gavin Screaton, Juthathip Mongkolsapaya, Sophie Yacoub, and Catherine Roberts. New insights into the immunopathology and control of dengue virus infection. *Nature Reviews Immunology*, 15(12):745–759, 2015.

[34] Ralf Bartenschlager and Sven Miller. Molecular aspects of dengue virus replication. 2008.

[35] REBECCA Littaua, ICHIRO Kurane, and FRANCIS A Ennis. Human igg fc receptor ii mediates antibody-dependent enhancement of dengue virus infection. *The Journal of Immunology*, 144(8):3183–3186, 1990.

[36] Kao-Jean Huang, Yu-Ching Yang, Yee-Shin Lin, Jyh-Hsiung Huang, Hsiao-Sheng Liu, Trai-Ming Yeh, Shun-Hua Chen, Ching-Chuan Liu, and Huan-Yao Lei. The dual-specific binding of dengue virus and target cells for the antibody-dependent enhancement of dengue virus infection. *The Journal of Immunology*, 176(5):2825–2832, 2006.

[37] Walter E Brandt, Dumrong Chiewsilp, Donald L Harris, and Philip K Russell. Partial purification and characterization of a dengue virus soluble complement-fixing antigen. *The Journal of Immunology*, 105(6):1565–1568, 1970.

[38] Greg W Smith and Peter J Wright. Synthesis of proteins and glycoproteins in dengue type 2 virus-infected vero and aedes albopictus cells. *Journal of General Virology*, 66(3):559–571, 1985.

[39] Charles M Rice, Edith M Lenches, Sean R Eddy, Se Jung Shin, Rebecca L Sheets, and James H Strauss. Nucleotide sequence of yellow fever virus: implications for flavivirus gene expression and evolution. *Science*, 229(4715):726–733, 1985.

[40] David A Muller and Paul R Young. The flavivirus ns1 protein: molecular and structural biology, immunology, role in pathogenesis and application as a diagnostic biomarker. *Antiviral research*, 98(2):192–208, 2013.

[41] David L Akey, W Clay Brown, Somnath Dutta, Jamie Konwerski, Joyce Jose, Thomas J Jurkiw, James DelProposto, Craig M Ogata, Georgios Skiniotis, Richard J Kuhn, et al. Flavivirus ns1 structures reveal surfaces for associations with membranes and the immune system. *Science*, 343(6173):881–885, 2014.

[42] B Falgout, R Chanock, and CJ Lai. Proper processing of dengue virus nonstructural glycoprotein ns1 requires the n-terminal hydrophobic signal sequence and the downstream nonstructural protein ns2a. *Journal of virology*, 63(5):1852–1860, 1989.

[43] Thomas Nowak, Petra M Färber, Gisela Wengler, and Gerd Wengler. Analyses of the terminal sequences of west nile virus structural proteins and of the in vitro translation of these proteins allow the proposal of a complete scheme of the proteolytic cleavages involved in their synthesis. *Virology*, 169(2):365–376, 1989.

[44] Melinda J Pryor and Peter J Wright. Glycosylation mutants of dengue virus ns1 protein. *Journal of general virology*, 75(5):1183–1187, 1994.

[45] Paulo R Post, Ricardo Carvalho, and Ricardo Galler. Glycosylation and secretion of yellow fever virus nonstmctural protein ns1. *Virus research*, 18(2-3):291–302, 1991.

[46] Marie Flamand, Françoise Megret, Magali Mathieu, Jean Lepault, Félix A Rey, and Vincent Deubel. Dengue virus type 1 nonstructural glycoprotein ns1 is secreted from mammalian cells as a soluble hexamer in a glycosylation-dependent fashion. *Journal of virology*, 73(7):6104–6110, 1999.

[47] Gunther Winkler, Valerie B Randolph, Graham R Cleaves, Terence E Ryan, and Victor Stollar. Evidence that the mature form of the flavivirus nonstructural protein ns1 is a dimer. *Virology*, 162(1):187–196, 1988.

[48] David A Muller and Paul R Young. The flavivirus ns1 protein: molecular and structural biology, immunology, role in pathogenesis and application as a diagnostic biomarker. *Antiviral research*, 98(2):192–208, 2013.

[49] Irina Gutsche, Fasséli Coulibaly, James E Voss, Jérôme Salmon, Jacques d'Alayer, Myriam Ermonval, Eric Larquet, Pierre Charneau, Thomas Krey, Françoise Mégret, et al. Secreted dengue virus nonstructural protein ns1 is an atypical barrel-shaped high-density lipoprotein. *Proceedings of the National Academy of Sciences*, 108(19):8003–8008, 2011.

[50] Joshua Fink, Feng Gu, and Subhash G Vasudevan. Role of t cells, cytokines and antibody in dengue fever and dengue haemorrhagic fever. *Reviews in medical virology*, 16(4):263–275, 2006.

[51] David G Nielsen. The relationship of interacting immunological components in dengue pathogenesis. *Virology journal*, 6(1):211, 2009.

[52] Martina Beltramello, Katherine L Williams, Cameron P Simmons, Annalisa Macagno, Luca Simonelli, Nguyen Than Ha Quyen, Soila Sukupolvi-Petty, Erika Navarro-Sanchez, Paul R Young, Aravinda M De Silva, et al. The human immune response to dengue virus is dominated by highly cross-reactive antibodies endowed with neutralizing and enhancing activity. *Cell host & microbe*, 8(3):271–283, 2010.

[53] Katherine L Williams, Simona Zompi, P Robert Beatty, and Eva Harris. A mouse model for studying dengue virus pathogenesis and immune response. *Annals of the New York Academy of Sciences*, 1171(s1):E12–E23, 2009.

[54] Corwin A Robertson, P David, and Daniel M Gordon. Prevention and control of influenza and dengue through vaccine development. *Pediatric annals*, 42(8):e182–e187, 2013.

[55] David M Morens. Dengue fever and dengue hemorrhagic fever. *The Pediatric infectious disease journal*, 28(7):635–636, 2009.

[56] Chuan-Liang Kao, Chwan-Chuen King, Day-Yu Chao, Hui-Lin Wu, and GJ Chang. Laboratory diagnosis of dengue virus infection: current and future perspectives in clinical diagnosis and public health. *J Microbiol Immunol Infect*, 38(1):5–16, 2005.

[57] RW Wood. Xlii. on a remarkable case of uneven distribution of light in a diffraction grating spectrum. *The London, Edinburgh, and Dublin Philosophical Magazine and Journal of Science*, 4(21):396–402, 1902.

[58] Andreas Otto. Excitation of nonradiative surface plasma waves in silver by the method of frustrated total reflection. *Zeitschrift für Physik*, 216(4):398–410, 1968.

[59] Erwin Kretschmann and Heinz Raether. Notizen: radiative decay of non radiative surface plasmons excited by light. *Zeitschrift für Naturforschung A*, 23(12):2135–2136, 1968.

[60] Andreas B Dahlin. *Plasmonic biosensors: an integrated view of refractometric detection*, volume 4. Ios Press, 2012.

[61] Bo Liedberg, Claes Nylander, and Ingemar Lunström. Surface plasmon resonance for gas detection and biosensing. *Sensors and actuators*, 4:299–304, 1983.

[62] Vitalii Silin and Anne Plant. Biotechnological applications of surface plasmon resonance. *Trends in Biotechnology*, 15(9):353–359, 1997.

[63] Nico J de Mol and Marcel JE Fischer. Kinetic and thermodynamic analysis of ligand-receptor interactions: Spr applications in drug development. *Handbook of Surface Plasmon Resonance*, pages 123–172, 2008.

[64] Patrick Englebienne, Anne Van Hoonacker, and Michel Verhas. Surface plasmon resonance: principles, methods and applications in biomedical sciences. *Journal of Spectroscopy*, 17(2-3):255–273, 2003.

[65] Stefan Löfås and Alan Mcwhirter. The art of immobilization for spr sensors. *Surface plasmon resonance based sensors*, pages 117–151, 2006.

[66] Jiri Homola, Sinclair S Yee, and Gunter Gauglitz. Surface plasmon resonance sensors: review. *Sensors and Actuators B: Chemical*, 54(1):3–15, 1999.

[67] Jiri Homola. Electromagnetic theory of surface plasmons. In *Surface plasmon resonance based sensors*, pages 3–44. Springer, 2006.

[68] Anatoly V Zayats, Igor I Smolyaninov, and Alexei A Maradudin. Nano-optics of surface plasmon polaritons. *Physics reports*, 408(3):131–314, 2005.

[69] Jiri Homola. Present and future of surface plasmon resonance biosensors. *Analytical and bioanalytical chemistry*, 377(3):528–539, 2003.

[70] P Cheyssac, VA Sterligov, SI Lysenko, and R Kofman. Surface plasmon-polaritons. *physica status solidi(a)*, 175(1):253–258, 1999.

[71] Nico J de Mol and Marcel JE Fischer. Surface plasmon resonance: a general introduction. *Surface plasmon resonance: methods and protocols*, pages 1–14, 2010.

[72] Leiva Casemiro Oliveira, Antonio Marcus Nogueira Lima, Carsten Thirstrup, and Helmut Franz Neff. *Surface Plasmon Resonance Sensors: A Materials Guide to Design and Optimization.* Number ISBN: 978-3-319-14926-4. Springer, 2015.

[73] Rebecca L Rich and David G Myszka. Advances in surface plasmon resonance biosensor analysis. *Current opinion in biotechnology*, 11(1):54–61, 2000.

[74] Jiri Homola. Surface plasmon resonance sensors for detection of chemical and biological species. *Chemical reviews*, 108(2):462–493, 2008.

[75] P Anton Van Der Merwe. Surface plasmon resonance. *Protein-Ligand Interactions: Hydrodynamics and Calorimetry*, 1:137–170, 2001.

[76] Stefan Löfås and Bo Johnsson. A novel hydrogel matrix on gold surfaces in surface plasmon resonance sensors for fast and efficient covalent immobilization of ligands. *Journal of the Chemical Society, Chemical Communications*, (21):1526–1528, 1990.

[77] Alexander A Kortt, Geoffrey W Oddie, Peter Iliades, L Clem Gruen, and Peter J Hudson. Nonspecific amine immobilization of ligand can be a potential source of error in biacore binding experiments and may reduce binding affinities. *Analytical biochemistry*, 253(1):103–111, 1997.

[78] Daniel J O'Shannessy, Michael Brigham-Burke, and Kim Peck. Immobilization chemistries suitable for use in the biacore surface plasmon resonance detector. *Analytical biochemistry*, 205(1):132–136, 1992.

[79] Marcel JE Fischer. Amine coupling through edc/nhs: a practical approach. *Surface plasmon resonance: methods and protocols*, pages 55–73, 2010.

[80] Karl Andersson, Markku Hämäläinen, and Magnus Malmqvist. Identification and optimization of regeneration conditions for affinity-based biosensor assays. a multivariate cocktail approach. *Analytical Chemistry*, 71(13):2475–2481, 1999.

[81] Iva Navratilova and David G Myszka. Investigating biomolecular interactions and binding properties using spr biosensors. *Surface Plasmon Resonance Based Sensors*, pages 155–176, 2006.

[82] Robert Karlsson and Anders Fält. Experimental design for kinetic analysis of protein-protein interactions with surface plasmon resonance biosensors. *Journal of immunological methods*, 200(1-2):121–133, 1997.

[83] David G Myszka. Kinetic analysis of macromolecular interactions using surface plasmon resonance biosensors. *Current opinion in biotechnology*, 8(1):50–57, 1997.

[84] Peter Schuck and Huaying Zhao. The role of mass transport limitation and surface heterogeneity in the biophysical characterization of macromolecular binding processes by spr biosensing. *Surface plasmon resonance: methods and protocols*, pages 15–54, 2010.

[85] *Xantec SPR sensor chips. www.xantec.com.*

[86] Robert Karlsson, Anne Michaelsson, and Lars Mattsson. Kinetic analysis of monoclonal antibody-antigen interactions with a new biosensor based analytical system. *Journal of immunological methods*, 145(1-2):229–240, 1991.

[87] *TraceDrawer 1.5 Handbook. Ridgeview Instruments AB, 2008.*

# Appendix A

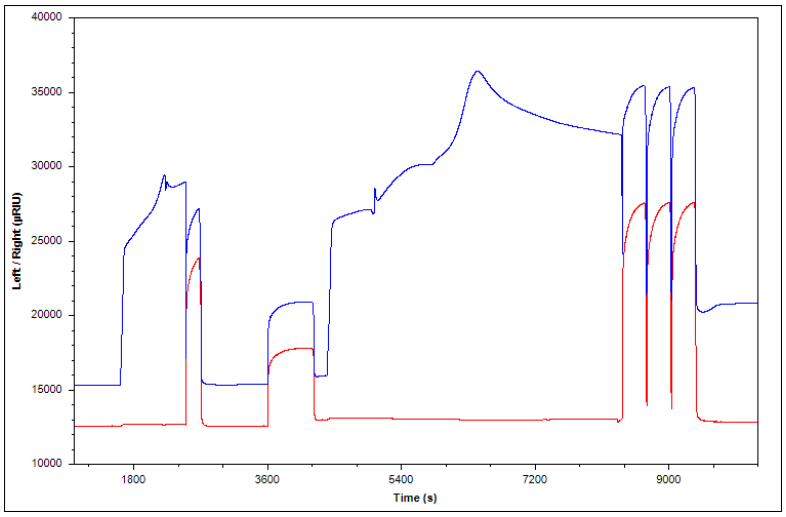


**Figure A.1:** Immobilization sensorgram of Mer 39 on CMD 50 m during run 2.

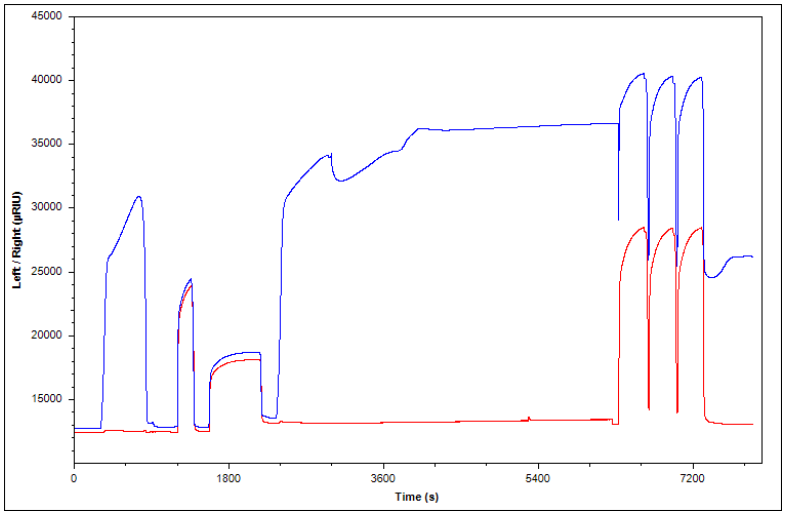


**Figure A.2:** Immobilization sensorgram of Mer 39 on CMD 50 m during run 5, showing different pre-concentration profile.

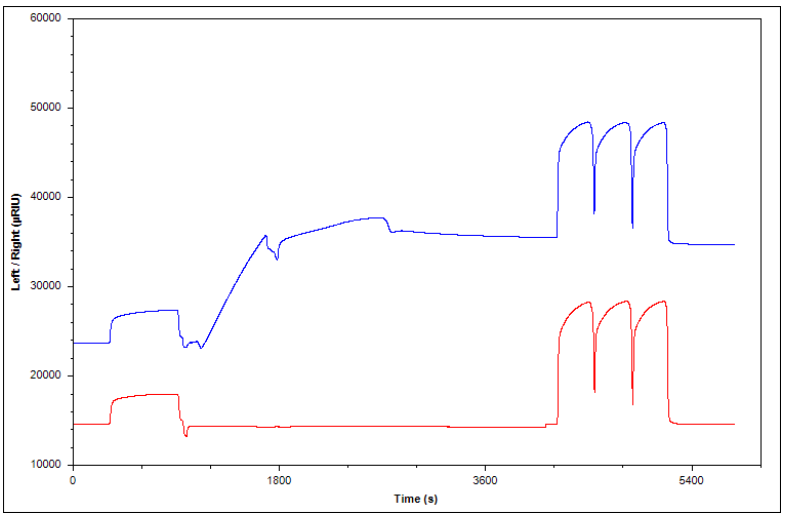


**Figure A.3:** Immobilization sensorgram of Mer 39-NPs on CMD 50 m during run 9 with Mer 39 already immobilized.

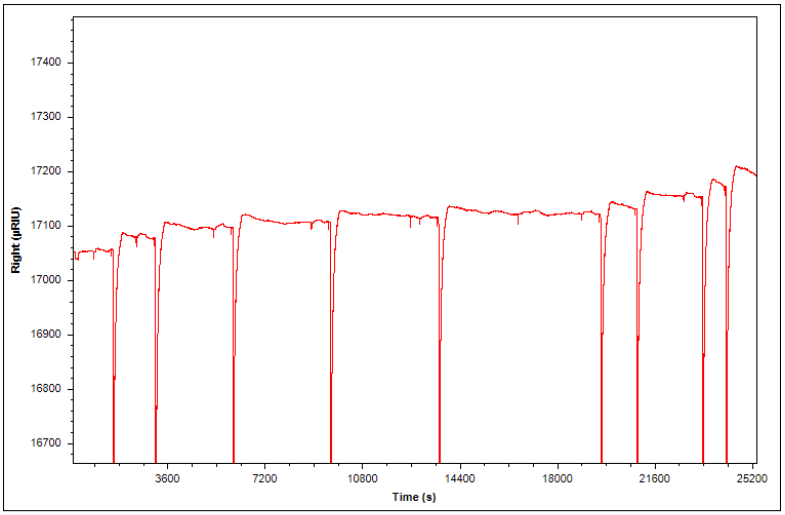


**Figure A.4:** An example of drifting reference channel baseline using hydrochloric acid for regeneration. The baseline was obtained during run 1 with Mer 39 immobilized on HC 1000 m sensor chip.

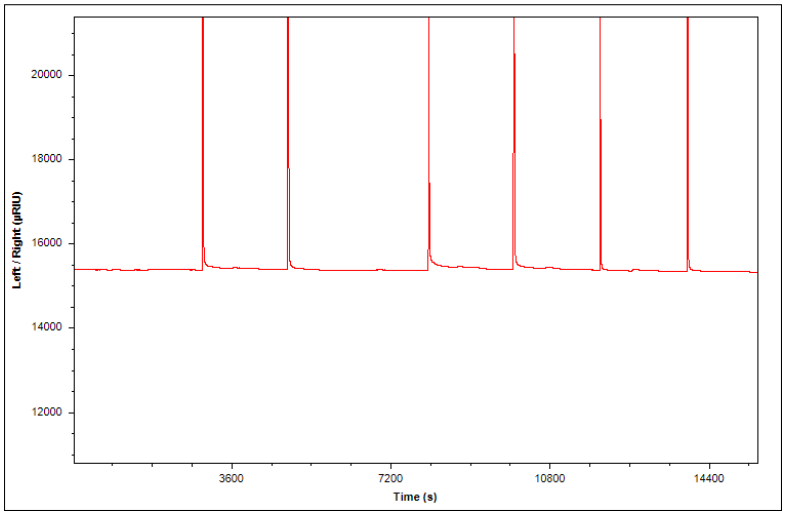


**Figure A.5:** An example of reference channel baseline after using glycine regeneration solution pH 2.2. The baseline was obtained during run 6 with Mer 39 immobilized on HC 200 m sensor chip.

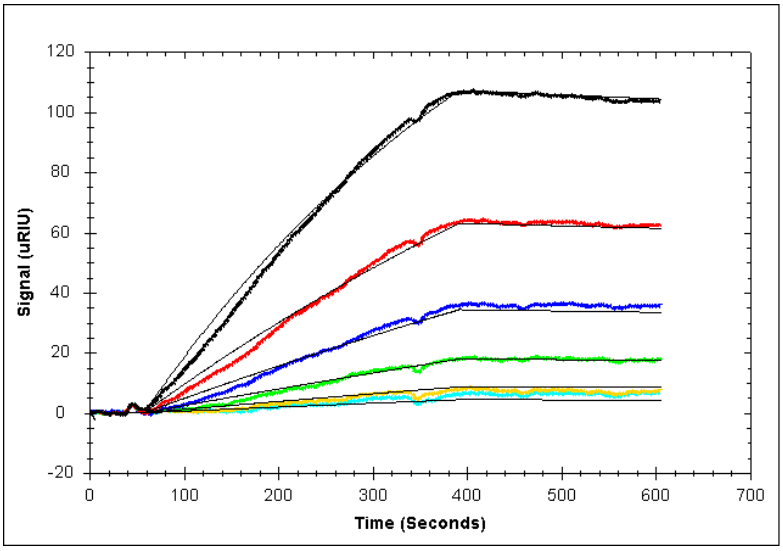


**Figure A.6:** Global fit of run 1 NS1 injection data using one to one model, sensor chip HC 1000 with immobilized Mer 39.

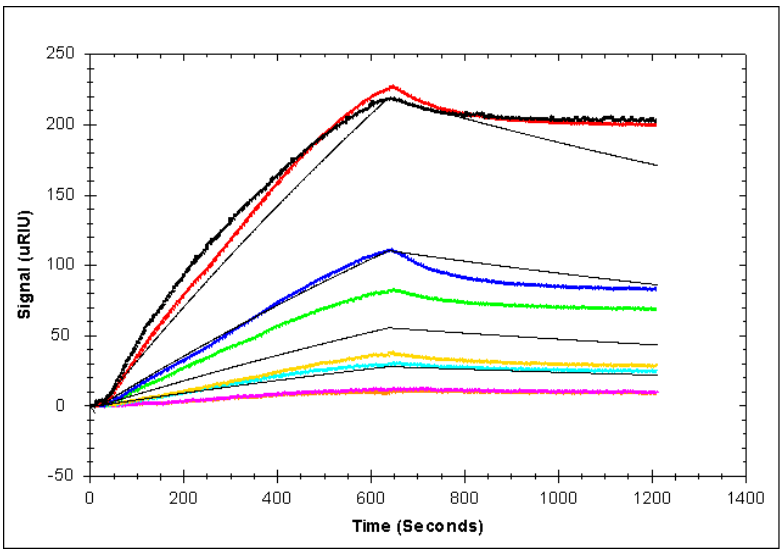


**Figure A.7:** Global fit of run 2 NS1 injection data using one to one model, sensor chip CMD 50 with immobilized Mer 39.

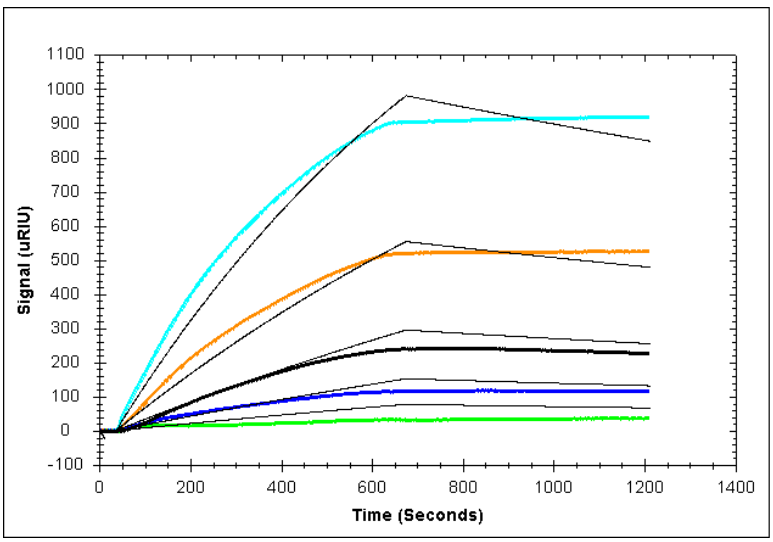


**Figure A.8:** Global fit of run 5 second day NS1 injection data using one to one model, sensor chip CMD 50 with immobilized Mer 39.

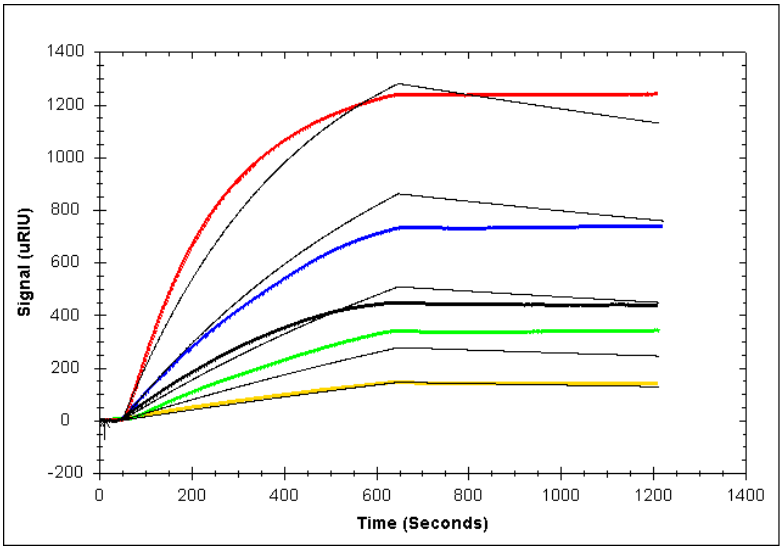


**Figure A.9:** Global fit of run 6 day 1 NS1 injection data using one to one model, sensor chip HC 200 with immobilized Mer 39.

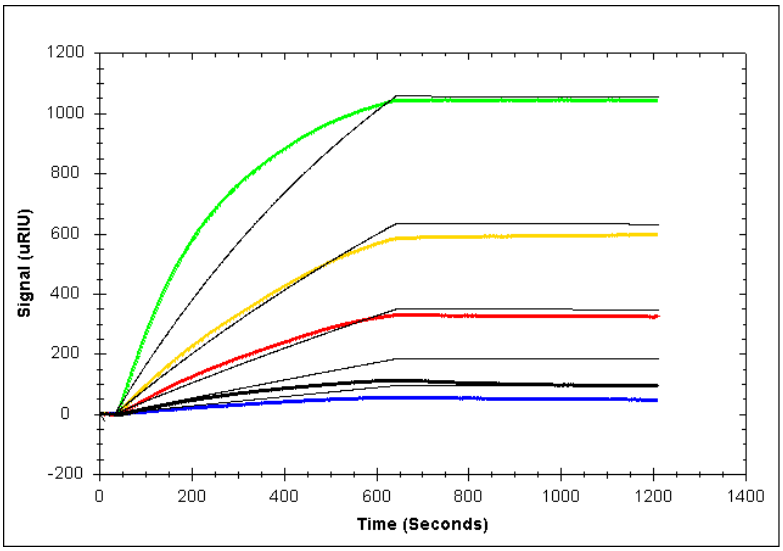


**Figure A.10:** Global fit of run 6 day 2 NS1 injection data using one to one model, sensor chip HC 200 with immobilized Mer 39.

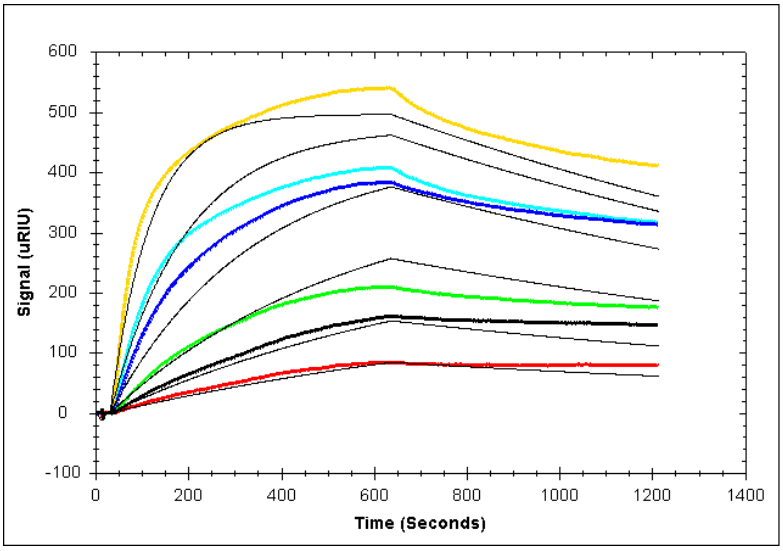


**Figure A.11:** Global fit of run 7 day 1 NS1 injection data using one to one model, sensor chip HC 200 with immobilized BBI5.

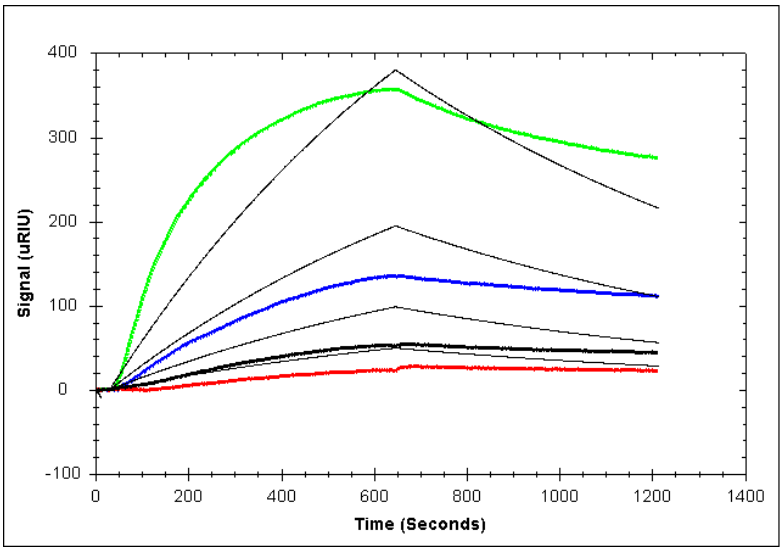


**Figure A.12:** Global fit of run 8 NS1 injection data using one to one model, sensor chip CMD 50 with immobilized BBI5.

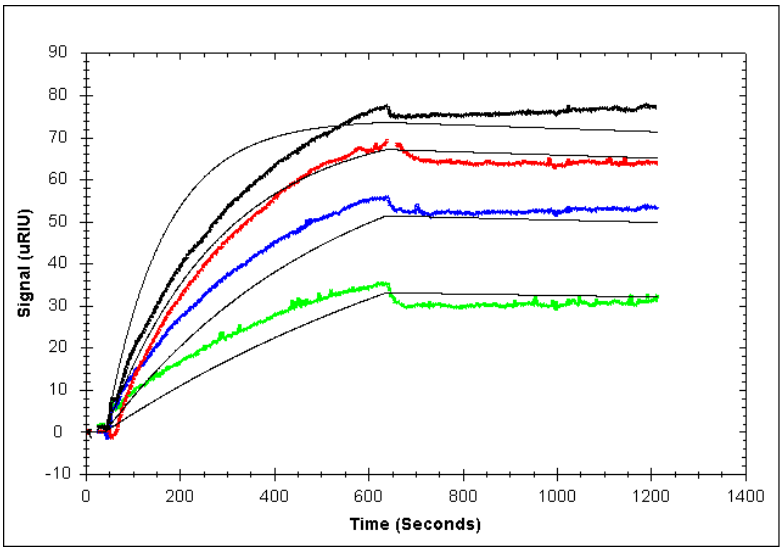


**Figure A.13:** Global fit of run 8 day 1 Mer 39 injection data using one to one model, sensor chip CMD 50 with immobilized BBI5.